January 2020

Polymer Flooding: Predicting Permafrost Stability For The WSak And Ugnu Alaska North Slope Reservoirs

Shane Namie

POLYMER FLOODING: PREDICTING PERMAFROST STABILITY FOR THE WSAK AND UGNU ALASKA NORTH SLOPE RESERVOIRS

By

Shane Scott Namie
Bachelor of Science, Montana Tech, 2018

A Thesis
Defense in the Field of Geological Engineering
Submitted to the Graduate Faculty

of the

University of North Dakota
in partial fulfillment of the requirements

for the degree of

Masters of Science

Grand Forks, North Dakota

August
2020

This thesis, submitted by Shane Namie in partial fulfillment of the requirements for the Degree of Master of Science in Geological Engineering from the University of North Dakota, has been read by the Faculty Advisory Committee under whom the work has been done and is hereby approved.

DocuSigned by:
Dr. Dongmei Wang
08C8564EBF15478...
Dr. Dongmei Wang

DocuSigned by:
B9143F10EA3F407...
Dr. I-Hsuan Ho

DocuSigned by:
Dr. Stephan Nordeng
313181BF2DED4CC...
Dr. Stephan Nordeng

This thesis (or dissertation) is being submitted by the appointed advisory committee as having met all of the requirements of the School of Graduate Studies at the University of North Dakota and is hereby approved.

DocuSigned by:
Chris Nelson
13D0157109424B1...
Chris Nelson
Dean of the School of Graduate Studies

7/21/2020
Date

PERMISSION

Title POLYMER FLOODING: PREDICTING PERMAFROST STABILITY FOR THE WSAK AND UGNU ALASKA NORTH SLOPE RESERVOIRS

Department The Harold Hamm School of Geology & Geological Engineering

Degree Masters of Science

In presenting this thesis in partial fulfillment of the requirements for a graduate degree from the University of North Dakota, I agree that the library of this University shall make it freely available for inspection. I further agree that permission for extensive copying for scholarly purposes may be granted by the professor who supervised my thesis work or, in her absence, by the Chairperson of the department or the dean of the School of Graduate Studies. It is understood that any copying or publication or other use of this thesis or part thereof for financial gain shall not be allowed without my written permission. It is also understood that due recognition shall be given to me and to the University of North Dakota in any scholarly use which may be made of any material in my thesis.

Shane Namie
July 15, 2020

ABSTRACT

The heavy oil reserves of the Ugnu and West Sak Formations in Alaska offer major production challenges, including proximity to the permafrost layer and exceptionally high viscosities. Despite deeper reserves, most of the untouched heavy oil deposits in the West Sak and Ugnu sands are at shallow depths with a low API gravity (< 15 degrees). The objective of this study is to evaluate permafrost subsidence while extracting heavy oil from shallow reservoir using polymer flooding. The approach to this study will focus on using geological properties taken from well logs, completion logs and available core data from 32 wells and applying them to a numerical fluid flow model. Calculations were completed for eight cross-sections taking into consideration the following outcomes: Formation tops, permafrost depth, porosity, water saturation, and permeability. Eleven numerical models were created showing polymer flooding is an effective enhanced oil recovery (EOR) process that minimizes permafrost subsidence.

Table of Contents

PERMISSION iii
ABSTRACT 1
LIST OF FIGURES 4
LIST OF TABLES 6
APPENDIX 7
CHAPTER I 8
INTRODUCTION 8
1.1 Heavy Oil Definition 8
1.2 Heavy Oil Reserve Potential 9
CHAPTER II - GEOLOGY 9
2.0 Geology of the Kuparuk Field 9
2.1 The Ugnu Reservoir Sands 10
2.2 The West Sak Reservoir Sands 11
2.3 West Sak and Ugnu Heavy Oil Potential 11
CHAPTER III – LITERATURE REVIEW 12
3.1 Alaska's State of Art 12
3.2 Conventional vs Unconventional Oil Recovery 14
3.3 API Gravity 15
3.4 Viscosity of Heavy Oil 16
3.5 Ugnu & West Sak Geological Properties 17
3.6 Geomechanical Properties 18
3.7 Permafrost Thawing and Subsidence 19
3.8 Well Casing Insulation Techniques 23
3.9 Oil Recovery Methods 24
3.10 Thermal EOR 25
3.11 Gas Injection 26
3.12 Chemical Flooding 27
3.13 History of Viscous Oil Development in ANS 28
3.14 Polymer Flood History 29
3.15 Framing the Problem 32
3.16 Framing the Question 33

3.17 Hypothesis 34
CHAPTER IV – METHODS 34
4.0 Geological Properties 35
4.1 Formation Tops 35
4.2 Formation Temperature 35
4.3 Porosity of the Formation 36
4.4 Resistivity of Formation Water 37
4.5 Water Saturation 37
4.6 Permeability 38
4.7 Numerical Methods 39
4.8 Permafrost Elastic Modulus (*E*) 40
4.9 Numerical Simulation Models 41
4.10 Overview of Simulation Models Initial Set Up 42
4.11 Simulation Experiments 43
CHAPTER V - RESULTS AND ANALYSIS 44
5.1 Permafrost and Reservoir Tops 45
5.2 Formation Temperature 47
5.3 Porosity 48
5.4 Water Saturation 49
5.6 Permeability 49
6.0 Numerical Models Horizontal Wells 50
6.1 Horizontal Wells Development Southwest Area West Sak 50
6.2 Vertical Wells Development Southwest Area West Sak 51
6.3 Horizontal Wells Development Southwest Area Ugnu 52
6.4 Horizontal Wells Development Northeast Area West Sak 53
6.5 Prior Study Comparison 54
CHAPTER VI – CONCLUSION 57
REFERENCES 60

LIST OF FIGURES

Figure 1. Location of world's heavy oil reserves…….67

Figure 2. The map location of the Kuparuk oil field on the ANS…….67

Figure 3. Lithology of Kuparuk oil Field……68

Figure 4. Carmen et al. (1983), Kuparuk reservoir isopach……68

Figure 5. The Petroleum System (Bird et al., 2002) ……69

Figure 6. The West Sak core area……69

Figure 7. Discovery of giant oil fields from 1945 to 2005……70

Figure 8. Viscosity comparison to household items……70

Figure 9. Werner (1987) structural contour map, top of West Sak Sands (ft)……71

Figure 10. Werner (1987) structural contour map, top of Ugnu sands (ft)……72

Figure 11. Panda et al. (1989) structural contour map, top of West Sak sands (ft)……73

Figure 12. Permafrost lays under 80 percent of Alaska's surface……74

Figure 13. Radii of thawing conventional production well……74

Figure 14. Thaw subsidence loading on production well……75

Figure 15. Electric downhole heating design on a horizontal well……75

Figure 16. Conceptual view of steam flooding……76

Figure 17. Multi-lateral technology……76

Figure 18. ANS heavy oil multi-lateral number of producers with production increased rates...77

Figure 19. ANS study area including cross-section layout...……78

Figure 20. Simulation break down for models……..79

Figure 21. Full scale model 300 x 300 x 7 = 630,000 grid blocks, 32 wells……80

Figure 22. Study area-1, 150 x 100 x 7 = 105,000 grid blocks……81

Figure 23. Study area-2, 150 x 150 x 7 = 157,500 grid blocks...……82

Figure 24. Technique identifying bottom of permafrost…….……83

Figure 25. Cross-section JJ-JJ'……84

Figure 26. Permafrost depth……85

Figure 27. Taliks form in the subsurface from water bodies…….……....85

Figure 28. Structural contour map of the top of Ugnu sands……...…...……86

Figure 29. Isopach map of the Ugnu reservoir……87

Figure 30. Structural contour map of the top of West Sak sands……88

Figure 31. Isopach map of the West Sak sands……...……89

Figure 32. Ugnu reservoir temperature graphed from cross-section A-H……...90

Figure 33. West Sak reservoir Temperature graphed from cross-section A-H……...……90

Figure 34. Case 1-6 total vertical subsidence southwest West Sak…….91

Figure 35. Case 1-6 Temperature profile southwest West Sak……...…….91

Figure 36. Case 7-8 total vertical subsidence southwest Ugnu……92

Figure 37. Case 7-8 temperature change southwest Ugnu……...……92

Figure 38. Case 9-11 total vertical subsidence northeast West Sak…….93

Figure 39. Case 9-11 total temperature change northeast West Sak……93

LIST OF TABLES

Table 1. Change in economically recoverable reserves……..94

Table 2. Crude oil classification by the American Petroleum Institute Agency…….94

Table 3. Static and Dynamic geomechanical properties…….95

Table 4. Geomechanical properties from prior numerical simulation Wang et al (2019)……..95

Table 5. Calculated reservoir properties from wireline logs……...……96

Table 6. Numerical model properties……..97

Table 7. Well geometry……...……98

Table 8. Estimated depths to TVD of the permafrost zone, Ugnu and West Sak sands.……99

Table 9. Wellbore temperature calculation…….100

Table 10. Average permafrost temperatures calculated……..……101

Table 11. Calculated variables used to build the mesh grids……..102

Table 12. Vertical subsidence and temperature results……..…….……103

APPENDIX

Appendix A, Table A1. Logs-derived data for selected wells in the West Sak Sands…….….104

Appendix A, Table 2A. Petrophysical properties of West Sak lower sands 1…….……...104

Appendix A, Table 3A. Petrophysical properties of West Sak upper Sands.…….……105

Appendix A, Table 4A. Petrophysical properties of West Sak lower sands 2…….....……105

Appendix A, Table 5A. Petrophysical properties of West Sak lower sands 3……..…..106

Appendix A, Table 6A. Petrophysical properties of West Sak lower sands 4……...……106

Appendix B, Figure 1B. Chart used to estimate Rmf from Rm)….……....…107

Appendix B, Figure 2B. Chart used to convert Rmf to reservoir temperature……..……..108

Appendix B, Figure 3B. Chart used to convert Rmf to Rmf_{eq} ……..…….……109

Appendix B, Figure 4B. Converting SP from the zone of interest water resistivity R_{we} ..…..…110

Appendix C, Figure 1C. Chart permeability from water saturation (sw) vs porosity (ϕ)…...…111

Appendix D, Figure 1D. Cross-section A-A’..…...…….…….....…….112

Appendix D, Figure 2D. Cross-section B-B’….…….....…….....…112

Appendix D, Figure 3D. Cross-section C-C’….……..…….……..…..…….113

Appendix D, Figure 4D. Cross-section D-D’……..…..…….…….…….……..113

Appendix D, Figure 5D. Cross-section E-E’……..…….…….…….114

Appendix D, Figure 6D. Cross-section F-F’…….…..…….…….…….114

Appendix D, Figure 7D. Cross-section G-G’……..……..…..……115

Appendix D, Figure 8D. Cross-section H-H’……..……..……..…..……..115

CHAPTER I

INTRODUCTION

The last frontier in US oil production may be in technology development for heavy oil production in seeking feasible enhanced oil recovery (EOR) methods in Artic regions. The heavy oil reserves in Alaska offer major production challenges deterring industry to date from production based on the following: proximity to the permafrost layer, and high viscosity. However, in recent years, increasing demand for oil and recent advancements in (EOR) technological developments have made heavy oil a viable consideration for extraction. Previous research has taken generalized geological properties from the Ugnu and West Sak deeper portions of the intervals and applied them to different areas of the reservoir field for modeling purposes. For example, Werner (1987) generalizes the reservoir property such as permeability, ranging from 10 to 800 mD in the West Sak sands and 200 to 3000 mD in the Ugnu sands.

While generalization in prior research can be valuable in developing a geological model, the research lacks completeness for building a unique geological field scale and EOR numerical fluid flow model. Additionally, to the authors knowledge to date prior research does not consider the relationship between the following three factors: permafrost, Ugnu and West Sak intervals. Specifically, the shallow depths of these reservoir sands in relation to temperature impact during production towards permafrost stability.

1.1 Heavy Oil Definition

Heavy oil is defined as viscous liquid that does not easily flow to production wells under normal reservoir conditions. In addition, the density or specific gravity is higher than light crude oil; density less than 20° API gravity or more than 200 cp viscosity at reservoir conditions (Dusseault, 2001). This type of oil originated as light oil that migrated to shallower traps,

undergo biodegradation and over time has turned into heavy oil. These types of reservoirs are comprised typically of unconsolidated sandstone existing at shallow depths with high porosity (28% to 36%) and oil viscosity ranging 500 to 15,000 cp (Dusseault, 2001).

1.2 Heavy Oil Reserve Potential

Heavy oil reservoirs characteristics are not all similar, they are influenced by fluid quality, rock properties, surface and subsurface temperature zones. In turn, the method of heavy oil recovery will vary from one part of the world to the next. Venezuela and Canada constitute around 35% of the total world heavy oil reserves followed by the Middle East, Russia and last US (Figure 1). Both Canada and Russia have experience addressing the unique challenge of producing such viscous oil from colder regions. For example, Canada has used water flooding along with polymer flooding in the past to recover both heavy and medium oil; with oil gravities of 22° to 15° API (Renouf, 2014). However, none of these countries have measured the long-term impacts on permafrost subsidence to the author's knowledge.

CHAPTER II - GEOLOGY

2.0 Geology of the Kuparuk Field

The Kuparuk oil field is located at the northern edge of the Alaskan North Slope (ANS) north of the arctic circle and approximately 20 mi. west of Prudhoe Bay Field (Figure 2). The field primarily stratigraphic column consists of the Kuparuk interval a lower member sequence of interbedded sandstone, siltstone, and mudstone. Above the Kuparuk sequence is two low gravity oil reservoirs, the West Sak sands and the overlying Ugnu sands (Figure 3). The Ugnu and Wsak sands combined stratigraphic intervals have an average thickness of 1050 ft (Werner, 1987). The stratigraphic sediments are comprised of the late Cretaceous and early Tertiary marine and deltaic deposits. The Kuparuk field deposits are part of the Alaska Arctic Basin

sequence which was influence over time by two events; the Barrows arch and the Colville Trough (Carmen et al., 1983). Today, located offshore and parallel to the Alaskan coastline is the paleo-high Barrow's arch which influenced the deposition of pre-Late Cretaceous sediments. The second basin sedimentary influence was the Colville trough; asymmetric with an east to west axis near the Brooks Range (Carmen et al., 1983). The overlying Brookian (Cretaceous to Tertiary) sediments were derived largely from the south continent to continent collision creating the Brooks Range Thrust (Figure 2).

During the development of Barrows arch the depositional environment was influenced from regional tectonics resulting in two structural high areas, the Colville and Prudhoe highs. Carmen et al (1983) research helps support the reservoir trap from an isopach map of the Lower Cretaceous sequence showing the extent of the Kuparuk oil field. Thinning of this sequence can be seen towards the Colville and Prudhoe highs south of Barrows arch (Figure 4). In general, oil is trapped in the Kuparuk field along an anticline that plunges 0.8 degrees to the southeast (Masterson, 2015). Furthermore, along the northeastern flank of the anticline, the field is contained by an oil water contact. The western and southern limits of the field are contained stratigraphically by sandstone pinch outs and truncated by unconformities (Masterson, 2015). This study briefly touches base on the Petroleum System events, for further detail see Figure 5.

2.1 The Ugnu Reservoir Sands

The Ugnu sands represent an interbedded fluvial sequence unconsolidated sand deposited in the Late Cretaceous and Early Tertiary marine deltaic environment. The sands are oriented in east-west direction with a stratum dipping approximately 2.0 degrees oriented from southwest to northeast. The oil viscosity in this reservoir is primarily affected by the proximity 1,600 ft TVD

of the permafrost layer. In turn, the permafrost temperature impacts the reservoir oil by driving down the API gravity to (< 15 degrees).

2.2 The West Sak Reservoir Sands

The West Sak heavy oil deposits are associated with the Orion and Polaris Fields within the Prudhoe Bay Unit and Schrader Bluff (Targac et al., 2005). The West Sak formation is a lower shoreface to inner shelf, unconsolidated sands in the Cretaceous-aged formation with an average gross thickness of approximately 500 ft TVD. The top of the West Sak reservoir ranges from 2,400 ft TVD located on the western edge of Kuparuk River Unit (KRU) to about 3,800 ft TVD on the eastern edge.

2.3 West Sak and Ugnu Heavy Oil Potential

West Sak and Ugnu's oil originated in similar places that the conventional "light" oil on the North Slope; the large Kingak Shale and Shublick Formation. Over millions of years, oil seeped out of the shale "source rocks" and migrated upward, and northward, along faults through the rocks. Some of it was trapped at deeper levels in the large sandstone formations that are now the deeper producing conventional oil fields (Kuparuk reservoir). While some kept migrating to shallower levels, where temperatures were cooler, and became the "viscous" oil deposits which are producing today; the West Sak core area.

The West Sak and Ugnu heavy oil deposits are located within the Kuparuk River Unit (KRU) on the (ANS). The deposits are associated with the Orion and Polaris Fields within the Prudhoe Bay Unit and the Schrader Bluff and Ugnu heavy oil sands within the Milne Point Unit and Kuparuk unit (Targac et al., 2005). The core area is located on the eastern edge (Figure 6); considered the warmest with an oil gravity ranging from 22° to 15° API with a reservoir temperature of 75°F.

Oil extraction has taken place from the West Sak deposits in the past from the Milne point unit further northeast from the Kuparuk field. However, majority of the untouched heavy oil deposits in the West Sak and Ugnu area are of low quality (<15 degrees API) and is located at shallow depths located in the Kuparuk field. This reservoir is close to the base of the permafrost (approx. 1,600 feet subsea), and relatively cold, which increases the viscosity of the oil. Low API gravity along with low temperatures results in the oil having viscosities greater than 300 cp.

CHAPTER III – LITERATURE REVIEW

3.1 Alaska's State of Art

At some point the continuous increase in world energy demand driven by economic development, dramatic population growth, and decline in giant conventional oil fields will stress our petroleum resources. This will require the industry to look towards unconventional methods to extract petroleum resources from reservoirs. Hirsch et al. (2005), defines peak oil as a theorized point in time when the maximum rate of extraction of petroleum is reached, after which it is expected to enter terminal decline. This peak period over the last few decades is a matter of debate with two agreement: 1) geologist all agree that eventually this will happen, 2) the discovery of giant oil fields (Figure 7), (more than 100,000 barrels per day) are the thing of the past (Hook et al., 2009).

Alaska's North Slope (ANS) has produced more than 17 billion barrels of oil since the discovery of Prudhoe Bay's oil Field. The ANS produces on average from year to year approximately 518,000 barrels per day currently, with forecasting for 2020 to meet consumer demand to be 529,000 barrels per day (Nelson, 2007). However, while the economic impact of oil and gas production is profound in Alaska, production has been in a long-term decline since peaking in 1988. It is not for the lack of resource in Alaska's subsurface that production has

declined for the state. There is plenty of conventional oil in the subsurface outside of the current fields in operation to make up the difference going forth. However, one proposal requires entering the north east section of Alaska's National Wildlife Refuge (ANWR) and will not start till ~2,031. It is estimated that this new area would add 3.4 billion barrels to production from 2031 to 2051.

The question that comes to mind is, "why doesn't the petroleum industry apply existing thermal (EOR) methods to the shallow portions of the West Sak and Ugnu Fields?" Because Petroleum companies do not have a viable solution in dealing with cold temperatures and a permanent permafrost subsidence in these shallow zones ranging ~1,200 ft to ~2,000 ft subsea.

Oil production is separated into three phases: primary, secondary and tertiary, which is also known as Enhanced Oil Recovery (EOR). Primary oil recovery is limited to hydrocarbons that naturally rise to the surface, or those that use artificial lift devices, such as pump jacks. Secondary recovery employs water or gas injection, displacing the oil and driving it to the surface. Last, tertiary involves three primary techniques of EOR: gas injection, thermal injection, and chemical injections, etc.

Alaska needs petroleum companies to work on advanced EOR technology to extract resources that exist already in developed areas. Such areas as West Sak and Ugnu sands already have existing wells (~512 wells in the Kuparuk field) moving through these sand formations to the deeper Kuparuk interval. Looking closer at the number to maintain production in the ANS without gaining new access to federal lands or offshore locations, industry will need to build upon existing infrastructure with the use of EOR methods to maintain forecast projections. As of December 31st, 2007, it was estimated that recoverable reserves for the producing fields in place now (Table 1), totaled between 14.65 and 15.7 BBO and 30.575 TCF (Thomas et al., 2009).

This range estimation includes reserve growth forecast that incorporates the viscous oil from the Ugnu, and West Sack accumulations. Looking to the future reserve growth has potential to add significant quantities of oil or gas without any additional exploration needed. However, in the past to present these unconventional reservoirs have remained untouched because they are near the permafrost. These types of reservoirs require a better understanding in reservoir geometry, EOR technology, and improved economic conditions to gain access. Going forth in the future to maintain and increase yields, fields such as Kuparuk River will need to rely on more efficient tertiary recovery methods for production (Masterson et al., 2001).

3.2 Conventional vs Unconventional Oil Recovery

The differences typically between conventional versus unconventional oil lie in the existing type oil. In the conventional oil extraction method, oil obtained is already flowing between rock formations underground. The natural pressure from the well is all it takes to pump this oil to the surface. After these types of oil fields are significantly depleted, the well's natural pressure might drop to where it cannot extract more oil. In the absence of water injection, pumping may be used to maintain oil recovery rate at an economical level. In this case, water or gas injection can be used. This type of extraction is still considered to be used for conventional resources.

Unconventional oil includes crude oil having API gravity lower than 20 degrees and other tight oils (Bakken oil, for example). If reservoir pressure falls below the oil bubble point pressure, gas that was initially dissolved in the oil will come out of solution. This gas has a considerably lower viscosity and will flow preferentially to the production well. While at the same time the viscosity of the remaining oil increases, reducing its mobility further; reducing the oil production rate further. Water (or gas) injection is routinely applied before this happens to

maintain reservoir pressure above the bubble point. For this reason, it is sometimes known as secondary recovery. For example, the shallow West Sak and Ugnu sands contain heavy oil, with a less effective seal due to the low seal pressure in the reservoir. It is presumed this may represent the cause for the dissolved gases to leave the oil, increasing the viscosity. This type of reservoir may require chemical methods along with horizontal drilling to reach the dispersed oil for extraction.

Currently, new discoveries of conventional oil are scarce and insufficient to meet the increase in energy demand going forth in the future. Parallel to the decline of conventional oil reserves, it has been observed that the new discoveries of oil are considered as unconventional resources with oil reserves that have API gravity lower than 20 degrees (Trevisan et al., 2006). The future development of new technologies will become crucial for the economic production of unconventional resources such as heavy oil and extra heavy oils.

3.3 API Gravity

Heavy oil or viscous oil, extra heavy oil, oil sand, tar sands, oil shale, and bitumen are all considered unconventional oil resources (Santos et al., 2014). Typically, heavy oil is comprised of a type of crude oil which is viscous with high density and low American Petroleum Institute (API) gravity. The API gravity system denotes that the higher the API Gravity the lighter the liquid is and the easier it will flow. API Gravity is a measure of how heavy or light a petroleum liquid is compared to water. For example, if the sources API gravity is greater than 10, it is lighter and floats on water; if less than 10, it is heavier and sinks. The formula to calculate API gravity from specific gravity (SG) is:

$$API\ gravity = \frac{141.5}{SG\ at\ 60°F} - 131.5 \quad \text{.....(1)}$$

The API degree range that defines and classifies oils to date has not been standardized. Comparatively, the World Petroleum Conference classifies heavy oil as those below 22.3 API degrees. The American Petroleum Institute, heavy oil classification is API smaller than 20 degrees and the North American taxation system relates to the American Petroleum Institute's version (Trevisan et al., 2009). This study has adopted the American Petroleum Institute's classification for API gravity measurements Table 2. Moreover, crude oil is also classified as light, medium, or heavy according to its measured API gravity.

3.4 Viscosity of Heavy Oil

Viscosity of heavy oils can be critical in reservoir simulators that are used to predict and optimize oil recovery from oil fields. These input properties for the reservoir fluids are considered a function of pressure, temperature and composition. Viscosity is directly related to all three of these characteristics and impacts the fluid's resistance to flow. The higher the viscosity value is, indicates more resistance to flow. Geochemical work done by Carmen and Hardwick (1983) indicates that crude oil from these shallow sands originated from the same source rock as the oil in the deeper Kuparuk reservoir; but biodegraded. Larter et al. (2006) believes the oil was expelled from its source rock as light or medium oil, and subsequently migrated to a trap. This was then converted into heavy oil through different processes such as water washing, bacterial degradation (aerobic), and evaporation, provided that the trap is elevated into an oxidizing zone. This light oil at one point lost all the small (light) molecules, leaving the heavy molecules behind (Brownbag, 2011). To clarify, most of the heavy oil is depleted in hydrogen leaving the longer chained molecules of heavy oil behind. An example of this is the viscosity of the West Sak ~30 cp to ~3,000 cp and Ugnu from ~10,000 cp to ~100,000 cp; which is a result of depleted hydrogen molecules. Meaning, the remaining oil has high

internal friction which is a characteristic of a liquid with high viscosity (Brownbag, 2011). To illustrate this, viscosity can be correlated by comparing to everyday things around the house (Figure 8).

3.5 Ugnu & West Sak Geological Properties

Current research work being done today in the Kuparuk field still uses geological research that was done prior to 1989. These studies are limited when considering the difference from one side of the field to the other. For example, Werner (1987) describes both the Ugnu and West Sak sands from a geological broad approach which included the stratigraphic and structural framework in the Kuparuk River Unit. His study entailed one cross-section from northeast to southwest including three wells all together (Figure 9 & 10). Although his study expanded the knowledge of the field with his structural contour maps of both the Ugnu and West Sak intervals, the source of his data is unclear on what he used to create his structural contour maps. The research paper shows the wireline logs for the three wells used in the cross-section, but fails to show the wells he used to expand the contour map to encompass the entire field. Furthermore, Werner (1987) study was an attempt to understand the entire field that includes the Ugnu and West Sak intervals from a geological stratigraphic standpoint with generalizing reservoir properties. Resulting in a broad viewpoint of the reservoir properties such as permeability; ranging from 10 to 800 mD in the West Sak sands and 200 to 3000 mD in the Ugnu sands.

Later, Panda et al (1989) research expanded in detail from well logs describing the West Sak reservoir to great lengths in two separate cross-sections (Figure 11). This study went further in combining log-derived data and petrophysical properties for the West Sak reservoir. The first cross-section (B-B') was on the east side using four wells going north to south in the deeper part of the reservoir. The second cross-section (A-A') is going northeast to southwest including four

wells. This study used thirteen wells all together for the West Sak reservoir to include: formation tops, net pay, average porosity, and average water saturation (Appendix A, Table 1A – 6A). Panda et al (1989) did the same thing Werner did and took the limited cross-section data and applied it to the entire field to represent the West Sak reservoir in structural contour maps. While Panda et al (1989) research expanded knowledge for the field, the two cross-sections are still insufficient when applying deeper reservoir properties to a shallow reservoir in an EOR numerical model that is sensitive to permafrost temperature and depth.

3.6 Geomechanical Properties

The geomechanical properties can reveal the mechanical behavior of rocks as fluid pressure is reduced in production which effectives stress from the overburden causing subsidence. In permafrost zones to date the subsidence has been minimal because the wells are deep enough to minimize temperature flow through the casing to the surface during production. However, in shallow reservoirs because of the short distance to the reservoir net pay area to the permafrost interval the potential for loss of wells, reduced production, and irreparable damage to the surface structures increases (Ranjbar et al., 2017). Looking to areas similar to the ANS to model the geomechanical properties the Malik, Mount Elbert and Toyoura Sands research cases all measure and model reservoir sediments as an unconsolidated sand with vertical compaction at Mallik and Mount Elbert limited within 0.4% (Rutqvist et al., 2009). To further support static to dynamic transforms the geomechanical properties the laboratory experiments on the Toyoura Sand (Masui et al., 2005), represented in the Rutquist et al. (2009) study are currently the most relevant mechanical properties for unconsolidated sand reservoir (Table 3).

The reservoir mechanical properties, the dynamic elastic modulus, dynamic shear modulus, and Poisson's ratio are essential in reflecting the geomechanical properties. Looking at

the relationship between elastic modulus as it increases Wang et al. (2003) showed that temperature decreases. Furthermore, the results in Wang et al. (2003) research showed in frozen Loess temperatures ranging from -2.0°C to -4.0°C that the elastic modulus was 1.7 GPa. Meaning, that the elastic modulus is affected and changes with temperature in a numerical model. Additionally, Wang et al. (2003) showed in the same study when the Poisson's ratio decreases so does temperature. However, in this same study the Poisson's ratio of frozen sand is not related to temperature. Concluding, that the law of dynamic Poisson's ratio varies with the type of soils such as silt or clay showing a decreased in elastic modulus with ascending temperatures.

3.7 Permafrost Thawing and Subsidence

In general, the bottom of the permafrost zone on the Alaska North Shore stays frozen year around (Collett et al., 2011). According to Collett et al (2011), all the North Slope oil fields are overlain by a layer of permafrost as illustrated in (Figure 12). In the Kuparuk field where the West Sak and Ugnu heavy oils reside, the first 300 ft of subsurface consist of permafrost made up of coarse sand, gravel, and conglomerates (Hallam et al., 1992). Approximately 900 ft is an unconformity of claystone intervals at ~ 150 ft thick. Below this unconformity is a series of silty-sand and silt beds that take up the whole Kuparuk field (Hallam et al., 1992). The depth of the "ice-bearing" permafrost varies from 1,200-1,700 ft in depth with temperature ranging approximately -10.5°C at the surface to 0 °C near the bottom (Lachenbruch, 1970). Furthermore, the surface temperature can impact the depth of the permafrost from near the cost at -12.0 °C where the permafrost is deeper to -8.0 °C near Brooks Range where permafrost is shallower. Additionally, this zone lacks load-bearing capacity; in turn immense care is needed to prevent thawing (Lachenbruch, 1970).

Permafrost is usually defined as any formation temperature that remains permanently below 32.0°F year around regardless of seasons. Lachenbruch (1970) research found that temperatures of permafrost away from bodies water can be determined by three factors: the mean annual surface temperature, the geothermal gradient, and the climate warming of the last hundred years. Specifically, the heat flow from the earth's interior is uniform and on the ANS the gradient is inversely proportional to the thermal conductivity of the permafrost (Lachenbruch, 1970). Where the conductivity is equal and the mean surface temperature is lower the permafrost is deeper. Additionally, when the mean surface temperature is equal, and the conductivity is higher the permafrost is deeper. For example, Lachenbruch (1970) found that Prudhoe bay has a permafrost thickness of 2,000 ft, Barrow's at 1,000 ft and Cape Simpson approximately 200 ft thick. Strange that all three areas have the same mean surface temperatures with different permafrost thicknesses. These differences in permafrost thicknesses were determined in Lachenbruch (1970) research to be contributed to the differences between the proportion of siliceous sediments in the stratigraphic column. His results conclude, an increase in conductivity with a decrease in geothermal gradient when traveling from Simpson to Barrow to Prudhoe. This study points out the differences in areas and the importance of using an heterogenous geological model for the use towards an EOR numerical fluid flow model that is sensitive to permafrost thawing and subsidence.

A potential problem exists when warm oil from deep producing formation flows up the producing well, losing heat as it passes through the permafrost zone. This in turn, may cause thawing of the permafrost and settlements of surrounding soils (Smith, 1971). Considering this study is using a cold chemical EOR method, the primary flow of heat from warm production wells to the surrounding formations represent a function of temperature. This temperature

difference will be present between the produced fluids and the formation, design of wells in a relationship to the permafrost zone and the thermal properties of the reservoir itself. The instability of permafrost and equipment failure on the surface is attributed to the following surface changes:

- Melting of permafrost can decrease ice volume, causing formation to compact due to loss of support.
- In permafrost zones, pressures that exceed hydrostatic are generated during thawing, pushing fluid flow resulting in soil compaction.
- As thawed permafrost compaction happens a phase change contraction of pore ice is accompanied by a decrease in pore pressure, resulting in an increase in intergranular stress.
- As permafrost thaws, the soil becomes softer and easier to deform due to loss of support provided by the pore ice.

In general, the rate of permafrost thaw will depend on the thermal properties between the well casing and the permafrost. For example, looking at Figure 13, at a reservoir temperature of 23.0°F the longer the well is producing shows a dramatic increase in the radius of thawing from the well (Smith, 1971). Additionally, Smith (1971) study found that over a period of 40-years using a vertical well permafrost thawing can spread ~80 ft. outward from the well. Moreover, after apparent surface subsidence, damage to surface equipment or loss of access to the wellbore, most of the time this is the first indication that thaw-induced subsidence has occurred. For example, BP reported on July 23rd, 2017 one of their wells in Prudhoe Bay was leaking at the well head. Upon investigating BP ended up shutting down 14 wells as a result regarding surface casing failures (Bailey, 2017). The investigation identified the cause of the incident was a

mechanical failure related to permafrost subsidence leading to shutting down 14 wells permanently (Bailey, 2017). The analysis determined that the upward movement of the well casing damaged the wellhead resulted from a tensile failure of the surface casing; the upper section of the casing becoming detached from the lower section where the surface casing had broken under a load resulting from subsidence of the permafrost surrounding the well.

While this study is not specifically looking at wellhead stresses and well casing insulation techniques it is good to understand how the thawing of permafrost impacts the well. The subsidence issue is caused by casing strain and not casing stress. As the permafrost thaws over time deformation in the soil occurs. In turn, strain occurs on the casing which is a consequence of the casing strain (Mitchel et al., 1978). Additionally, the induced casing strain is bounded and controlled by the amount of permafrost deformation. Wells on the ANS all have design techniques implemented to reducing thawing around both the production well and the injections well such as: insulated tubing, active refrigerating systems and gels. BP's wells in the example above all were specifically designed for permafrost regions and 14 of them have failed over time due to subsidence. Mitchel et al (1978), refers to four permafrost subsidence loading mechanisms for inducing casing strain as shown in the (Figure 14). The pore pressure reduction mechanism produces an upward rebound of the permafrost base, resulting in compressive casing strains above the base and tensile strains below (Mitchel et al., 1978). The pore pressure loading also produces an inward lateral motion of the thawed-frozen interface. The inward motion, together with layers of different soil types, produce the alternating compressive and tensile strains (Mitchel et al., 1978).

3.8 Well Casing Insulation Techniques

Depending on the permafrost's mechanical behavior, special packer fluids only limit the thawing and subsidence around wellbore casing. Typically, nonfreezing un-gelled fluids such as alcohol, diesel oil, potassium chloride, and calcium chloride solution are used in casings (Mitchel et al., 1978). However, as seen with the BP well subsidence failure in 2017 with production time of twenty years or more the well casing may undergo stress due to slow thawing. In addition, cooling the flowing stream may cause hydrate plugging in gas wells and higher viscosity and pressure loss in oil wells. A problem that can arise with heavy oil recovery in shallow low temperature reservoirs.

One of the primary design flaws with using solid insulation in a permafrost zone is it needs to be dry and placed in a low-pressure environment (Mitchel et al., 1978). Contact with fluids such as thawing permafrost will degrade the thermal effectiveness of low density, solid foam systems. To combat this issue a double walled insulated casing design to seal in the insulation within the wellbore could be used. However, while this is effective in minimizing heat loss across a section of pipe, it loses its effectiveness at the coupling points. Additionally, this system experiences differential expansion between inner and outer casings, shifting the weight of each joint from the inner casing to the outer casing at the coupled points. As a result, failure happens at the joint from heat lose and strain on the well casing at the coupling joints.

Refrigeration and Heat Pipes Insulation can reduce heat loss and hence permafrost thaw, but cannot prevent it (Davies, 1979). Moreover, a major disadvantage of mechanical refrigeration compared to passive thermal protection methods such as insulation or heat pipes is the requirement for circulation and refrigeration equipment to be on location and maintained and could drive up the cost on an expensive EOR process making the production none economical.

3.9 Oil Recovery Methods

Oil companies today are focusing on maximizing the recovery factor (RF) from their oilfields as well as maintaining an economic oil rate. However, most of the sedimentary basins that might contain big conventional oil plays have already been realized. Resulting in the realization of any new discoveries will be small going forth in the future. Nonetheless, there are still vast volumes of unconventional hydrocarbons, such as the very viscous oils, oil shales, shale gas and gas hydrates that have yet to be exploited. Presently many of the technologies for exploiting these resources are energy intensive, expensive, in pilot testing or still undiscovered. Despite these obstacles, Enhanced Oil Recovery (EOR) methods in unconventional resource fields have represented a significant role in changing oil production in North America. For example, shale formations in the Bakken have 900 billion of recoverable oil in place (Alfarge et al., 2017). How much of the generated oil is recoverable remains to be determined; estimates range from 3% to 18% have been published (Lefever et al., 2006). To meet the future demand in energy throughout the world, the petroleum industry will need to look towards the difficult to recover resources in known reservoirs. In other words, to support the sustain demand for petroleum, the need for applying advanced Improved-Oil-Recovery (IOR) or EOR (tertiary recovery) technologies are going to be required. These tertiary recovery methods will fulfil a key role in meeting the energy demand for years to come. Traditionally, the major predominant methods used in EOR for heavy oils are: thermal recovery, gas injection and chemical flooding. EOR are the current methods that have been implemented in some heavy oil reservoirs and can be considered for the target formations in this study.

3.10 Thermal EOR

Traditionally there are only two thermal recovery methods for heavy oil: (1) a process with which heat is generated within the reservoir, (2) the process of injecting heat into a reservoir. Thermal recovery introduces heat to the reservoir to reduce the viscosity of the oil. Many countries to date including the United States have been extracting heavy oil for over the last forty years or longer utilizing these methods. The thermal recovery process reduces the viscosity by means of heat, while producing the force that increases flow rates of the oil to the production well. For example, the Kern River field, located near Bakersfield California, was discovered in 1899 at 43 ft below the surface with low initial reservoir temperature and pressure, resulting in low primary recovery. The field is ~6-miles-long and ~4-mile-wide consisting of heavy oil. The oil density had ~10° to ~15° API gravity with a viscosity of ~500 cp to ~10,000 cp, similar to that of the ANS (Curtis et al., 2002). Production peaked at just over 40,000 Barrels per day in the early 1900.

Poor reservoir performance and low demand caused production to decline to low levels until technological advancements were made in the mid-1950. This led to advancement in generating heat within the reservoir, downhole electrical heating. Electric downhole heating (EDH) systems were implemented to lower the viscosity of oil in the reservoir and increase the flow rates of crude and improve the oil recovery (Figure 15). For Example, the Kern field wellbore configuration consists of two zones: a high watt density zone installed in the producing zone and a cold lead extending to the surface. Furthermore, as technology advanced in the early 1960's, both Venezuela and California represented the first to apply steam (Figure 16) to the reservoir; thinning the oil and enhancing its ability to flow (Santos et al., 2013). Presently, thermal recovery currently accounts for more than 50% of applied EOR methods in the United

States and Venezuela (Santos et al., 2013). While these two methods are successful in various parts of the world, these methods will not work for the shallow reservoirs on ANS. The heat from these tertiary methods would melt the permafrost layers creating an unstable reservoir as well as instability on the surface.

3.11 Gas Injection

Gas injection used as a second or tertiary method of recovery involves injecting natural gas (nitrogen or carbon dioxide) into a reservoir. The gas can either expand and push gases through the reservoir or mixed with or dissolved within the oil, decreasing viscosity and increasing flow. Starting in the early 1970's CO_2-EOR was successfully used in Texas and New Mexico. Currently half of all EOR methods being employed today in North American unconventional fields are being done by some form of gas injection (Santos et al., 2013). Despite this method showing success, Deruiter et al (1994) demonstrated this method will not work on the West Sak reservoir. Their research looked at static equilibrium experiments measuring the solubilities of CO_2 injected into two types of oil, 18.5° API and 14.0° API gravity. Additionally, this study goes even farther to include measurements of viscosity, density, and miscibility of the two materials. The results show that CO_2 solubility increased with pressure for both API gravity oils up to the liquefaction pressure of CO_2 (~800 psi at 65°F), after which CO_2 solubility effects remain constant. Both oils exhibit an increase in phase density with increased CO_2 solubility. However, this density increase may be the result of an increase in total system pressure. Considering the slopes of the density curve does not appear to change at pressures greater than the pressure where CO_2 solubility plateaus. Furthermore, a slim-tube displacement was performed with pure CO_2 on the 18°API gravity oil at 2000 psi, (CO_2 at this pressure is in liquid phase), oil recovery was very low and CO_2 breakthrough behavior was indicative of an

immiscible displacement; not forming a homogeneous mixture with the oil (DeRuiter et al., 1994). This study concluded that CO_2 is found to have only limited solubility at pressures greater than that of CO_2 liquefaction pressure and was determined to be an ineffective recovery method on the ANS.

3.12 Chemical Flooding

Looking to the world for other possible successful EOR methods: chemical flooding (polymer flooding, alkali-polymer flooding, alkali-surfactant-polymer flooding) accounts for 76% of the recovered reserves out of all EOR methods used in China (Zhang et al., 2016). Chemical flooding encompasses the injection processes that use special chemical solutions as displacing fluid. These solutions are usually composed of alkaline, polymer, and surfactant (Donaldson et al., 1985). In chemical flooding, the oil recovery is enhanced either by an improvement in the performance of the injected water, such as by polymer addition, or by an increase in the displacement efficiency by means of the formation of surfactant micelles (Yang et al., 1991).

The injection of various chemicals, dilute solutions, can been used to aid mobility improvement and the reduction in interfacial tension. Injection of alkaline solutions into reservoirs with oil that contain organic acids naturally occurring will result in the production of soap. This can lower the interfacial tension enough to increase production (Temizel et al., 2018). For example, the use of sodium dioxide or sodium carbonate will react with the acid fractions from the heavy oil, producing in-situ surfactants (Cook et al., 1974). This natural occurring surfactant will reduce the oil to water interfacial tension (Campbell, 1981). Polymer flooding process is based on the injection of a water-soluble polymer consisting of high molecular weight compounds. These compounds promote an increase in the water viscosity, in turn, increase the

resistance to flow, improving the reservoir sweep efficiency in high permeability regions (Santos et al., 2013). Last, surfactant EOR represents the surface-active agents that reduce interfacial tension by modifying wettability, allowing oil to be pulled off rock surfaces easier. This diluted solution works by lowering the interfacial tension or capillary pressure that impedes oil droplets from moving through a reservoir (Santos et al., 2013).

3.13 History of Viscous Oil Development in ANS

The existence, on the ANS of two vastly large, shallow, heavy oil sands with a combined oil-in-place of over ~40 MMBO has been known since 1985. Both the Ugnu (8-12 API), at 2,000 to 3,000 ft subsea and the West Sak (16-22 API), from 3,300 to 5,500 ft subsea, sit under 1,200 to 1,800 ft of Permafrost. In the early 1980 the DS-1J area was selected for the location of the one of the first pilot project for extracting oil from the West Sak sands. A total of 15 vertical wells was drilled in a five-acre inverted nine-spot well pattern, using a waterflood EOR method with vertical wells in tight spacing. The pilot project operated for approximately two years producing 900,000 barrels of oil and proved that waterflooding could be used in the deeper portions of the reservoir (Targac et al., 2005).

More than a decade later from 1997 through 1998 a second attempt to develop the West Sak reservoir with vertical wells was made at DS-1D. This pilot test consisted of 18 vertical producer wells with 11 vertical water injectors. The key difference in this project was the vertical well spacing was wider at 40-acres intervals vs DS-1J's 5-acres spacing. Technology advancements since the first pilot test allowed producers to utilize more modern fracture stimulated completions and sand control methods for production. While this project produced marginal economic results, it was still valuable from the sense of information gained. The second oil recovery method waterflooding response matched up with DS-1D earlier pilot test,

particularly with production rates ranging from 100 to 400 BOPD (Targac et al., 2005). At this point in time it had become clear that it is not economically viable to continue with vertical production wells using water flooding.

Research during and prior to this time period in spite the attempts to development, already indicated that water flooding may not be the most successful for oil production improvement for heavy oil reservoirs. For example, Jin et al (1985) looked to waterflooding as a primary means of extraction in a reservoir, specifically what was happening to the formation. Analyzing long-term injection of cold water resulted in a temperature drop around an injection wellbore. After injecting water volume equivalent to 2.705-fold PV into the injection well, the reservoir temperature decreased by 6.7°C below the initial reservoir temperature (Jin et al., 1985). This bottom hole temperature drops are concerning when considering this tertiary method in shallow reservoirs on the ANS. This may be one of the primary reasons this method was not viable.

At year-end 2000, technology experienced advancements to where the use of horizontal multi-lateral production wells were starting to be used; allowing for two or more West Sak pay sands being accesses at a time (Figure 17). A total of 12 multi-lateral or single horizontal wells had been drilled on the ANS, including nine wells at Milne Point during this period. By year-end 2001, the combined number of multi-laterals wells had increased to 25, with sustained growth occurring every year in this core area (Figure 18).

3.14 Polymer Flood History

From 1997 to 2007 significant changes were made to the completion, design and production strategies regarding extraction from the West Sak heavy oil reservoir. Specifically, in 2003, where very long laterals where being drilled over 6,000 ft. This created reduction in

recovery per drill in terms of production cost per barrel of oil. In addition, changes also included sand exclusion to sand management, adding standard electrical submersible pump (ESP) to multi-lateral wells. Last, the EOR process evolved from waterflood to viscosity reducing water-alternating-gas (VRWAG) (Targac et al., 2005). Success for extracting West Sak viscous oil had been achieved with the use of (ESP). However, this success has only been achieved at the West Sak and Milne point core areas, where the reservoir sands are deeper by almost a 1,000 ft in comparison. It is important to emphasize this is not the entire field and does not include the shallower Ugnu reservoir. The core area only makes up approximately one-fourth of the field. The remaining field raises up as it travels south west from Milne point. Heavy oil extraction methods in the rest of the shallower reservoir will have to consider the permafrost.

From a technology standpoint, preliminary laboratory and simulation studies indicated that polymer flooding possesses potential in extracting heavy oil from the shallow portions of the ANS. Looking back in history, Sandiford (1964) was the first to release research regarding the reduction in mobility of water when small amounts of partially hydrolyzed polyacrylamide (HPAM) were included. Moving forward in history, the Daqing oil field located in the Songliao basin, with three commercial reservoir formations Saertu, Putaohua, and Gaotaizi are similar to the ANS. The Daqing reservoirs are made up of unconsolidated shallow sands at ~2,295 to 3,934 ft subsurface (Yusun et al., 1985). In Addition, these reservoirs have similar reservoir characteristics as the Ugnu and West Sak sands. For example, Both the ANS and Daqing Fields are terrestrial fluvial-delta deposit, mainly fining upward, multi-interval with shallow oil reservoir at low temperatures (Yusun et al., 1985). Since 1989 there has been thirteen successful field test that led to the development of 37 polymer flooding areas in Daqing. Furthermore, from

1996 the primary EOR method for the Daqing oil field is polymer flooding with water-cut dropping more than 20% or higher in most areas (Renquing, 2013).

The Chinese petroleum industry moved forward in the Daqing oil fields applying pilot test and new technology in the late 1980's and 1990's. In comparison to the ANS, the U.S. petroleum industry over the same period continued to apply conventional technology to an unconventional problem. For the U.S. petroleum industry this resulted in high development costs, significant logistical and environmental challenges, and low oil recovery (Dandekar et al., 2019). Furthermore, to date the United States still does not have any large-scale polymer flood projects going in any oil fields, despite that this EOR method has been tested and implemented in other countries; Canada and China (Dandekar et al., 2019).

August 2018, a pilot test was initiated on the ANS. (HPAM) polymer was injected with an initial goal to maintain an average concentration of 1,800 ppm over a 3-week period. Milne Point is the initial pilot test for the ANS, using two pre-existing pairs of horizontal injection and production wells in an isolated fault block of the Schrader Bluff heavy oil reservoir (Dandekar et al., 2019). The pilot test overall objective is to perform a successful field experiment that will validate the use of polymer flooding for extraction on the ANS. The field data and scientific knowledge that have been collected since the start of the injection indicate that the field pilot is performing as predicted (Dandekar et al., 2019). While the Dandekar et al (2019) study, acknowledge a concern for permafrost thawing, as one of many reasons to use polymer flooding over other types of EOR methods. The study did not address measuring permafrost from the beginning for a future comparison measurement in their pilot field test. In addition, the author does not mention future studies that may be needed to determine long-term effects on permafrost stability utilizing this tertiary method.

3.15 Framing the Problem

From a geological view, previous research has considered the Ugnu and West Sak geological characteristics and properties roughly at a certain range. For example, Werner (1987) describes both the Ugnu and West Sak sands from a geological broad approach which included the stratigraphic and structural framework in the Kuparuk River Unit. However, the study generalized the reservoir properties such as average permeability. Later, Panda et al (1989) research expanded further from well logs describing the West Sak reservoir to great lengths in two separate cross-sections. However, that study with two cross-sections which generalized the reservoir properties and characterization to the entire field still showed a homogenous reservoir.

Looking at the Milne point pilot test results should be of no surprise that polymer flooding is working as predicted in the lab. This method in other parts of the world with similar characteristics has shown to work; Canada for example. To date there are no heterogeneous numerical models illustrating how polymer flooding effects permafrost thawing or subsidence, when the reservoir separation from this zone is ~200 to 1000 ft. However, a prior study carried out by Wang et al (2019) regarding a homogeneous numerical model shows promise that subsidence is negligible when using in combination the following tertiary methods: water flooding and polymer flooding.

While previous studies are still relative in developing a geological model. In this research, a heterogeneous geological model was built, and then applied to an EOR numerical fluid flow model. The numerical model will consider the relationship between the following three factors: permafrost, Ugnu and West Sak intervals. Specifically, the shallow depths of these reservoir sands, along with temperature due to the proximity of the permafrost.

3.16 Framing the Question

Alaska is considered an isolated area that is expensive to develop in new oil exploration and production. As light oil is depleted in this area, future oil companies will want to extract the heavy oil to keep production up. Depending on when this companies start producing from these reservoir intervals will determine if the production can be economical and possible. To date there has never been production of heavy oil from Ugnu and West Sak intervals in the Kuparuk oil field. For economical purposes, these companies will need to start extracting this heavier oil and mix in the lighter currently existing oil for transportation to refineries. Assuming this is the case, today is the time to ask the following questions:

1. Is the data that exist regarding the Kuparuk oil field for the targeted intervals (literature, wireline logs, completion logs and core samples) complete enough to create a full field scale geological model specific to the Kuparuk oil field that includes the permafrost, West Sak and Ugnu reservoirs?
2. Can applying geological properties specific to a study area in the Kuparuk oil field show less permafrost subsidence in horizontal wells that Wang et al (2019) research using polymer injection.

This research study expanded upon Wang et al. (2019)'s paper and was limited to polymer flooding. To achieve our goal, a field scale geological model was built using Petra to expand the prior research from homogenous to a heterogenous model with the following properties: formation tops, porosity, permeability, water saturation and temperature. Additionally, polymer flooding effectiveness was analyzed as variables in relationship to the effects on permafrost subsidence using Computer Modeling Group (CMG) software.

3.17 Hypothesis

Three hypotheses were tested in the research proposal:

(1) If the temperature in the SW reservoir cross-sections is colder than the NE reservoirs cross-sections, then the permafrost temperature must influence both Ugnu and Wsak reservoirs in the SW section while the earth's interior heat is influencing the Ugnu and Wsak reservoirs in the NE section.

(2) By applying reservoir geological properties specific to the West Sak and Ugnu reservoirs in the Kuparuk Oil Field when compared to Wang et al. (2019) numerical simulated model, the specific reservoir properties will result in a further decrease in subsidence when using an EOR polymer flooding method.

(3) Horizontal wells have greater thawing of permafrost overall with less permafrost subsidence then vertical wells, when using an EOR polymer flooding method.

CHAPTER IV – METHODS

A geological field scale model was done using Petra, and then upscaled to the Computer Modeling Group (CMG) software applying numerical simulations involving polymer EOR methods. This study expands upon Werner (1987) who has one cross-section with limited geological properties (Figure 9). In additions, to this prior study Panda et al (1989) had two cross-sections illustrating limited reservoir properties for the West Sak Reservoir (Figure 11). The analysis is comprised of two goals that attempts to support all three hypotheses: 1) build a full field scale geological model specific to the Kuparuk oil field that encompasses unique geological properties to the permafrost, West Sak and Ugnu reservoirs, 2) apply the geological field scale model to a numerical simulation model to show permafrost sensitivity in various combination of polymer flood methods in vertical and horizontal wells that are sensitive to permafrost.

4.0 Geological Properties

To depict a heterogenous reservoir that includes the permafrost, Ugnu and West Sak reservoirs, the geological model accounts for six intervals. Well logs, core descriptions, and well completion reports were obtained from the Alaska Oil and Gas Conservation Commission (AOGCC). The objective was to exhibit the various geological properties for these six intervals such as the formation tops, temperature, porosity, water saturation, and permeability from the existing wells. Geomechanical properties were taken from prior studies with the exception of the elastic modulus of the permafrost. The research started out compiling data from 512 wells that include wireline logs, core reports, and completion logs that were most complete. These wells in the Kuparuk Oil Field were then reduced to 9 cross-sections containing 32 wells in total (Figure 19).

4.1 Formation Tops

Data collected was input into Petra to determine the depth of each interval in this study and creating nine cross-sections for the entire field. For the purpose of this research thesis, the Upper and Lower Ugnu sands were combined into one reservoir. Likewise, the upper and lower West Sak sands were combined into one reservoir. These intervals inside the reservoir sands was less than 100 ft to 300 ft thick and the geological property differences are marginal. Three separate sections of silt-clay-sand intervals separate the permafrost and both reservoirs.

4.2 Formation Temperature

Reservoir formation temperature is required to interpret electrical log outputs in the determination of the physical properties of reservoir fluid such as: resistivity of formation, water saturation, and permeability. The formation temperature (T_f) was estimated based on an

assumption of a linear temperature gradient between the bottom of the well, and the topographic surface using the following equation from Hartman et al (1999):

$$T_f = T_s + D_f \frac{BHT - T_s}{TD} \quad \text{.....(1)}$$

Where, T_s is the bottom of the permafrost set constant at 0 °C, D_f is the depth to the formation minus permafrost zone, BHT is the bottom hole temperature, and TD represents the total depth of well minus permafrost. Each well was independently calculated with each reservoir section averaged. The independent well averages were then applied to each appropriate cross-section, and then averaged again to represent the entirety of the cross-section.

The permafrost zone was done similarly as the lower intervals, with the exception of T_s with an average surface temperature -10.5 ° C taken form Lachenbruch et al (1987) study, BHT was set at 0 ° C, D_f represents the depth of the permafrost, and TD was considered the total depth of the permafrost. The permafrost temperatures were averaged for three independent depths (surface – 500 ft TVD, 501-1,000 ft TVD, and 1,000 ft TVD to bottom of permafrost) in each well.

4.3 Porosity of the Formation

One of the purposes of the study was to determine the formation porosity for the Ugnu, West Sak reservoirs and silt-sand-clay zones. Davis (1954) porosity equation used in his research, shown when calculating porosity from bulk density to have a mean error rate of ~ 3.0% in several classes of sediments. For purpose of establishing a heterogeneous model, the mean error rate of ~3$\pm$ is acceptable. Using Davis (1954) porosity equation:

$$\phi = \left[\frac{\rho_G - \rho_B}{\rho_G - \rho_L}\right] x\ 100 \quad \text{.....(2).}$$

Where, ϕ is the porosity, ρ_G represents the grain density for unconsolidated sand at 2.654 g/cm^3, ρ_B is the bulk density taken directly off the wireline log, ρ_L is the saturated fluid density constant at 1.05 cgm (Davis 1954). The porosity was calculated at half a foot interval for both reservoir sands in each of the 32 wells. Each reservoir was then isolated, and the porosity was then averaged for each of the Ugnu, West Sak reservoir and silt-sand-clay (stone) intervals.

4.4 Resistivity of Formation Water

Resistivity of formation water (R_w) is required to determine formation water saturation (S_w) and formation permeability (K) when lab data is unavailable. The most direct way of finding water resistivity (R_w) is to obtain a sample of the formation water and measure the resistivity. However, in this study this was not possible and required using an empirical approximation formula; spontaneous potential (SP) log data. To determine R_w this study employed Hartman et al (1999) using the following five steps: 1) estimate formation temperature from calculations, 2) convert R_{mf} to formation temperature, 3) Convert R_{mf} to R_{mfeq}, 4) read SP response and estimate R_{we}, and 5) convert R_{we} to R_w and NaCl at formation temperature (Appendix B, Figure 1B – 4B).

4.5 Water Saturation

Water saturation (S_w) is the ratio of water to pore volume and is needed to calculate an estimation of formation permeability (K). Archie's equation is the most widely used calculation when estimating the water saturation of reservoirs when core samples are not available. Archie (1941)'s equation that was used in this study is a combination of three equation derived down to the following:

$$Sw = (\Phi^{-m} * Rw/Rt)^{1/n} \quad \text{.....(3).}$$

Were, S_w is the water saturation, R_w is the resistivity of formation water, R_t is the estimated deep resistivity log, *m* is a factor related to porous medium (1.54 for unconsolidated sand) estimated from Jackson et al (1978), and *n* is an empirically derived saturation exponent, typically 2.00 for unconsolidated sandstone (Williams et al., 2008). Water saturation was calculated at half a foot interval for both reservoir sands in each of the 32 wells. Each reservoir was then isolated and averaged for each of the Ugnu, West Sak reservoir and silt-sand-clay intervals.

4.6 Permeability

The relationships between permeability, porosity and residual water saturation for unconsolidated reservoir sands enables permeability to be estimated when both porosity and residual water saturation is known (Timur, 1968). Timur used many different equations related to each other in his research. As a result, the parameters of $K = \phi^{4.4}/S^2_{wr}$ was the best general estimator of permeability (*K*) from measurements of ϕ and S_{wr} resulting in a standard error of 0.2937 when used in these types of formations. The following equation was used to calculate permeability (*K*):

$$K = 0.136 * \frac{\Phi^{4.4}}{S_{wr}^2} \quad \text{.....(4).}$$

Where, 0.136 and the exponent of 4.4 are correlation coefficient statistically determined in Timur (1968) study, ϕ is the porosity given from wireline logs, and S_{wr} was calculated. Permeability was calculated at half a foot interval for both reservoir sands in each of the 32 wells. Where ϕ was calculated using equation (2), and S_{wr} was calculated from equation (3). Each reservoir was then isolated and averaged for each of the Ugnu and West Sak reservoir segments and compared to Timur (1968) chart (Appendix C, Figure 1C) for comparison and verification.

4.7 Numerical Methods

Numerical reservoir simulation can be defined as the process of constructing a model that simulates the flow dynamics of an actual reservoir system. This includes for example, the subsurface porous, permeability, and other physical components. The unique geological model of the Ugnu and West Sak reservoirs in the Kuparuk oil field were integrated into the numerical model. These integrated properties included but are not limited to the following: reservoir temperature, oil viscosity, porosity, water saturation, and permeability. The geomechanical properties (Table 4) were taken from the Malik and Mount Elbert studies which were used in Wang et al. (2019) study (with exception of the Elastic Modulus in permafrost). Malik, Mount Elbert and Kuparuk reservoirs are all comprised of unconsolidated sands. Furthermore, these geomechanical properties have been adopted in prior reservoir studies on the ANS done by Rutquist et al (2009) and Maui et al (2005).

The STARS program in the Computer Model Group (CMG) software was selected as the numerical simulation tool. The CMG software uses a finite element method (FEM) which is a particular numerical method for solving partial differential equations. To solve a problem, the FEM subdivides a large system into smaller, simpler parts that are called finite elements. This is achieved by a particular space discretization in the space dimensions, which is implemented by the construction of a mesh of the object: the numerical domain for the solution, which has a finite number of points. The finite element method formulation of a boundary value problem finally results in a system of algebraic equations. The method approximates the unknown function over the domain. The simple equations that model these finite elements are then assembled into a larger system of equations that models the entire problem. The FEM then uses variational methods from the calculus of variations to approximate a solution by minimizing an associated

error function. Additionally, one of the primary mathematical equation used in the STARS program is the material-balance equation which is an expression of the conservation of mass in a reservoir.

The equation mathematically defines the different producing mechanisms and effectively relates the reservoir fluid and rock expansion to the subsequent fluid withdrawal. Material balance analysis is an interpretation method used to determine original fluids-in-place (OFIP) based on production and static pressure data. The general material balance equation relates the original oil and water in the reservoir to production volumes and current pressure conditions / fluid properties. The equation assumes a tank type behavior at any given datum depth - the reservoir is considered to have the same pressure and fluid properties at any location in the reservoir. The mass conservation equation for the polymer solution combined with Darcy's law results in the following transport equation:

$$\nabla \cdot \left(C_p T_w k(\nabla P_w - \gamma_w \nabla h)\right) + \nabla \left(\frac{\phi_p S_w D_e}{B_w}\right) \cdot \nabla C_p + q_w C_p = \frac{\partial}{\partial t}\left(\frac{\phi_p C_p S_w}{B_w} + \phi A_d\right) \ldots\ldots\ldots(5).$$

Where C_p the polymer concentration, T_w is the transmissibility for the water phase, P_w is the pressure of the water phase, Υ_w is the specific gravity of water, h is the height, ϕ_2 is the pore space accessible for the polymer solution, S_w is the water saturation, B_w is the formation volume factor for water, D_e is the effective dispersion coefficient for the polymer component in the water phase, q_w is the water injection rate and A_d is the adsorption/desorption coefficient.

4.8 Permafrost Elastic Modulus (E)

Permafrost is considered to be linear elastic material where the Elastic Modulus in permafrost is related to the permafrost thickness (Smith, 1971). Subsidence of thawed permafrost will be caused by the loss of the load-carrying capacity of the interstitial ice and/or the reduction of pore pressure (Smith, 1971). To account for permafrost thickness difference in each well an

Elastic Modulus mathematical model was used. Reasoning, subsidence of thawed permafrost will cause the loss of the load carrying capacity of the interstitial ice and/or the reduction in pore pressure and thickness contributes to these failures. For this reason, the Elastic Modulus will be calculated independently for each well using the following equation developed by Smith (1971):

$$Modulus\ of\ Elastic = (500 + Z) * 10^3\ lb/ft^2 \ldots\ldots\ldots\ldots\ldots\ldots\ (6)$$

where Z is the thickness of the permafrost in feet. The equation was derived by lab properties that were based on stress-strain data obtained from the thaw consolidation test done in Smith (2009) study.

4.9 Numerical Simulation Models

The numerical methods are made up of three different models that include: Full scale field model, study area-1 and study area-2 (Figure 20). Each of these reservoir simulations was developed using data from the geological field scale model done for the Kuparuk field that included the permafrost, Ugnu and West Sak sands. Reservoir rock properties such as average porosity, average permeability, water saturation, temperature, well locations and intervals depths are all shown in Table 5.

To simulate the oil field production as close as possible the model was set up to mimic the true start dates of oil production in this field. The numerical model is designed to match when the original vertical wells that are deeper in the Kuparuk reservoir to start injecting and producing January 1st, 1984 and shut down January 1st, 1996. The experimental vertical and horizontal wells for cases 1-11 all start injection and production January 1st, 2021 and end on January 1st 2040.

4.10 Overview of Simulation Models Initial Set Up

Full Scale Model. In this study the full-scale model is set up using 300 x 300 x 7 = 630,000 grid blocks representing a 20.6 x 21.7-mile surface area. Where an individual block in the I-direction is 364.4 ft, Y-direction is 380.9 ft and the Z-direction is variable and is dependent on the depth of the nearest well for a specific interval that was imported into a mesh grid from PETRA representing a total depth of 6,578 ft TVD (Figure 21).

Study Area -1. This model is set up using 150 x 100 x 7 = 105,000 grids blocks. representing 4.2-mile-long by 1.5-mile-wide surface area (Figure 22). Where the individual block in the I-direction is 146.9 ft, Y-direction is 80.6 ft and the Z-direction is variable and is dependent on the depth of the nearest well for a specific interval that was imported into a mesh grid from PETRA representing a depth of ~ 6,104 ft TVD. The wells for this study were set up in both the West Sak and Ugnu reservoirs. Cases 1-5 were two horizontal wells placed in the West Sak reservoir at a length of 5,000 ft with a spacing between the injector and producer at 560 ft. Case-6, two vertical wells were used at 480 ft spacing and perforated in the West Sak reservoir interval. Cases 7-8, were two horizontal wells placed in the Ugnu reservoir at a length of 5,000 ft with a spacing between the injector and producer at 560 ft.

Study Area-2. The deeper section of the two study areas. This model is 150 x 150 x 7 = 157,500 grids representing 3.2-mile-long by 4.0-mile-wide surface area. Individual grid block dimensions are in the I-direction 112.3 ft, Y-direction 134.4 ft and in the Z-direction variable with a depth of ~6,504 (Figure 23). The wells for this study were set up in the West Sak reservoir only. Cases 9-11 were two horizontal wells placed in the West Sak reservoir at a length of 5,000 ft with a spacing between the injector and producer at 584 ft.

4.11 Simulation Experiments

There were eleven simulation case studies between study area-1 and study area-2 that include the following: well geometry, well type, location, perforation interval, polymer concentration, and calculated Elastic Modulus below is a detail break down (Table 6 & 7).

Study area-1, Cases 1-8 West Sak Reservoir. Eight individual simulation models were done to capture the differences in temperature and subsidence from a production wells over a twenty-year period.

- Cases-1 is a horizontal well, (1 injector and 1 producer, at 560ft spacing) that were perforated in the West Sak reservoir at 5,000 ft in length. This case was done using waterflooding where measurements for permafrost temperature and subsidence was taken from one specific block on the surface where the production well rises out of the subsurface.
- Cases 2-5 were done using horizontal wells, (1 injector and 1 producer, at 560 ft spacing) perforated in the West Sak reservoir at 5,000 ft in length. These cases were done using polymer flooding (1,000ppm, 1,800ppm, 2,150ppm and 2,500ppm) where measurements were taken from one specific block on the surface where the production well rises out of the subsurface.
- Case-6 was done using vertical wells (1 injector well and 1 production well, at 584 ft spacing) perforated in the West Sak reservoir. This case was done using polymer concentration at 1,000 ppm, where measurements were taken from one specific block on the surface where the production well rises out of the subsurface.
- Case-7 was done using horizontal wells (1 injector well and 1 production well) perforations in the Ugnu reservoir at 5,000 ft in length with waterflooding.

- Case-8 was done using horizontal wells (1 injector well and 1 production well) perforated in the Ugnu reservoir at 5,000 ft lateral length, injected with 1,800 ppm polymer concentration.

Study area-2, Cases 9-11. Three simulation were done to capture the difference between these cases, Wang et al. (2019) study and the southwestern West Sak reservoir with relationship to the permafrost temperature and subsidence differences. Wang et al. (2019), the initial grid cells were set up to illustrate the area of the model. For comparison, in Wang et al (2019) study the grid cells were set up at 51 x 31 x 18 = 28,454 grids representing a 3-mile-long by 1-mile-long wide surface with a depth of 4,930 ft.

- Case-9 was done using horizontal wells (1 injector well and 1 production well, spacing at 50 ft) perforated in the West Sak reservoir at 5,000 ft lateral length, waterflood injection.
- Cases 10-11 were done using horizontal wells, (1 injector and 1 producer, at 560 ft spacing) perforated in the West Sak reservoir at 5,000 ft in length. These cases were done using polymer flooding (1,800ppm and 2,500ppm) where measurements were taken from one specific block on the surface where the production well rises out of the subsurface.

CHAPTER V - RESULTS AND ANALYSIS

The main objectives are to determine if the hypothesis is testable to answer the following questions regarding permafrost subsidence in the Kuparuk oil field on the Alaska North Slope:

1. Is the data that exist today regarding the Kuparuk oil field for the targeted intervals (literature, wireline logs, completion logs and core samples) complete enough to create a full field scale geological model specific to the Kuparuk oil field that includes the permafrost, West Sak and Ugnu reservoirs?

2. Can applying geological properties specific to a study area in the Kuparuk oil field show less permafrost subsidence in horizontals wells than Wang et al (2019) using polymer?

This study started out with 512 wells that were reduced to 32 wells that make up 9 cross-sections built using Petra software that resulted in unique geological properties. These unique geological properties included: permafrost depth, formation tops, porosity, temperature, water saturation, and permeability for the Kuparuk oil field (Table 5). The results allow for a more accurate interpretation of the reservoir field when applying these properties to a numerical simulation model for fluid flow.

5.1 Permafrost and Reservoir Tops

Majority of the wells that were drilled in the Kuparuk River Unit were for the intention of producing oil from the deeper and lighter oil in the Kuparuk sands. The targeted research reservoir is the Ugnu and West Sak sands located between ~2,200 ft to ~4,000 ft subsurface. The bottom of the permafrost zone (Figure 24) along with the tops Ugnu and West Sak sands were determined by correlating data between wireline logs, well completions reports from AOGCC and research results from Collette et al. (1983). Cutting through the middle of the field with a cross-section JJ-JJ' (Figure 25) results indicate the permafrost, West Sak and Ugnu reservoirs are shallower in the southwest area versus the northeast area. Moreover, Table 7 shows the results of individual well depths for the permafrost, Ugnu and Wsak reservoir tops. The table is laid out from the top down approach representing the Northeast section to the southwest section of the field.

Specifically, the results indicate that the permafrost decreases in depth by ~200 to ~300 ft TVD traveling from the northeast section to the southwest section of the field. This make sense

and may be supported by Lachenbruch et al (1987) study where the increase in the thermal conductivity acts as an insulator from the Earth's interior heat. Additionally, looking at (Figure 26) the permafrost cross-section (JJ-JJ') shows variations in the permafrost thicknesses (spikes). This may indicate the presence of areas that have an active layer that includes taliks that may extend into the permafrost (Figure 27). A talik is a layer of unfrozen ground that lies between the permafrost and active layer such as the underlying silt zone in this study above the Ugnu reservoir (Connon et al., 2018).

The measured depth to the top of the Ugnu sands can be seen in all the cross sections residing with ~200 to ~600 ft from the bottom of the permafrost. Additionally, a structural contour map was done of the entire field showing ~1,595 ft TVD in the southwest to ~2,694 ft TVD in the northeast following the same depth profile as the permafrost (Figure 28). Additionally, the reservoir intervals of Ugnu, the lower and upper sand intervals were measured as one sand unit in this research. Because to the author's knowledge there are no existing studies to date that have isolated the specific net pay area of the Ugnu reservoir. An Isopach map was done (Figure 29) for the Ugnu reservoir showing a thickness of ~220 ft in the southwest versus ~370 ft in the section. This may support the deeper permafrost thickness that Lachenbruch (1970) research found that contributed to the differences between the proportion of siliceous sediments in the stratigraphic column.

The measured depth to the top of the West Sak sands can be seen in the cross-sections residing with a ~600 ft in the southwest section to ~1,400 ft from the bottom of the permafrost (Figure 27). Additionally, a structural contour map was done using Petra of the entire field showing ~2,140 ft TVD in the southern vs ~3,180 ft TVD in the northeastern section (Figure 30). Panda et al. (1989) prior study split the West Sak sands into two separate intervals: upper sands

and lower sands with four subintervals of sand 1-4. Panda et al. (1989) study appears to be more detailed with a smaller area with core samples that allowed them to detail the net pay thickness. This study combined the sand intervals into one reservoir for two reasons: 1) this research did not have access to core sample lab work beyond literature available; 2) the geological properties through the sand intervals are consistent from top to bottom in the reservoir sands both in literature and from wireline logs. An Isopach map was done (Figure 31) for the Ugnu reservoir showing a thickness of ~220 ft in the southwest versus ~370 ft in the section.

5.2 Formation Temperature

To measure formation temperature through a borehole requires that borehole to be undisturbed for an extended period after the drilling has taken place (Lachenbruch et al., 1982). However, for the purpose of this study the bottom whole temperatures used were taken from the well completion logs representing an estimation of formation temperatures. Previous studies frequently have one specific temperature that represents the entire reservoir. For example, Targac et al (2005) represents the core area of the West Sak reservoir to be 23.9° C. The West Sak reservoir depth to this area ranges from 5,000 ft to 6,000 ft TVD with a subsurface permafrost separation of 1,700 ft to 2,000 ft. Additionally, prior research Werner (1987) and Panda et al. (1989) have taken generalized values such as a specific values of one area in Kuparuk field and generalized them for the entire field. To measure permafrost potential instabilities in temperature and subsidence it may not be entirely correct to use unique geological properties: porosity, water saturation, temperature, permeability, permafrost thickness, and reservoir depths outside the Kuparuk field for this type of study.

There are not any studies to date that have analyzed and calculated both the Ugnu and West Sak reservoir temperature across the entire reservoir. Both Collett et al (1993) and

Lachenbruch et al (1982) have studied permafrost temperatures. However, neither study has provided temperatures for the Ugnu and West Sak reservoirs in the Kuparuk field. The temperature calculation results in this study (Table 9) show a trend that may be correlated to the average surface temperature and permafrost depth as well as Earth's interior. The Ugnu formation ranges from approximately 14.8°C in the northeast area to 4.3°C in the southwest area of the reservoir (Figure 32). Similarly, the West Sak reservoir ranges approximately 24.8°C in the northeast area to 15.6°C in the southwest area (Figure 33).

Permafrost ranges from 1,400 ft thick to 1,700 ft thick TVD in some areas and can cause difficulties in developing a heterogenous geothermal interpretation. In considering the geothermal aspects of subsequent models, the permafrost temperature was calculated for each well and averaged. The results indicate no difference in borehole temperature averages from one section of the field to the next (Table 10). The surface temperature across the entire field is steady at -10.5 °C and the calculated temperature gradient to the bottom of the permafrost is consistent completion reports and Lachenbruch et al (1982) study.

5.3 Porosity

Prior research has covered the Ugnu and West Sak intervals from a broad representation of the geological parameters. For example, Werner (1987) generalized that the West Sak sand had a typical porosity ranging from 25 to 35 percent and Ugnu ranged from 30 to 35 percent. Furthermore, Panda et al (1989) research reported the water saturation from the West Sak sands from 13 wells. While these porosities are close in nature, they fail to cover the entire West Sak and Ugnu reservoir. The results from the porosity calculations in this research considered six intervals that included: the permafrost, Ugnu reservoir, West Sak reservoir, and the silt/clay/sand (stone) layers. The Ugnu reservoir cross-section averages range from 33.0% to 35.0%, no north

to south trend. Additionally, the porosity cross-section averages for the West Sak reservoir are a bit lower and range from 31.5 in the northeast section to 27.0% in the southwest section (Table 5). However, the last cross-section (H) was missing the wireline log for these specific reservoirs. Silt layer 1 cross-section averages ranges were 39.0% to 32.0% with no observation trend. Silt layer 2 were a bit lower in range from 32.3% to 27.5% in cross-sectional averages. The deeper silt layer cross-section averages were 30.0% to 29.7% with no observational trend.

5.4 Water Saturation

Panda et al (1989) is the closest research that has captured a comprehensive set of geological parameters for the West Sak reservoir. In this previous study water saturation was calculated for two cross-sections that included 13 wells. Nonetheless, this analysis lacks covering the entire Ugnu and West Sak reservoir. Similarly, porosity computations for water saturation were calculated for the following six layers: Permafrost, Ugnu reservoir, West Sak reservoir and the three siltstone-claystone-sandstone layers that are between these reservoirs. The results indicate an increasing trend in the cross-section averages from the northeast area to the southwest area (Table 5). Ugnu reservoir cross-section (A) 25.0% versus the cross section (F) at 32.7%. However, the West Sak sands demonstrate the opposite in the cross-section water saturation with a decreasing trend. Cross-section (A) averages 34.5% and cross-section (F) averages 28.7%. In the silt zones the cross-sectional average in each cross-section decrease with depth with minor trend from the northeast to the southwest areas.

5.6 Permeability

Werner (1987) found permeabilities in the Ugnu reservoirs ranging from 200 to 3,000 md and the West Sak sand ranging from 10 to 800 mD. This broad view of permeability is not adequate to build a heterogenous numerical fluid flow model. The result of this research shows

permeability cross-sectional averages indicate a northeast to southwest decreasing trend (Table 5). The Ugnu sands section (A) cross-section average is 879 mD versus section (F) cross-section average8 of 682 mD. Similarly, the West Sak sands section (A) cross-section average is 684 mD versus section (F) cross-section average of 337 mD. The siltstone layers between the permafrost, Ugnu sands and the West Sak sands show an overall decrease in permeability with increased depth.

6.0 Numerical Models Horizontal Wells

The numerical results include 11 Cases that cover both the shallow southwest area (study-1) and the deeper northeast area (study-2). Study-1 includes the following (Case 1-5) horizontal wells which includes one water flood case and four polymer simulations. Case-6 includes a simulation using polymer in a vertical well. Additionally, Case 7-8 include one water flood and one polymer simulation in the Ugnu reservoir. Study-2 includes the following (Case 9-11) horizontal wells which includes one water flood case and two polymer simulation. The results of the simulation measuring permafrost subsidence and temperature change from form Jan 1, 2021 through Jan 1, 2040 can be found (Table 12).

6.1 Horizontal Wells Development Southwest Area West Sak

The horizontal well lengths were 5,000 ft and spaced 550 ft apart in the West Sak reservoir layer 5 (Cases 1-5). The simulation results for Case-1 (water flood) the subsidence average was (-8.52e-09 ft per year), and (-1.99e-07 ft per 20-year period) (Figure 34). Additionally, the results water flooding over the 20-year period predicted the most subsidence among Cases 1-6. Furthermore, when looking at the results just in the horizontal wells, polymer concentrations at 1,000 ppm Case-2 (horizontal well) had the largest subsidence (-1.15e-07 ft per year), for a total of (-9.24e-08 ft per 20-year period). Moreover, Case-5 (horizontal well) when

using polymer concentration at 2,500 ppm had the least amount of subsidence (-1.28e-07 ft per year) for a total of (-7.93e-08 ft per 20-year period).

Temperatures for the West Sak reservoir interval 5 (Cases 1-5, horizontal wells) indicate that the permafrost shows no significant impact from polymer injection with either models (Figures 35). However, there were small difference in temperature trends between water flooding (Case-1) and the horizontals wells (Case 2-5) in the permafrost. While both methods (waterflooding and polymer flooding) show a decrease in temperature near the production well at the permafrost surface when comparing the two. However, when using polymer injection, the temperature decrease was greater than the watering flooding temperature over a 20-year period. Specifically, the water flood method decreased the temperature in the permafrost by -1.3e-03 °F per year for a total decrease of -2.53e-02 °F over a 20-year period. In comparison, polymer in the horizontal's wells (Cases 2-5) all have a similar steep decreasing temperature change of ~ -2.43e-03 °F per year regardless of concentration.

6.2 Vertical Wells Development Southwest Area West Sak

In the vertical well development studies (Case-6), the producer and injector wells were perforated in interval 5 the West Sak reservoir spaced at 584 ft apart. The vertical simulation was only done using polymer concentration of 1,000 ppm. Reasoning, prior research shows that vertical wells are not sufficient in heavy oil extraction in this region. The results indicate that subsidence is minimal with an average of (-3.44e-07 ft per year), and (-8.37e-08 ft per 20-year period) of subsidence (Figure 34). Additionally, as mentioned in previous results Cases 1-5 over the 20-year period created the most subsidence among all the simulated studies including the vertical well (Case-6).

Temperatures for the West Sak reservoir interval 5 (Cases 6, vertical) indicate that permafrost shows no significant impact from 1,000 ppm polymer injection (Figures 35). However, there was a small difference in temperature trends between horizontal and vertical wells. While both methods show a decrease in temperature the vertical model has a very steep slope (decrease in temperature) at a small scale. Specifically, a decrease in temperature of -3.19e-03 °F per year for a total decrease of -6.39e-02 °F over a 20-year period.

In comparison, the vertical wells in this study appeared to show very little vertical subsidence effecting the permafrost. However, in Wang et al. (2019) research the vertical well had increased in temperature and showed an increase in subsidence. The answer between these two results may be supported by an earlier study done by Jin et al. (1985). This prior research analyzed long-term injection of cold water into vertical wells. Which resulted in a temperature drop around an injection wellbore. After injecting water volume equivalent to 2.705-fold pore volume of injection (PV) into the injection well, the reservoir temperature decreased by 6.7°C below the initial reservoir temperature (Jin et al., 1985). So, why does this not happen in a horizontal well as dramatically? The possible reason for the dramatic decrease in reservoir temperature is that the area around the well is less than that of horizontal wells. In turn, the polymer injection does not have enough time to reach a steady state between the water/polymer mix and the reservoir temperature. Whereas, a horizontal well may be a mile long reducing the temperature of the mixture the farther out it travels horizontally from the surface injection entry and production exit points.

6.3 Horizontal Wells Development Southwest Area Ugnu

In the horizontal well development studies, the two horizontal wells were 5,000 ft in length spaced 550 ft apart in the Ugnu reservoir layer 3 (Cases 7-8). The results for Case-7

(water flood) the subsidence average was (-2.4e-08 ft per year), and (-4.77e-07 ft per 20-year period) (Figure 36). Additionally, in some areas of the model the permafrost was only 300 ft above the reservoir. Furthermore, when looking at the results just in the horizontal wells when injecting polymer concentrations at 1,800 ppm Case-7 (horizontal well) had the least amount of subsidence between the two cases at (-6.0e-09 ft per year), for a total of (-6.35e-08 ft per 20-year period).

Temperatures for the permafrost from injecting and producing from the Ugnu reservoir horizontal wells (Case-8) indicate that the permafrost shows no significant impact from polymer injection at 1,800 ppm (Figures 37). However, there was a small difference in temperature trends between water flooding (Case-7) and the horizontals wells (Case-8). Specifically, water flooding increased the temperature by 3.46e-03 °F per year for a total decrease of 6.92e-02 °F over the 20-year period. Additionally, polymer in the horizontal's wells (Cases 8) results show a decrease in temperature of -1.46e-03 °F per year for a total decrease of -2.91e-02 °F over the 20-year period.

6.4 Horizontal Wells Development Northeast Area West Sak

In the horizontal well development studies, the two horizontal wells were 5,000 ft in length spaced 600 ft apart in the West Sak reservoir layer 5 (Cases 9-11). The results for Case-9 (water flood) the subsidence average was (-1.3e-08 ft per year), and (-2.78e-07 ft per 20-year period) (Figure 38). Case-10 used the same set up as the water flood with the exception that it was now using a polymer concentration of 1,800 ppm in the injection. The results show an increase in subsidence over water flooding of (-8.0e-08 ft per year), and (-1.65e-07 ft per a 20-year period). Case-11 was a duplication of the experiment with the exception of using a 2,500-ppm polymer concentration in the injection at (-6.0e-08 ft per year), and (-1.20e-07 ft per 20-year period). The results show a decrease in subsidence when using the 2,500 ppm versus 1,800-ppm

polymer concentration. Additionally, for all three cases the difference between the bottom of the permafrost zone and the reservoir was ~1700 ft. Furthermore, when looking at the results just in the horizontal wells when injecting polymer concentrations at 1,800 and 2,500 ppm, Case-9 (water flooding) had the least amount of subsidence between the three cases.

Temperatures for the permafrost from injecting and producing from the northeast West Sak reservoir horizontal wells (Case-10 & 11) indicate that the permafrost shows no significant impact from polymer injection at 1,800 ppm or 2,500 ppm (Figures 39). However, there was a small increase in temperature in all the cases with water flooding leading. Furthermore, when comparing the two polymer injection cases with water flooding, Case-11 temperature increased the least over a 20-year period. Specifically looking at individual cases, water flooding increased the temperature by 2.2e-04 °F per year for a total increase of 4.6e-03 °F over the 20-year period. Additionally, polymer in the horizontal's wells (Cases 10) results show an increase in temperature of 1.8e-04 °F per year for a total increase of 3.8e-03 °F over the 20-year period. Last, Case-11 temperature increased by 1.7e-04 °F per year for a total increase of 3.7e-3 °F over the 20-year period.

6.5 Prior Study Comparison

Wang et al. (2019) did three comparison models using different polymer concentration: 1,800, 2,150 and 2,500 ppm. Comparing this study with Wangs et al. (2019) previous research, the reservoir in this study was similar in distance at 1,700 ft in comparison to Wang et al. (2019) 1,640 ft. Furthermore, there were substantial difference between result outcomes between the two studies. For example, in Wang et al. (2019) study a horizontal well using 1,800-ppm polymer concentration resulted in total vertical subsidence of ~0.62 ft, compared to this studies Case-10 results at (-8.0e-08 ft per year), and (-1.65e-07 ft per a 20-year period). Additionally,

Wang et al. (2019) horizontal models using 1,800 polymer concentration had a 1.78°F increase in the permafrost temperature over a 20-year period compared to this study at 1.8e-04 °F per year for a total increase of 3.8e-03 °F. While Wang et al. (2019) may have had more intervals (18) built into the model compared to six in this study. It is possible that the heterogeneous aspect of the prior research was lost in using the general geological properties taken from Prudhoe Bay studies. Meaning, the number of layers does not necessarily determine if a model is heterogeneous. Furthermore, the small differences in cell size between this study and Wang et al. (2019) study may have contributed to these differences. Further research applying core sample measurements from lab experiments may provide better accuracy and verification.

In looking at Wang et al. (2019) research in comparing an 18-layer model to a geological heterogeneous 6-layer model. This study does support Wang et al. (2019) final conclusion assumptions that higher polymer concentration does not necessarily lead to increased subsidence. While this study supports that assumption, Wang et al. (2019) results were considerable larger in value than the results in this study. Which model may be closer to what reality is? There are three major differences between the models: number of intervals layers used, differences in geological properties, and difference in permafrost to reservoir separation. It may be argued that the 18 intervals with geological properties from an adjoining field reduces the accuracy of Wang et al. (2019) results. In Wang et al. (2019) prior study the geological properties are less than 10 miles away. In analyzing Wang et al. (2019) prior research and this study, two assumptions come to mind for the differences in temperature and subsidence outcomes between the studies. First, the closer and colder the reservoir is the more influence it has on permafrost subsidence. Second, the deeper and warmer the reservoir is the more influence it has on permafrost subsidence. While

this is true in the bigger picture, there are some finite difference that may account for the different assumptions.

This study shows the possible differences between geological properties unique to the Kuparuk Field versus from Prudhoe Bay. There are a few factors that support using a heterogeneous geological model unique to a specific location:

1) Regardless of which polymer concentration was used the subsidence was considerable smaller in this study.
2) When using any of the two polymer concentrations in the northeast area-2 in this study the temperature increased with very little differences between case-10 and 11, indicating polymer concentration does not impact the permafrost stability.
3) It is plausible that the only differences between this study and Wang et al. (2019) research is in the heterogeneous geological model versus the adjoining field geological properties.
4) It may be as simple as the temperature difference in the West Sak reservoir between studies. In Wang et al. (2019) the oil reservoir was at 70° F compared to this study area-2 at 66.7° F on average.

When using the same heterogeneous geological properties, reducing the distance between the permafrost and the reservoir to ~ 300 to 600 ft, the temperature and subsidence increased. This indicates possibly that the ranges of polymer concentrations used in both of these studies in the West Sack reservoir does not impacted substantially the temperature or subsidence over a 20-year period. Furthermore, in analyzing the Ugnu (Case-8) the only difference between this model and the West Sak model was the reduction in the separation between the reservoir and the permafrost. The same field, well separation, and geological properties were used. This may

indicate that the proximity of the permafrost to the reservoir is reduced to 300 to 600 ft the temperature of the permafrost influences the polymer injection fluid. This resulted in a decrease in temperature to the permafrost. Furthermore, it is plausible at deeper sections of the reservoir such as Wang et al. 2019 study and Cases-11 &12 in this research that the warmer reservoir influences the fluid temperature resulting in increased permafrost subsidence and temperature not necessarily the polymer concentration itself based on the increased travel time through the reservoir over water flood method.

CHAPTER VI – CONCLUSION

As the United States works towards replacing carbon energy with renewable energy resources in the next fifty to sixty years, oil extraction using conventional methods during this period is running out. Revisiting these mature fields with previous research methods and knowledge is useful for designing a homogeneous model for a conventional field. However, unconventional fields require the use of Enhance Oil Recovery methods that require more specific and less generalized geological models for application in numerical simulated fluid models. When considering an area that has subdivision of active layers, permafrost, siltstone-claystone-sandstone, and unconsolidated sands, applying a unique geological model to a specific location that is intended for production should be considered for permafrost sensitivity.

The cross-section JJ-JJ' (Figure 25) shows the Ugnu and West Sak reservoirs are deeper and thicker in the northeast section versus the southwest section. The permafrost is also slightly deeper in the northeast section compared to the southwest section. However, the mean surface temperature has little impact on the northeastern section in comparison to the southwest section. This study supports the first hypothesis that the temperatures of the Ugnu and West Sak reservoir can be influence by three factors: the mean annual surface temperature, the Earths' interior

geothermal gradient and siliceous sediments. Specifically, drawing upon Lachenbruch (1970) research regarding proportion of siliceous sediments in the stratigraphic column. The shallow end of the reservoir while closer to the surface should be impacted more by the mean surface temperature and have deeper permafrost. While the permafrost on northeastern deeper impacted by the mean surface temperature should be similar in thickness. However, this is not the case, the thickness of the permafrost is thicker in northeast sections of the Kuparuk field. This concludes the following is happening in the Kuparuk field, an increase in conductivity with a decrease in geothermal gradient when traveling from the south western to the north eastern section. This is a result of thicker siliceous sediments restricting heat flow from the earths' interior.

Case-11 and 12 in the deeper section of the field do support the hypothesis by applying a unique geological model. These two cases do support less subsidence in comparison to Wang et al (2019) research study. Furthermore, there appears to be very little differences in subsidence between the polymer concentration when applied to the West Sack reservoir on the southwest section. This may be a result of the reservoir temperature influencing the polymer temperature. For example, the difference in temperature between the reservoir and the permafrost in the southwest section is 30°F. Whereas, the northeast section the difference between the reservoir and permafrost is 70°F.

This study looked to collaborate Wang et al (2019) study in showing that horizontal wells will have greater permafrost thawing then vertical wells at a limited distance from the injector well. However, greater overall subsidence using the horizontal versus vertical wells over time was observed and did not support the hypothesis.

An interesting result took place looking at cases 1-8 in Study area-1, the results showed a decrease in permafrost temperature regardless in which method was used. Traditionally, it can be

argued that the surface temperature of a fluid being injected into the Earth's interior will not continue decreasing in temperature and reduce the surface temperature of the permafrost once entering and exiting the production well. However, there are no studies to date that look at shallow reservoir polymer injection at -10.5° F to 32° F with injectors and producer well lengths at +5,000 ft. This result will require future lab studies and follow up to validate these results. However, a start in looking into these results and future work will take into consideration an earlier study done by Jin et al. (1985). This prior research analyzed long-term injection of cold water into vertical wells in cold regions. Which resulted in a temperature drop around an injection wellbore. After injecting water volume equivalent to 2.705-fold pore volume of injection (PV) into the injection well, the reservoir temperature decreased by 6.7°C below the initial reservoir temperature (Jin et al., 1985). Future research should replicate this study analyzing the West Sak and Ugnu reservoirs sand from a core laboratory to verify the geological properties that were calculated in this study. This would collaborate the effects polymer concentration has on permafrost in relationship to subsidence and temperature change. Furthermore, to increase heterogeneity in the reservoir sands, the one intervals layer in both West Sak and Ugnu should be increased to represent the actual reservoir characteristics of four individual layers.

REFERENCES

Abraham, J., 2011. “A Promising Tool for Subsurface Permafrost Mapping: An Application of Airborne Geophysics from the Yukon River Basin, Alaska. USGS, Fact Sheet 2011-3133.

Alfarge, D., Wei, M., Bai B., 2017. "IOR methods in unconventional reservoirs of North America: comprehensive review." In SPE Western Regional Meeting. Society of Petroleum Engineers.

API 1980: API Manual of Petroleum Measurements Standards, Chapter 11.1-Vol XI/XII, adjunct to ASTM D1250-80 and IP 200/80.

Amendt, D., Busetti, S., and Wenning Q., 2013. "Mechanical characterization in unconventional reservoirs: a facies-based methodology." Petrophysics 54, no. 05, 457-464.

ANDMIR, 2020. “Downhole Electric Heater – ADDHEAT^{TM}, http://www.andmir.com/downhole-electric-heater.

Bailey, A., 2017. “BP reports spill cause, shuts in 14 Prudhoe Bay wells pending a risk analysis for problem well design. Petroleum news vol. 22, no 30.

Bird, K.J. and Houseknecht, D.W., 2002. US Geological Survey 2002 petroleum resource assessment of the National Petroleum Reserve in Alaska (NPRA): Play maps and technically recoverable resource estimates. US Department of the Interior, US Geological Survey.

Bockheim J. G., Walker, A., Everett, L.R., 2018: Soil carbon distribution in nonacidic and acidic tundra of Artic Alaska. In Soil processes and carbon cycle, pp 143-155.

Brownbag, L., 2011: Heavy oil vs. Light Oil, www.aoga.org/wp-content/uploads/2011/03/HRES-3.10.11-Lunch-Learn_BP-Heavy oil.pdf.

Campbell, T. C., 1981: "The role of alkaline chemicals in oil displacement mechanisms." In Surface Phenomena in Enhanced Oil Recovery, pp. 293-306. Springer, Boston, MA.

Carman, J.G., Hardwick, P., 1983. Geology and Regional Setting of Kuparuk Oil Field, Alaska, The AAPG Bulletin, v. 67, no. 6 p. 1014-1031.

Chmielowski, J., 2013: BP Alaska Heavy Oil Production from the Ugnu Fluvial Deltaic Reservoir, Monterey, California, AAPG, SEG and SEPM Joint Technical Conference, 19 April 2013.

Climatenexus, 2020. “Alaska: Climate Change Ground Zero”, https://climatenexus.org/climate-change-news/alaska-climate-change-ground-zero/.

Collett, T. S., Myung W. L., Agena, F. W., Miller, J. J., Lewis, A. L., Zyrianova, V. M., Boswell, R., Inks, L. T., 2011: Permafrost-associated natural gas hydrate occurrences on the Alaska North Slope, Marine and Petroleum Geology 28, no 2, pp 278-294.

Connon, R., Devoie, É., Hayashi, M., Veness, T. and Quinton, W., 2018. The influence of shallow taliks on permafrost thaw and active layer dynamics in subarctic Canada. Journal of Geophysical Research: Earth Surface, 123(2), pp.281-297.

Cooke Jr, C. E., Williams E. R., Kolodzie A. P., 1974. "Oil recovery by alkaline waterflooding." Journal of petroleum technology 26, no. 12, 1-365.

Couch, E.J., Keller, H.H., Watts, J.W., 1970: Permafrost Thawing Around Producing Oil Wells, Technology, Montreal, Canada, April-June 1970.

Dandekar, A., Bai, B., Bames, J., Cercone, D., Cifermo, J., Ning, S., Seright, R., Sheets, B., Wang, D., Zhang, Y., 2019: First Ever Polymer Flood Field Pilot-A Game Changer to Enhance The Recovery of Heavy Oils on Alaska's North Slope, San Jose, California, SPE Western Regional Meeting, 23 April 2019.

DeRuiter, R.A., Nash, L.J., Singletary, M.S., 1994. Solubility and Displacement Behavior of a Viscous Crude with CO2 and Hydrocarbon Gases.

Dusseault, M.b., 2008: Comparing Venezuelan and Canadian Heavy Oil and Tar Sands, Calgary, Canada, Canadian International Petroleum Conference, 5 May 2008.

Hallam, R.J., Plekenbrock E.J., Abou-Sayed A.S., Garon, A.M., Putnam, T.W., Weggeland, M.C., Webb, K.J., 1992. Resource Description and Development Potential of the Ugnu Reservoir, North Slope, Alaska. Society of Petroleum Engineers, doi 10.2118/21779-PA.

Hirsch, R., Bezdek, R., Wendling, R., 2005: Peaking of World Oil Production: Impacts, Mitigation, & Risk Management, Researchgate, DOI 10.2172/939271.

Hook, M., Soderbergh, B., Jakobsson, K., Aleklett, K., 2009: The evolution of giant oil field production behavior, Natural Resource Link, vol 19, No 1, 39-56.

Househnecht, D., Bird, K., 2005. Alaska North Slope basin map from U.S. Geological Survey Professional Paper 1732-A.

Jin, Y., Liu, D., Luo, C., 1985: "Development of Daqing oil field by waterflooding." Journal of petroleum technology 37, no. 02, 269-274.

Larter, S., Whilhelms, A., Head, I., Koopman, M., Aplin, A., Di Primio, R., Zwach, C., Erdmann, M., and Telnaes, N., 2003, The controls on the composition of biodegraded oils in deep subsurface-part 1, Organic Geochemistry, 34 (3), 601-613.

LeFever, J.A. and Helms, L.D., 2006. Bakken Formation reserve estimates. North Dakota Geological Survey.

Masterson, W. D., Dzou, L. L., Holba, G. A., Fincannon, L. A., Ellis, L., 2001: Evidence for biodegradation and evaporative fractionation in West Sak, Kuparuk and Prudhoe Bay Field area, North Slope, Alaska, Elsevier, Vol. 32, No. 3, 411-441.

Masui, A., Haneda, H., Ogata, Y., Aoki, K., 2005: "The effect of saturation degree of methane hydrate on the shear strength of synthetic methane hydrate sediments." In Proceedings of the 5th International Conference on Gas Hydrates, Trondheim, Norway, vol. 2037, pp. 657-663.

Namie, S., Wang, D., 2019: An Expanded Geological Reservoir Model of the West Sak and Ugnu Heavy Oil Reservoirs: A First Step in Exploring EOR Methods on Alaska's North Slope. Abstract submission, AAPG Europe Region Conference, January 28-29, Athens Greece.

Nelson, K., 2007, Alaska North Slope production breaks 800,000 bpd barrier, Petroleum news, vol. 12 no, 1.

Paskvan, F., Turak, J., Jerauld, G., Gould, T., Skinner, R., Garg A., 2016: Alaskan Viscous Oil: EOR Opportunity, or Waterflood Sand Control First, Society of Petroleum Engineers, SPE Conference Paper 180463_MS, 26 May 2016.

Pospisil, G., 2011. "Heavy Oil Challenges & Opportunities North Slope Alaska', https://www.aoga.org/wp-content/uploads/2011/01/8.-Pospisil-Heavy-Viscous-Oil.pdf.

Ranjbar, A., Hassani, H., Shahriar K., and Mohammad Javad Ameri, K., 2018. "Hybrid numerical modeling of Mandel's problem and investigating its various aspects." In Geomechanics and Geodynamics of Rock Masses-Volume 2, pp. 1413-1418. CRC Press.

Renouf, G., 2014: A Survey of Polymer Flooding in Western Canada, Tulsa, Oklahoma, SPE Improved Symposium, 12 April 2014.

Renqing, L., 2013: "Development of enhanced oil recovery in Daqing." J Pet Gas Eng 4, 46-50.

Robelius, F., 2007: Giant Oil Fields – The Highway to Oil: Giant Oil Fields and their Importance for Future Oil Production, doctoral thesis from Uppsala University, 156p.

Rosen, Y., 2005: North Slope's Vast Viscous-Oil Targeted, Reuters, May.

Sheng, J., 2011: Modern Chemical Enhanced Oil Recovery, Gulf Professional Publishing, 2010, 1001-206.

Rutqvist, J., Moridis, G. J., Grover, T., and Collett, T., 2009. "Geomechanical response of permafrost-associated hydrate deposits to depressurization-induced gas production." Journal of petroleum science and engineering 67, no. 1-2: 1-12.

Sandiford, B. B., 1964: "Laboratory and field studies of water floods using polymer solutions to increase oil recoveries." Journal of Petroleum Technology 16, no. 08, 917-922.

Santos, R. G., Loh, R. G., Bannwart C. A., and Trevisan O. V., 2014. "An overview of heavy oil properties and its recovery and transportation methods." Brazilian Journal of Chemical Engineering 31, no. 3, 571-590.

Seright, R.S., Zhang, G., Akanni, O.O., Wang, D., 2012: A Comparison of Polymer Flooding with In-Depth Profile Modification, Calgary, Canada, SPE Canadian Unconventional Resources Conference, 15 November 2011.

Smith, R. E., Clegg W. M., 1971. "Analysis and design of production wells through thick permafrost." In 8th World Petroleum Congress. World Petroleum Congress.

Targac, G.W., Redman R.S., Davis E.R., Rennie S.B., Mckeever, S.O., 2005: Unlocking the Value in West Sack Heavy Oil, Calgary, Canada, International Thermal Operations and Heavy Oil Symposium, 1 November 2005.

Temizel, C., Canbaz, C.H., Minh, T., Elsayed, A., Jia, B., Putra, D., Irani, M., Alkouh, A., 2018. A Comprehensive Review Heavy Oil Reservoirs, Latest Techniques, Discoveries, Technologies and Applications in the Oil and Gas Industry. Society of Petroleum Engineers. doi:10.2118/193646-MS.

Thomas, P. C., North, B. W., Doughty, C. T., Hite, M. D., 2009: Alaska North Slope Oil and Gas A Promising Future or an Area in Decline, DOE/NETL 2009, NETL Addendum Report.

Trevisan, F., Bannwart C. A., 2006: "Three-phase flow patterns and pressure drop for heavy crude oil-water-gas horizontal flow." In International Heat Transfer Conference 13. Begel House Inc.

Van Wagener, D., 2018. Development of Alaska’s ANWR would increase U.S. crude oil production after 2030, Energy Information Administration, June 18

Wang, D., Namie, S., Li, C., 2019: Impact of Polymer or Surfactant Flooding on Permafrost Stability, Denver, Colorado, Unconventional Resources Technology Conference, 22 July 2019.

Werner, M. R., 1987. West Sak and Ugnu Sands: Low-Gravity Oil Zones of The Kuparuk River Area, Alaskan North Slope, Pacific Section SEPM and The Alaska Geological Society 50, pp. 109-118.

Xie, J. and Matthews, C.M., 2011, January. Methodology to assess thaw subsidence impacts on the design and integrity of oil and gas wells in Arctic regions. In SPE Arctic and Extreme Environments Conference and Exhibition. Society of Petroleum Engineers.

Yang, C., Han D., 1991: "Present status of EOR in the Chinese petroleum industry and its future." Journal of Petroleum Science and Engineering 6, no. 2, 175-189.

Zhang, Y., Wei M., Bai, B., Yang H., Kang W., 2016. "Survey and data analysis of the pilot and field polymer flooding projects in China." In SPE improved oil recovery conference. Society of Petroleum Engineers.

FIGURES

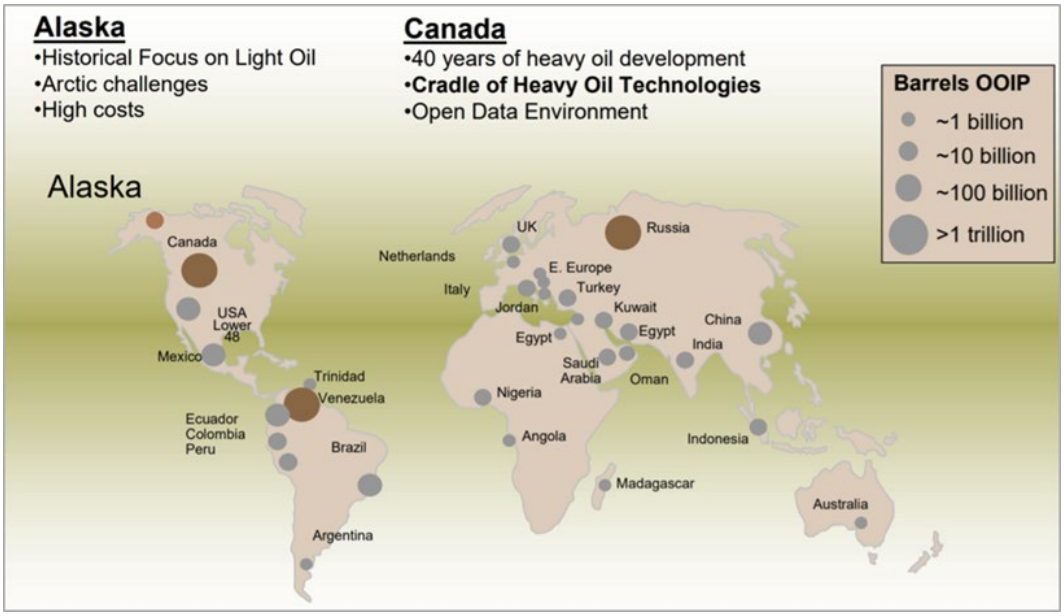

Figure 1. Location of world's heavy oil reserves (Chmielowski, 2013).

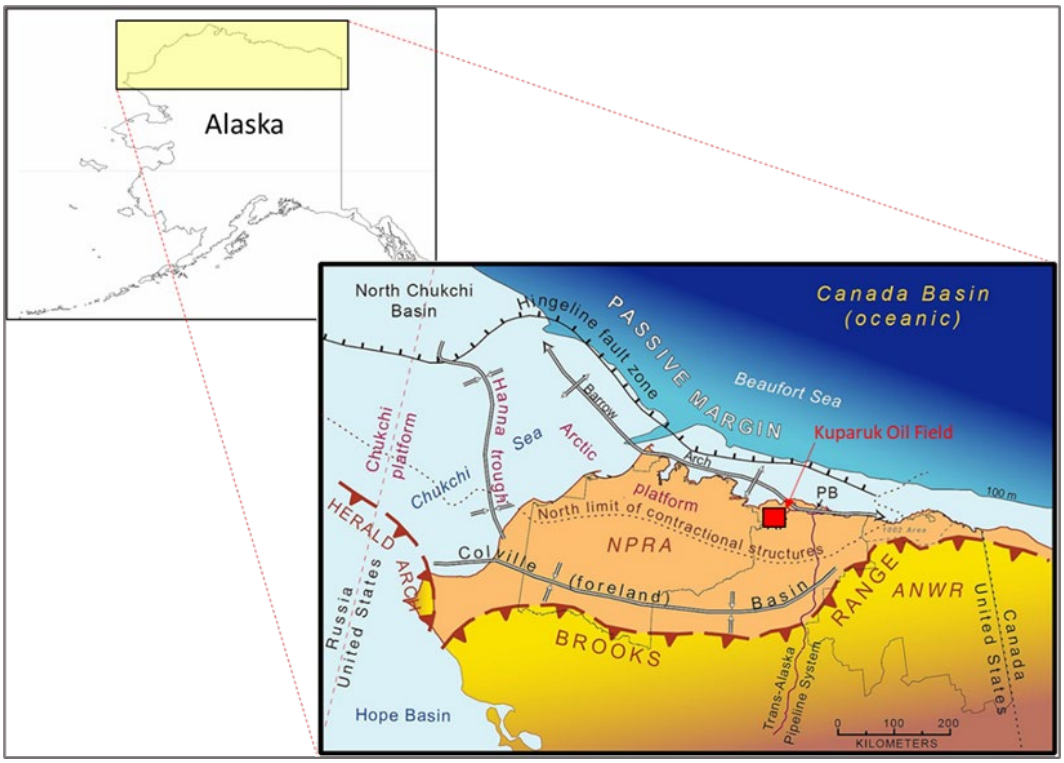

Figure 2. The map location of the Kuparuk oil field on the ANS, modified from Houseknecht et al. (2005).

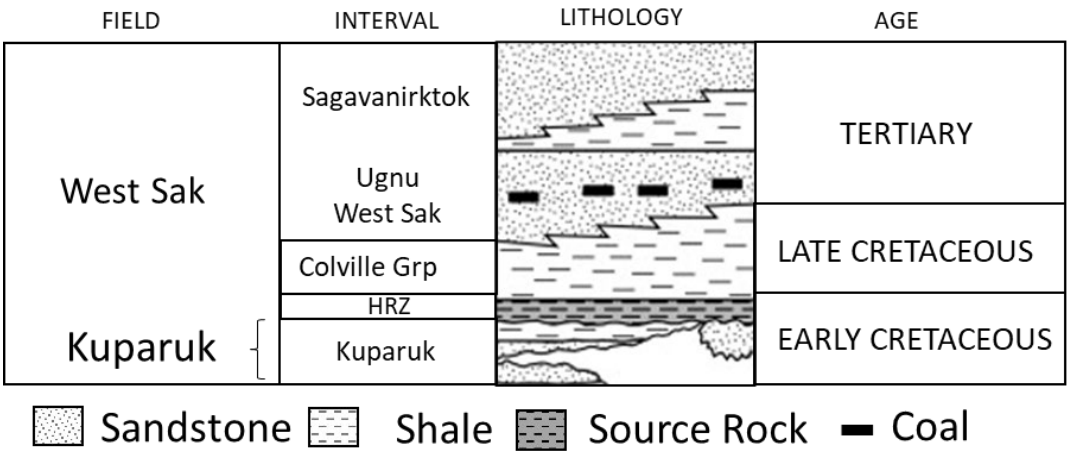

Figure 3. Lithology of Kuparuk oil Field (Masterson et al., 2001).

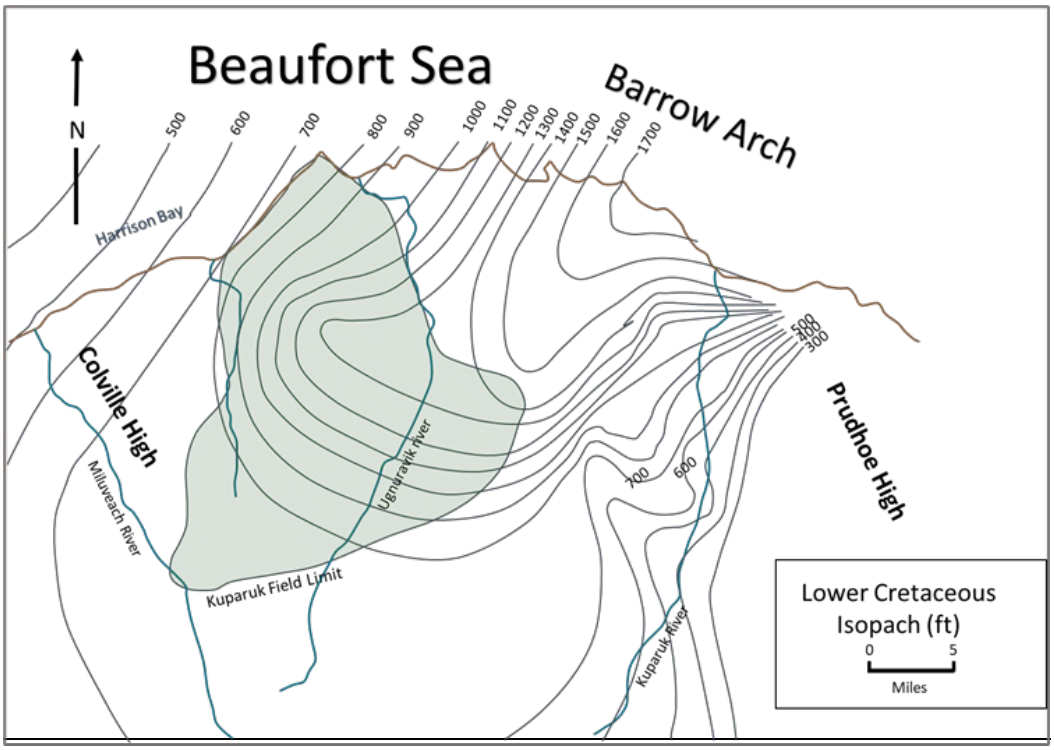

Figure 4. Carmen et al. (1983), Kuparuk reservoir isopach map showing the Prudhoe and Colville high.

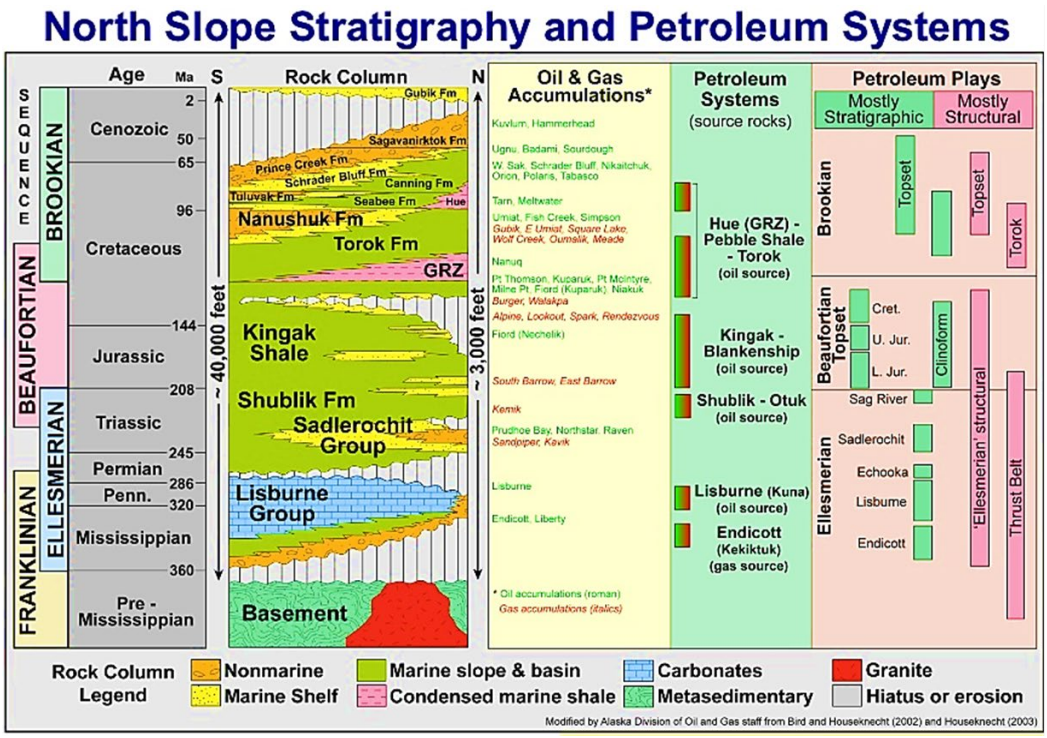

Figure 5. The Petroleum System (Bird et al., 2002).

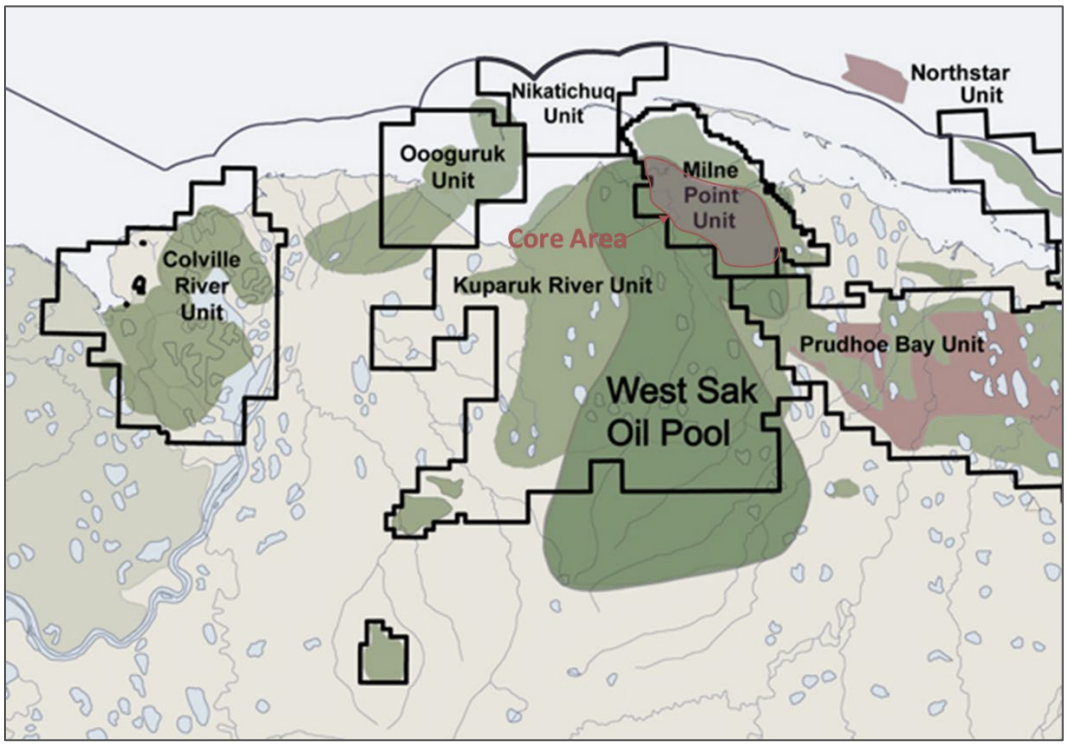

Figure 6. The West Sak and Ugnu oil pool location (Pospisil, 2011).

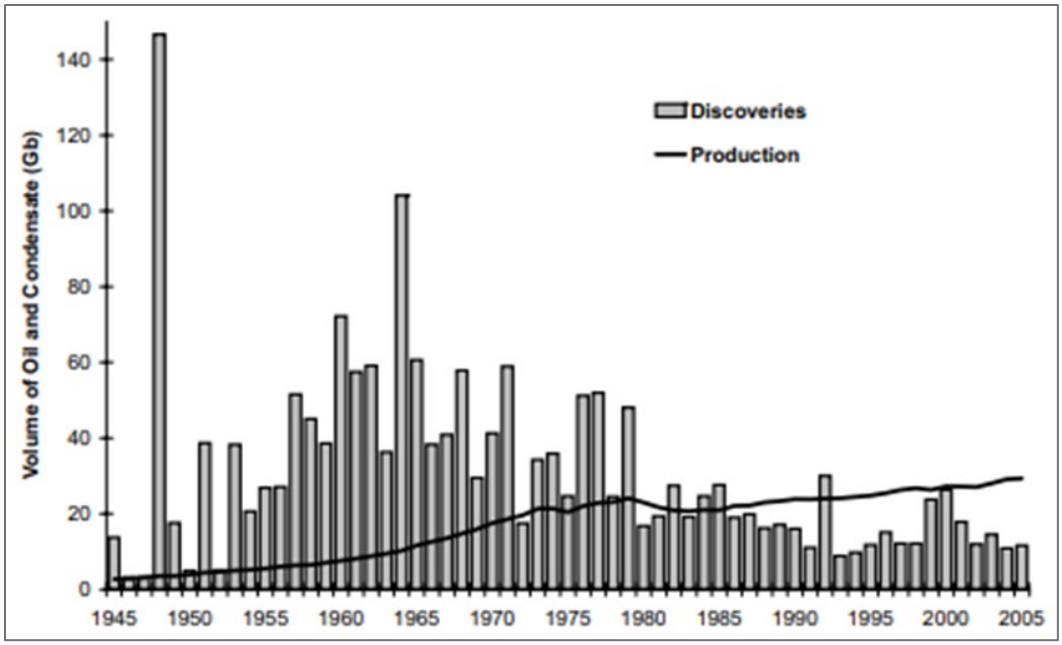

Figure 7. Discovery of giant oil fields from 1945 to 2005, showing production (black line) outpacing discovery (Robeliue, 2007).

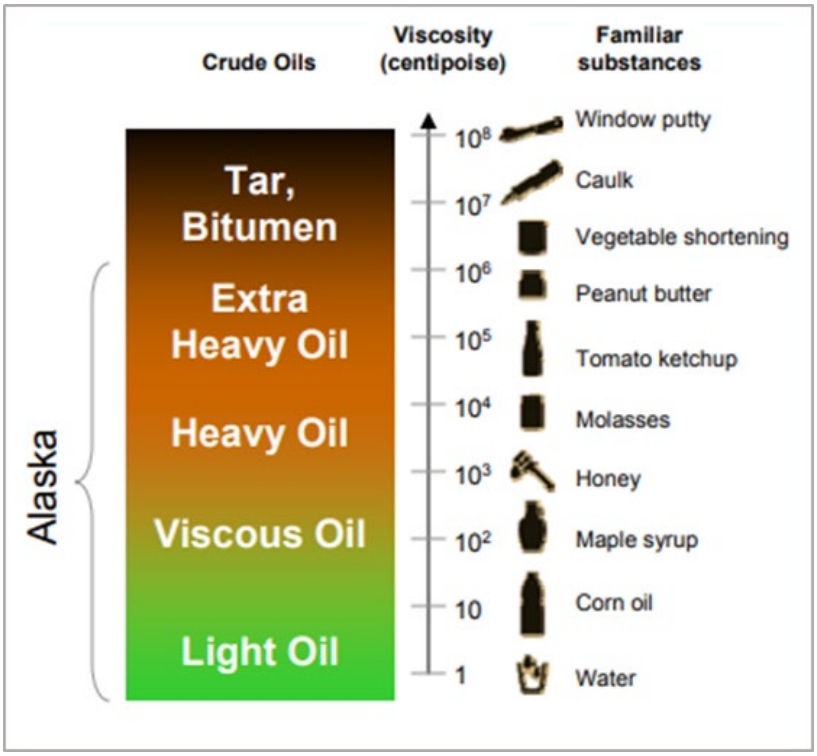

Figure 8. Viscosity comparison to household items (Brownbag, 2011).

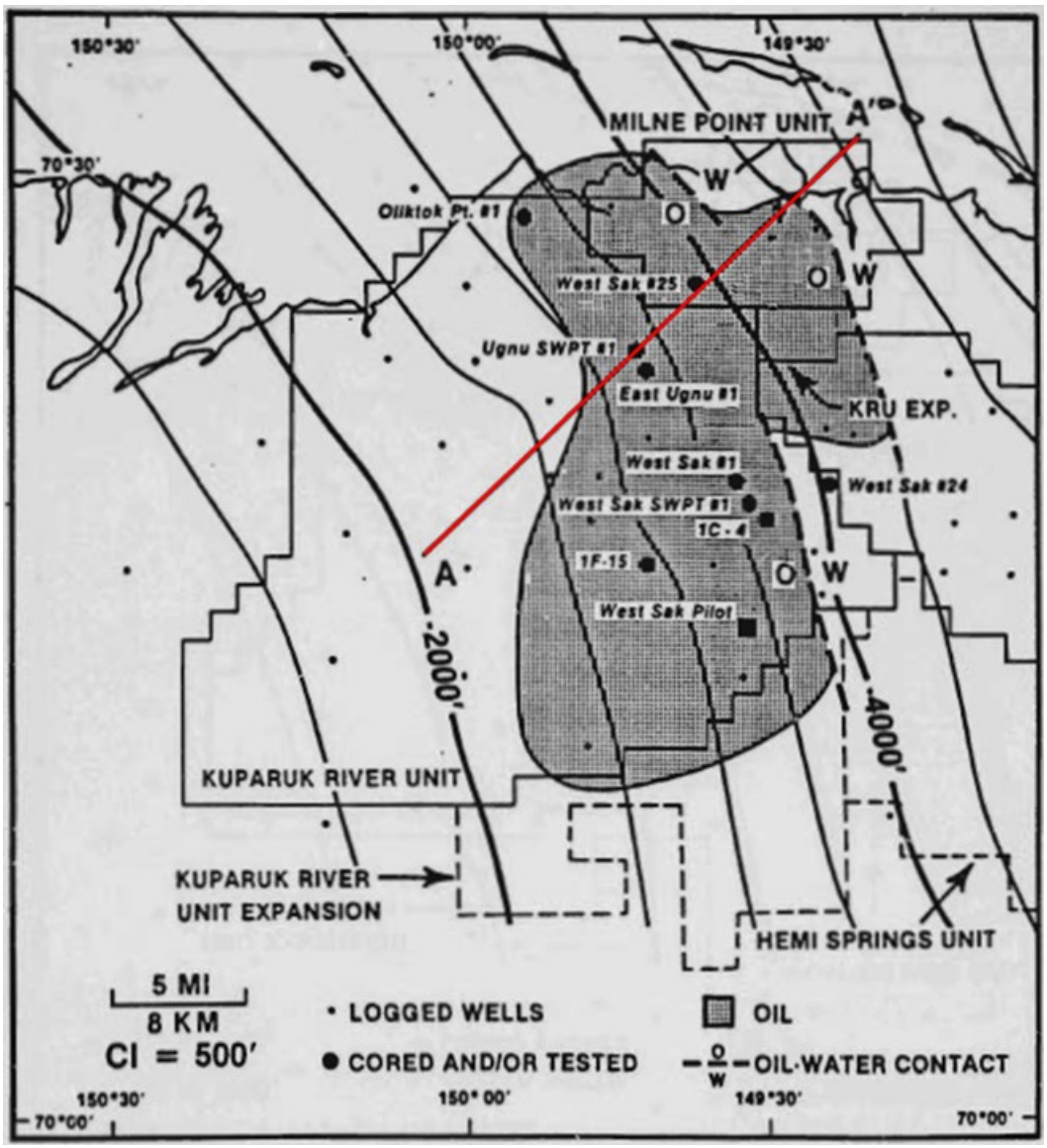

Figure 9. Werner (1987) structural contour map, top of West Sak Sands (ft).

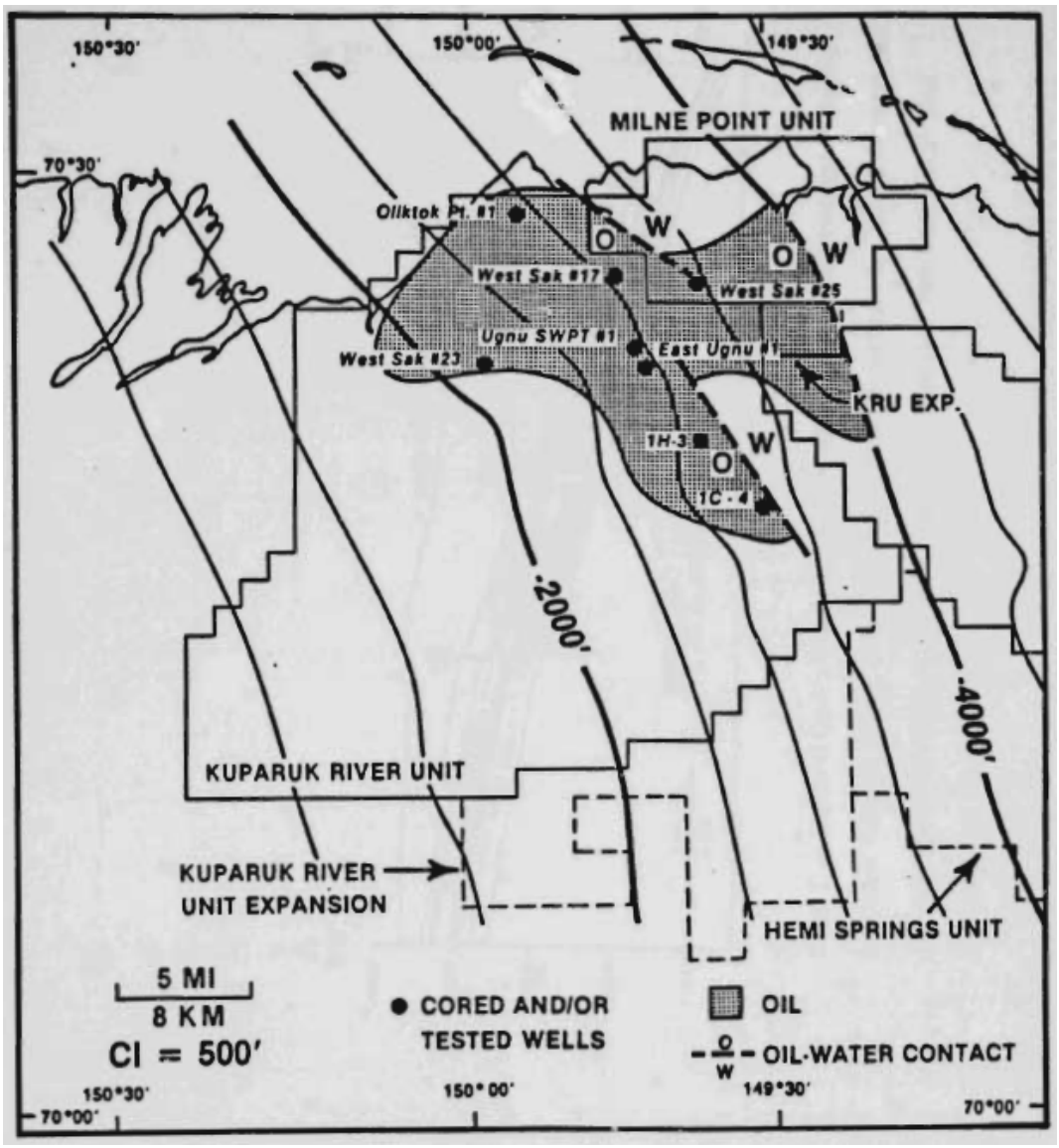

Figure 10. Werner (1987) structural contour map, top of Ugnu sands (ft).

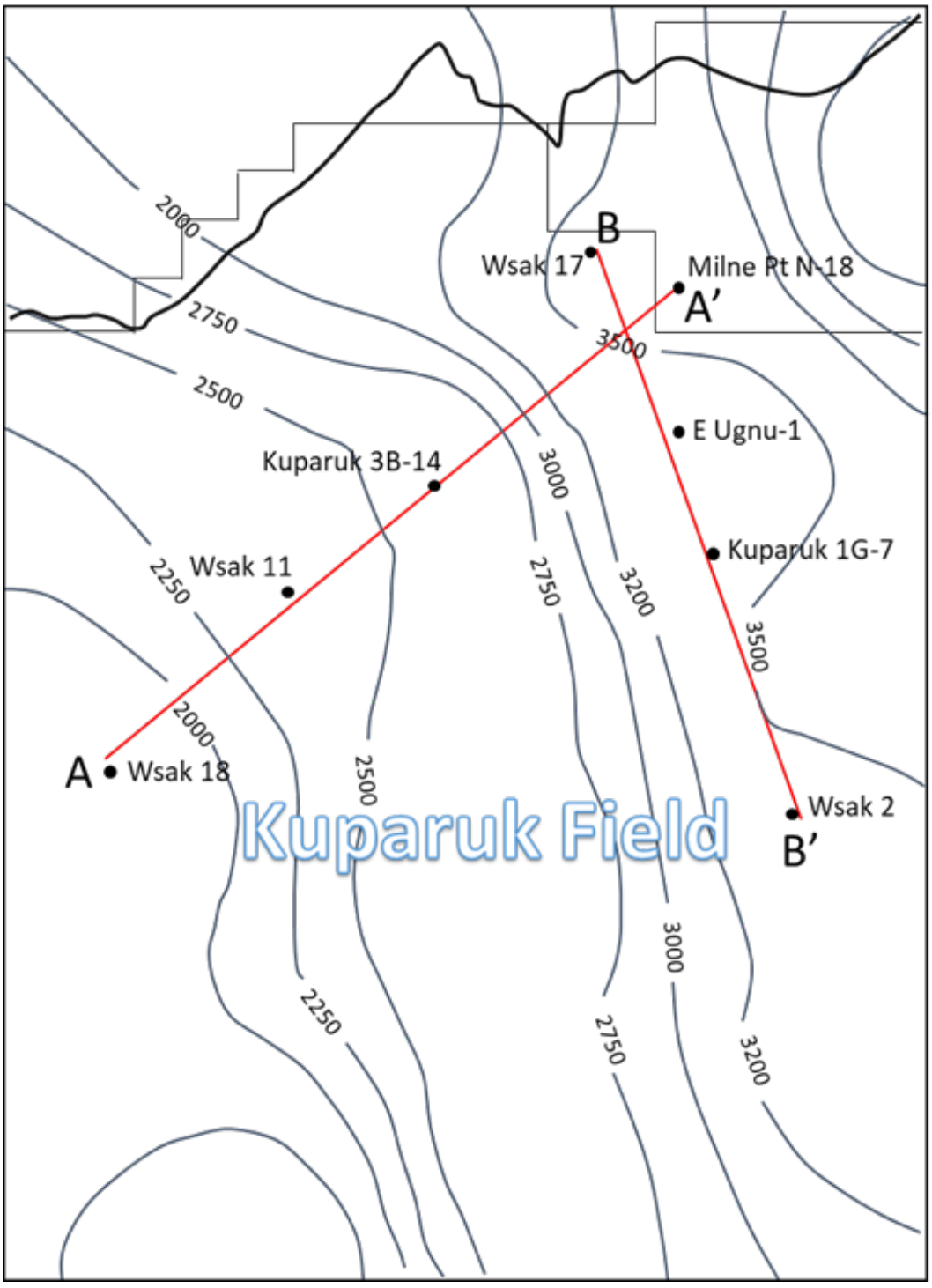

Figure 11. Panda et al. (1989) structural contour map, top of West Sak sands (ft).

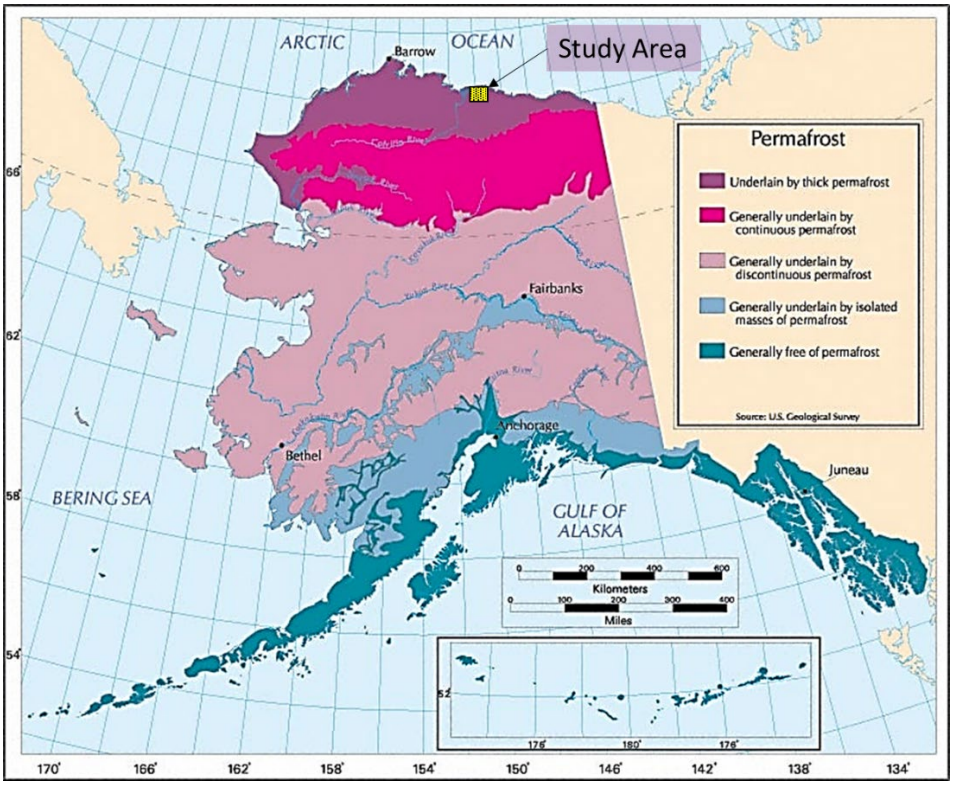

Figure 12. Permafrost lays under 80 percent of Alaska's surface (Climatenexus, 2020).

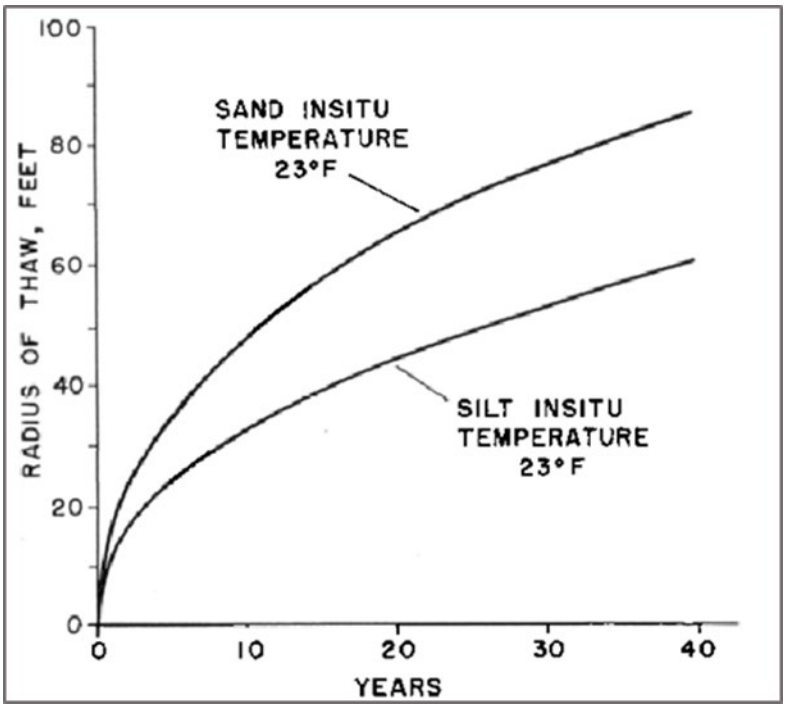

Figure 13. Radii of thawing conventional production well (Smith, 1971).

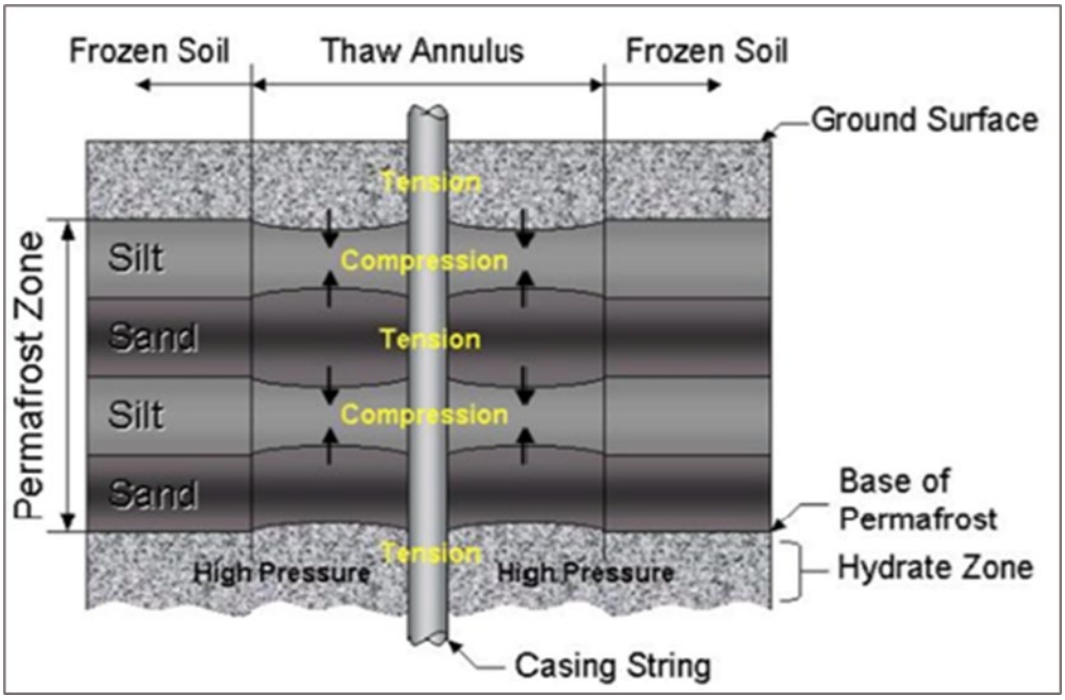

Figure 14. Thaw subsidence loading on production well (Xie et al, 2011).

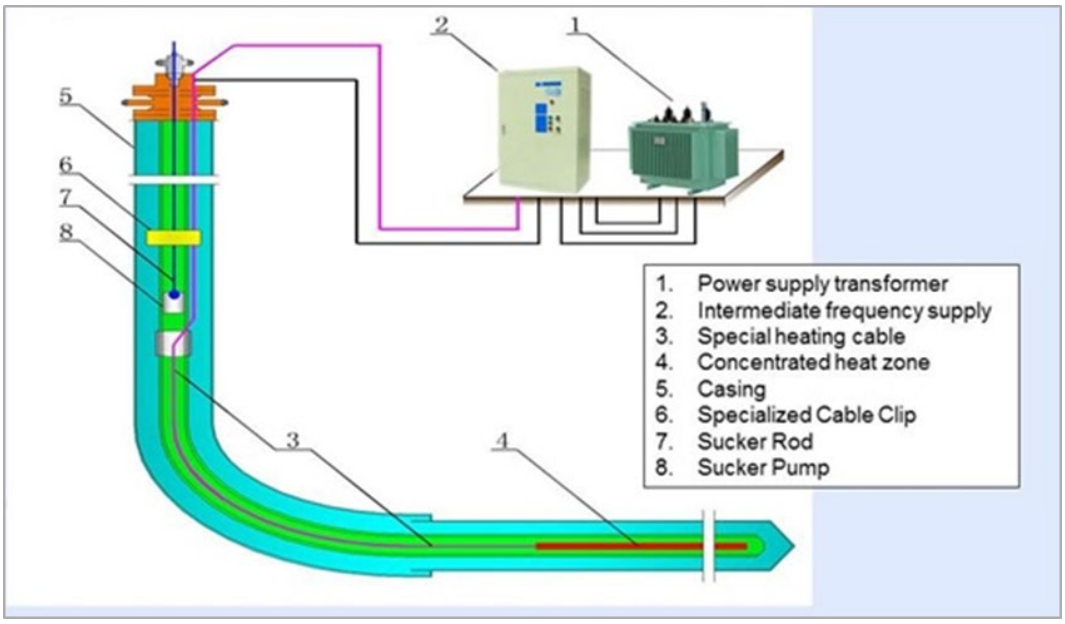

Figure 15. Electric downhole heating design on a horizontal well (ANDMIR, 2020).

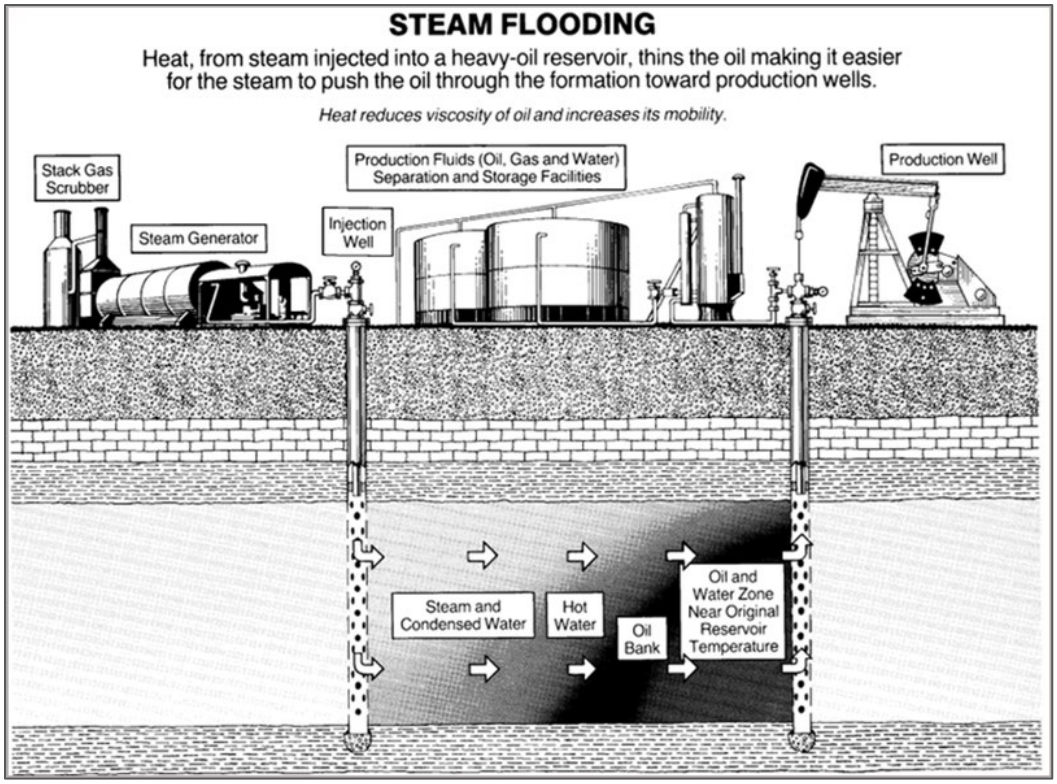

Figure 16. Conceptual view of steam flooding (Donaldson et al., 1985).

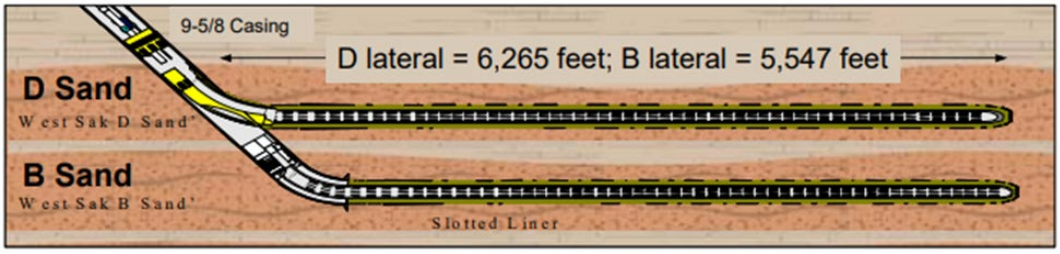

Figure 17. Multi-lateral technology (Targac et al., 2005).

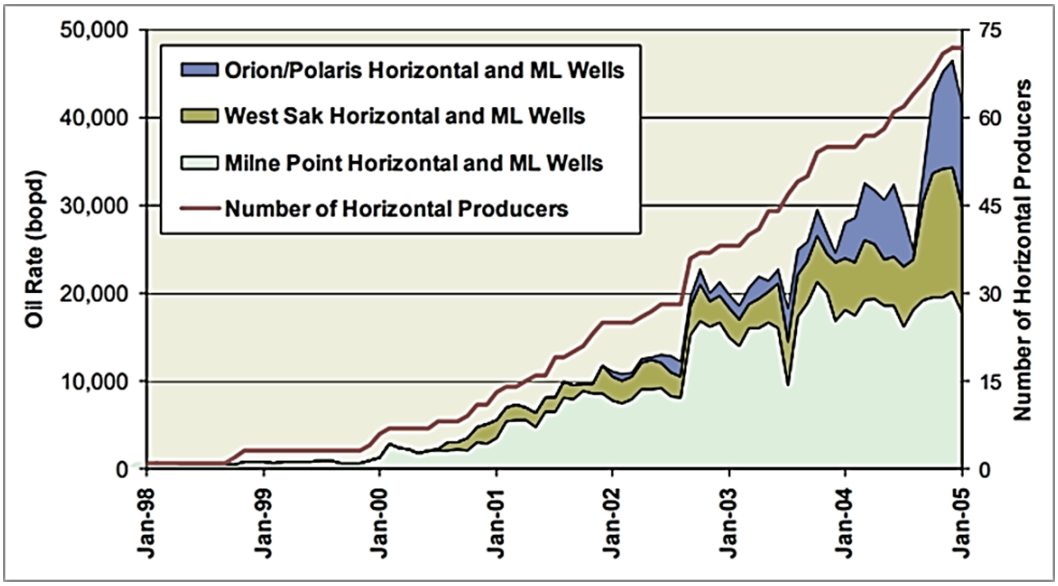

Figure 18. ANS heavy oil multi-lateral number of producers with production increased rates (Targac et al., 2005).

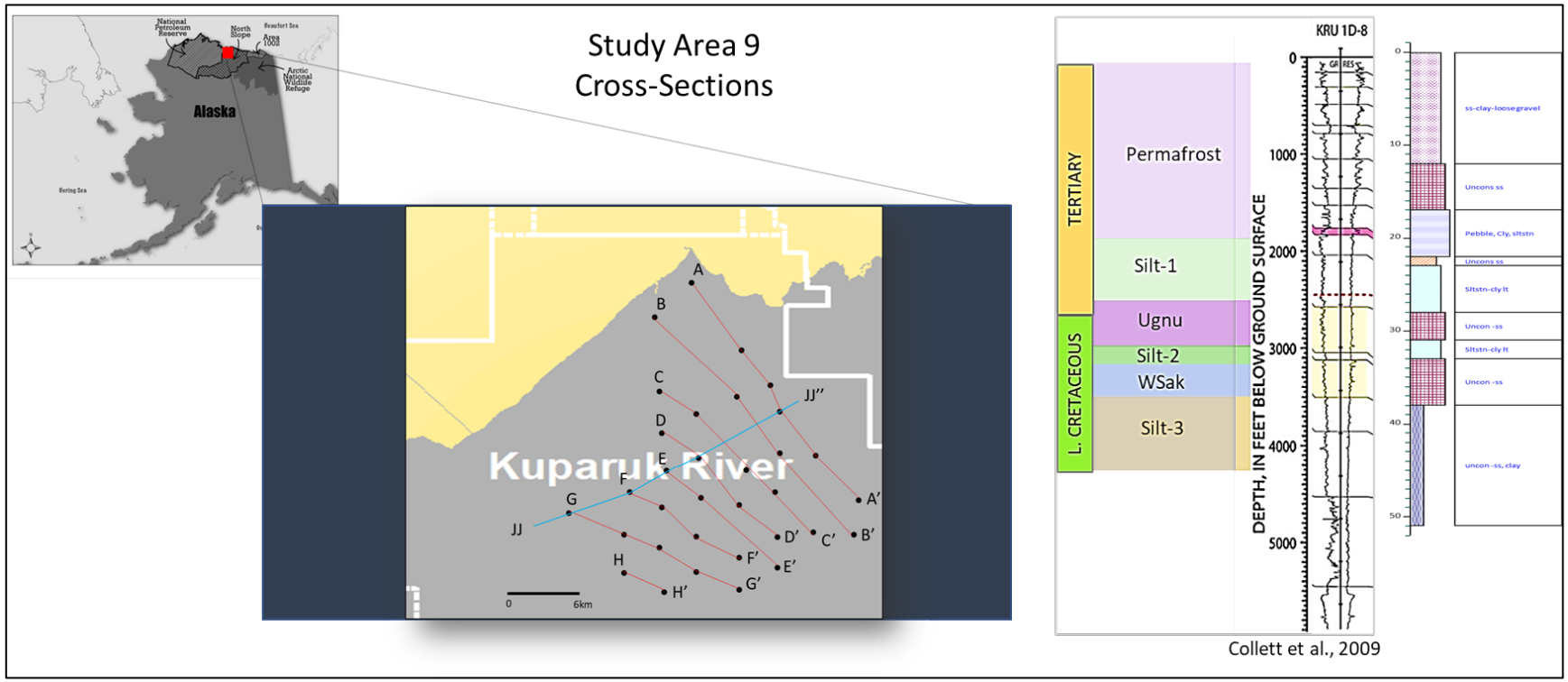

Figure 19. Study area illustrating the 9 cross-sections, include reference well.

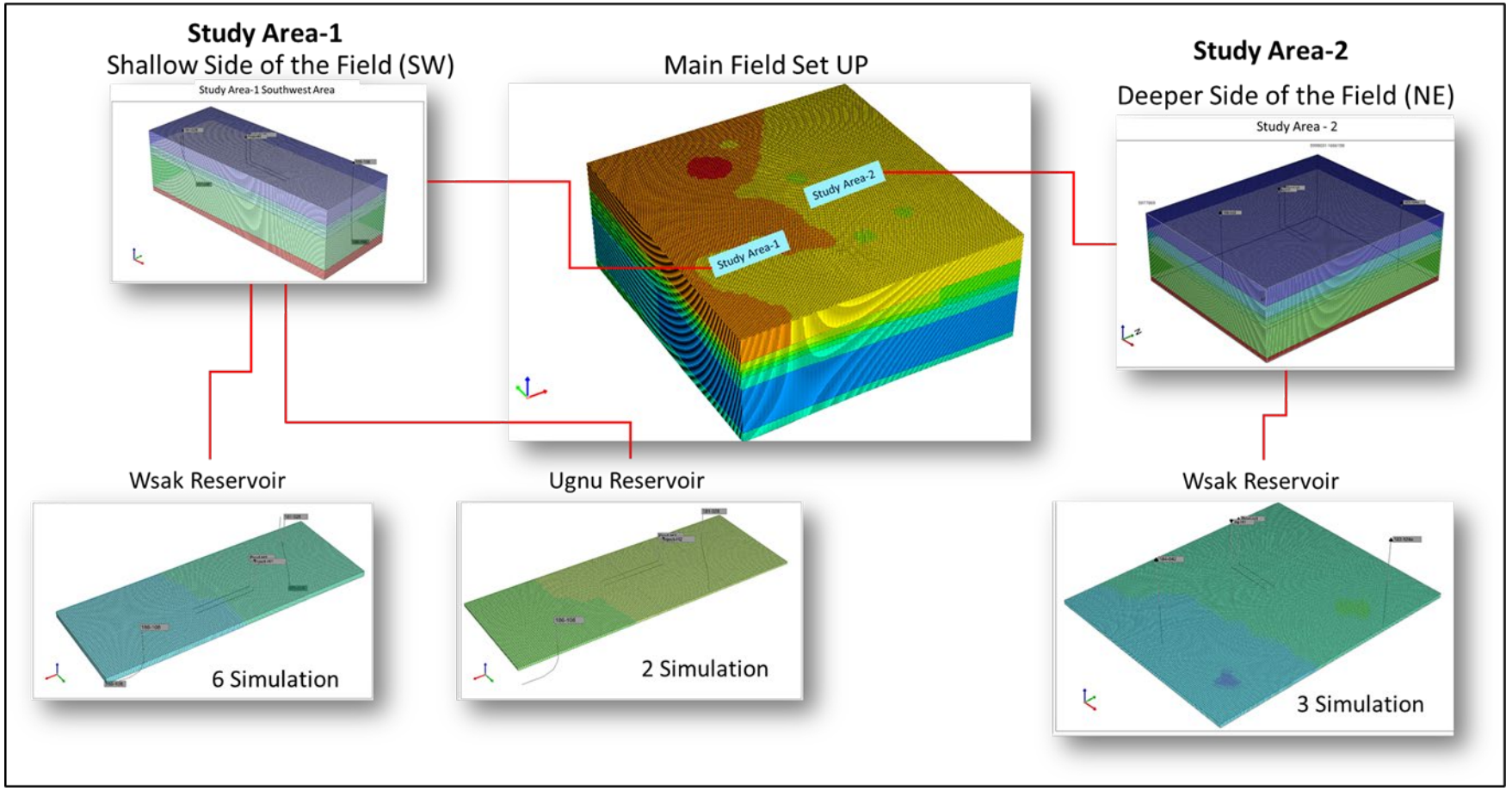

Figure 20. Illustrating the breakdown of where the simulation take place.

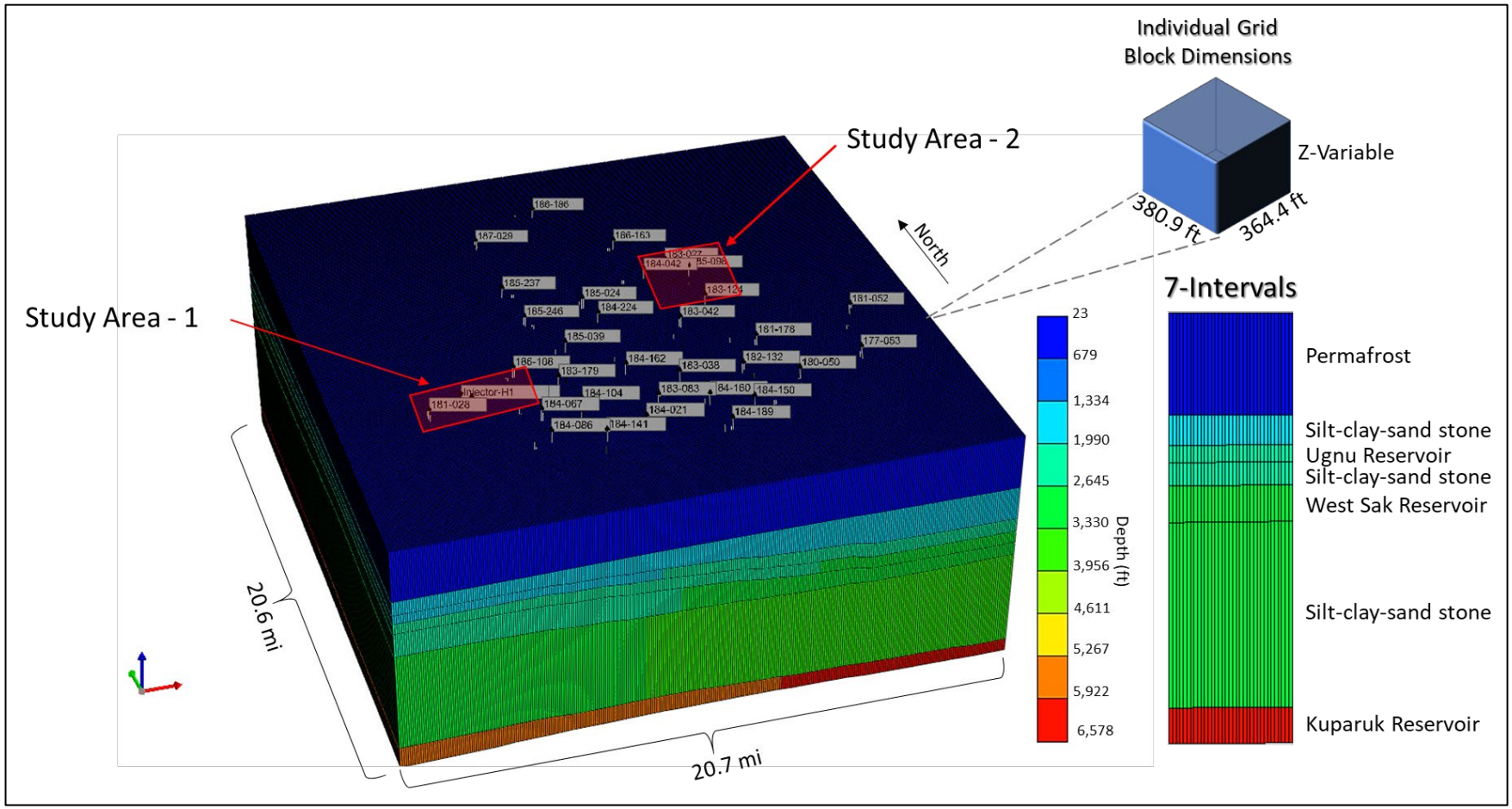

Figure 21. Main numerical model illustrating where study area 1 and 2 are located including block dimensions and interval set up.

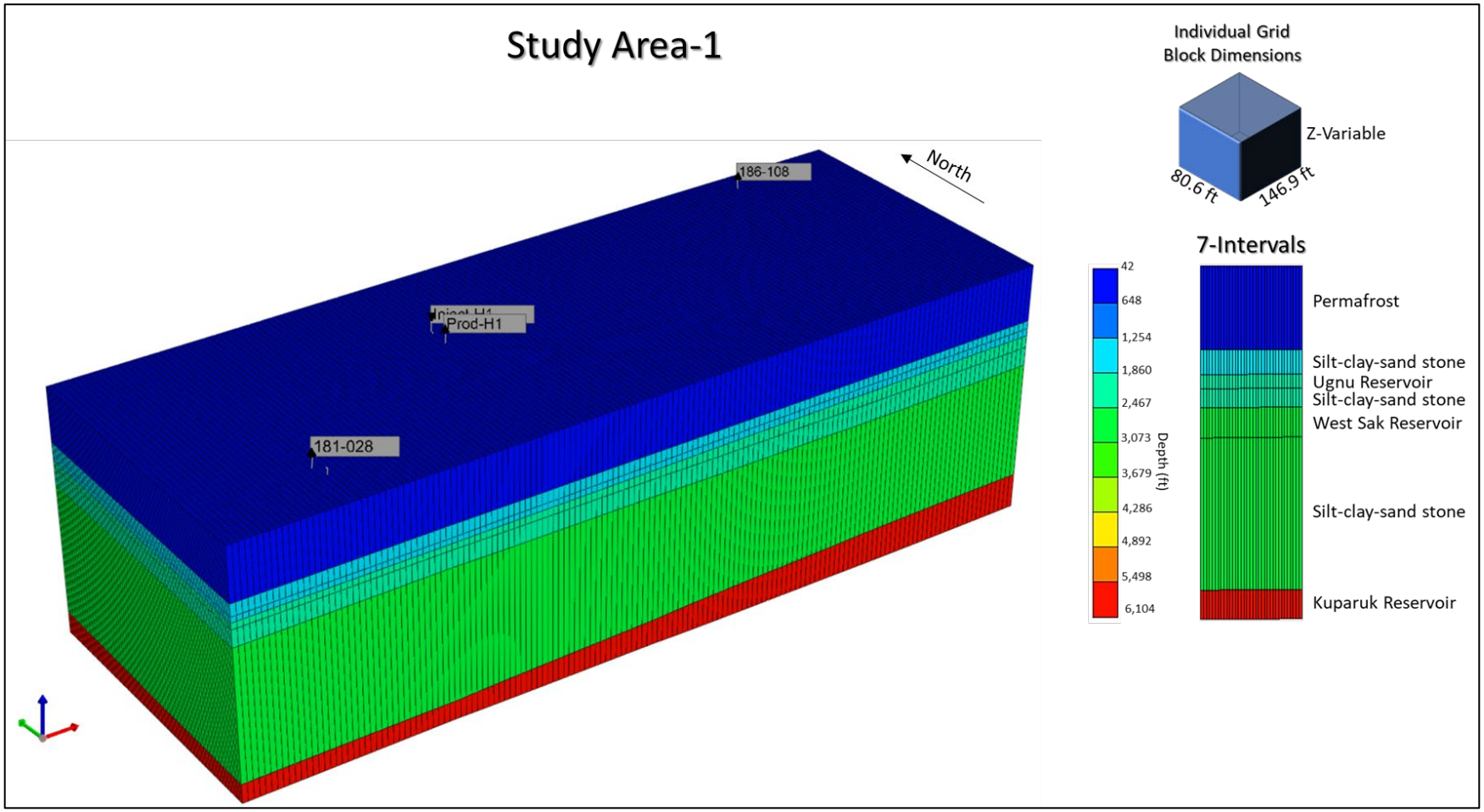

Figure 22. Study area-1 including grid block dimensions and interval set up.

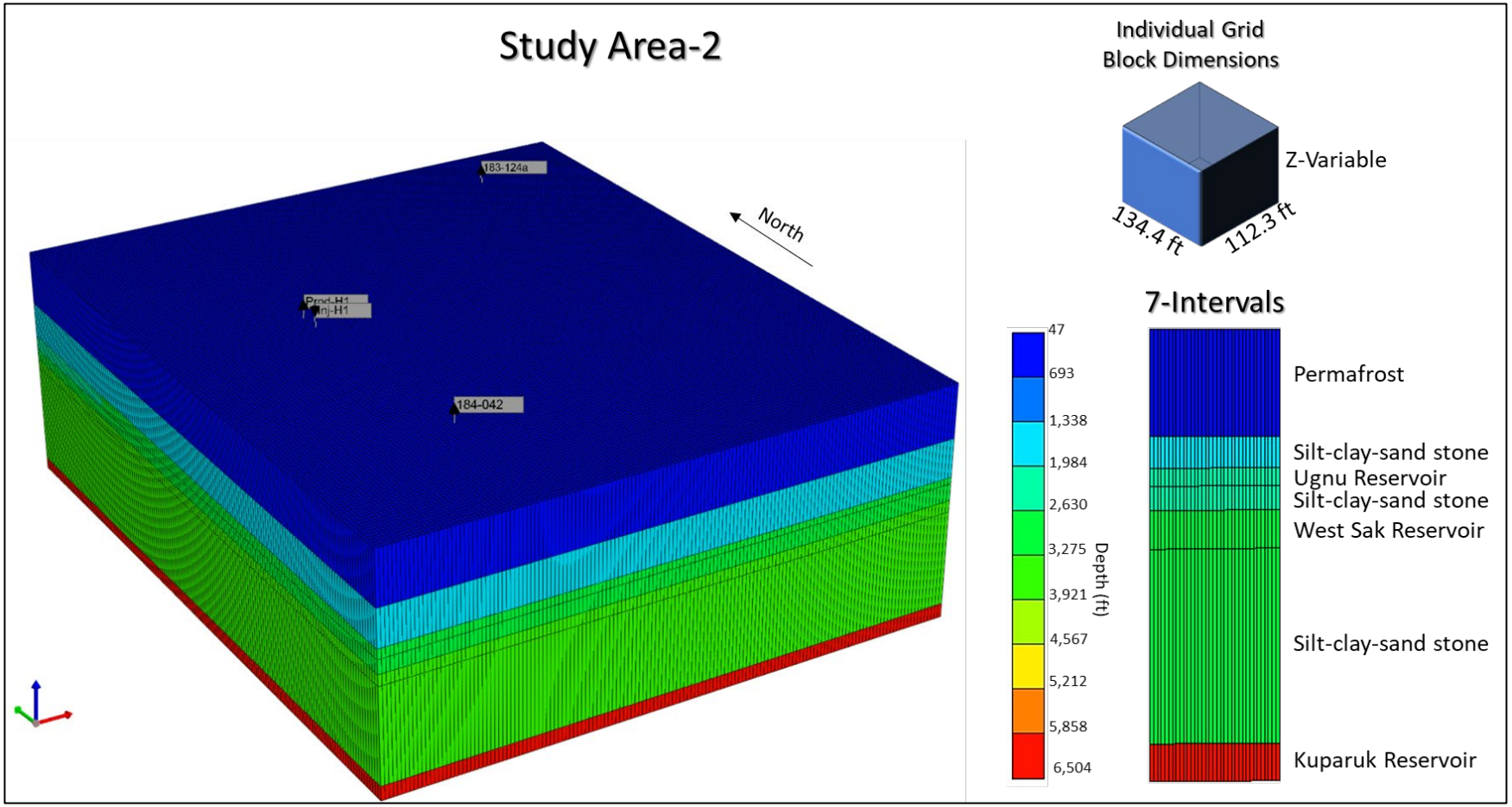

Figure 23. Study area-2 including grid block dimensions and interval set up.

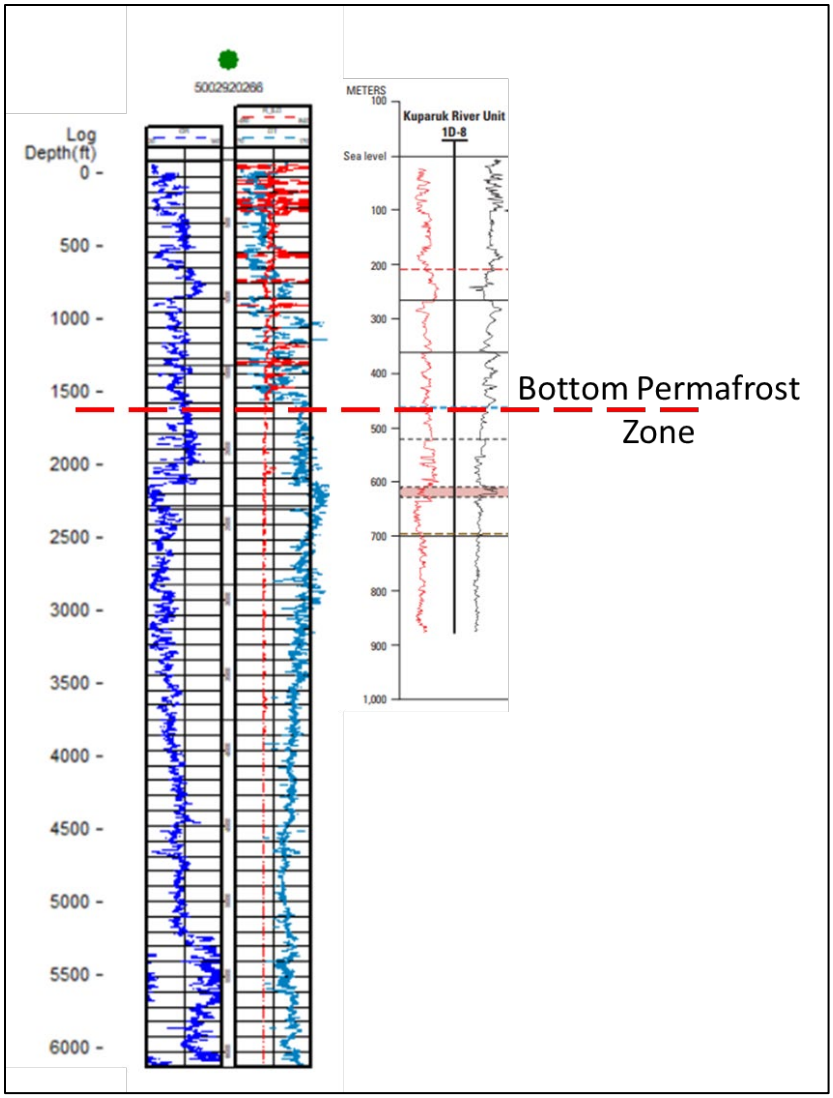

Figure 24. Technique in identifying the bottom of the permafrost zone, reference a study done by Collette et al., 1983.

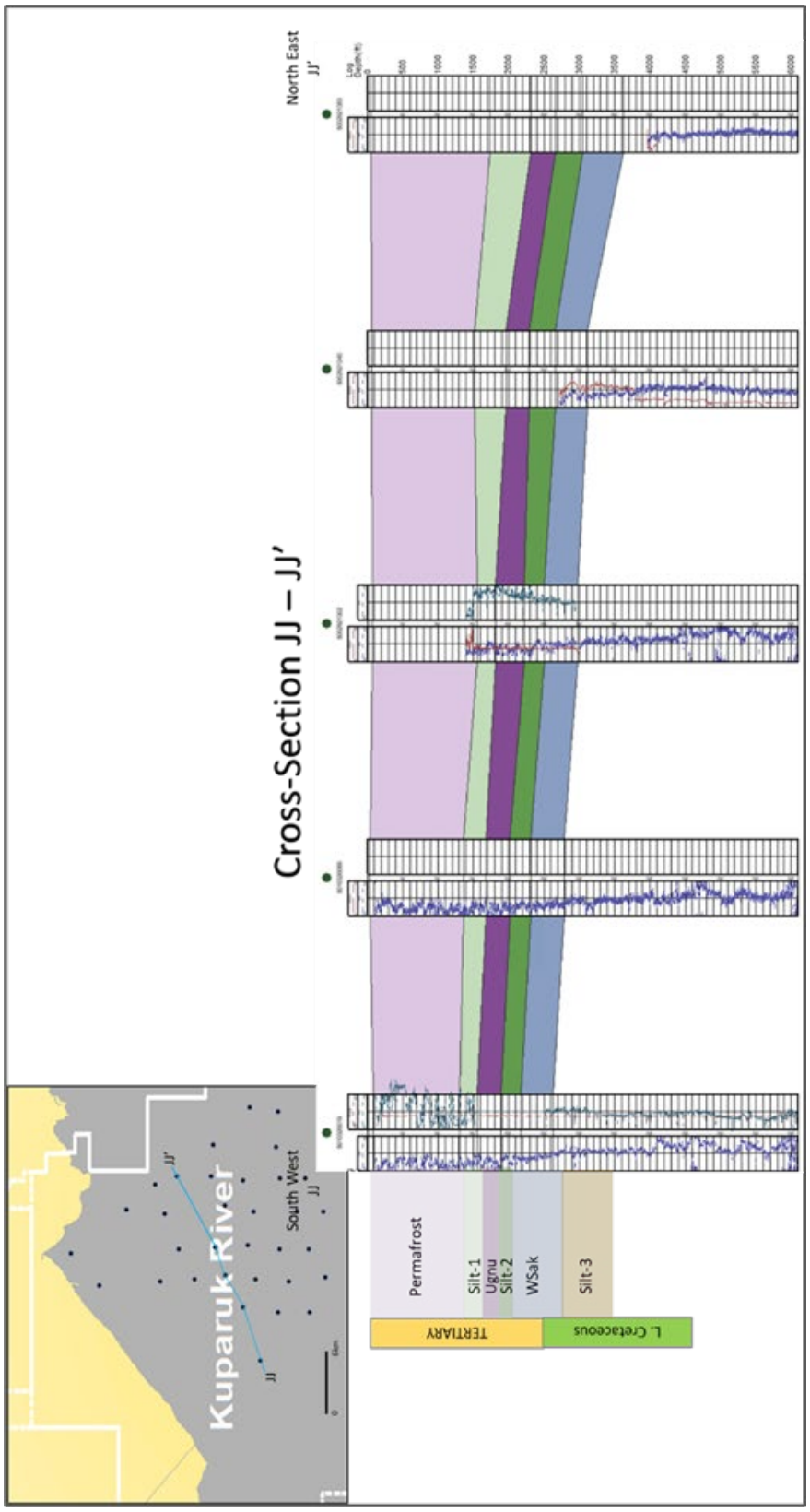

Figure 25. Cross-section JJ-JJ' cutting across the middle of the field showing a down dip with all intervals trending from the southwest to the northeast in the Kuparuk field.

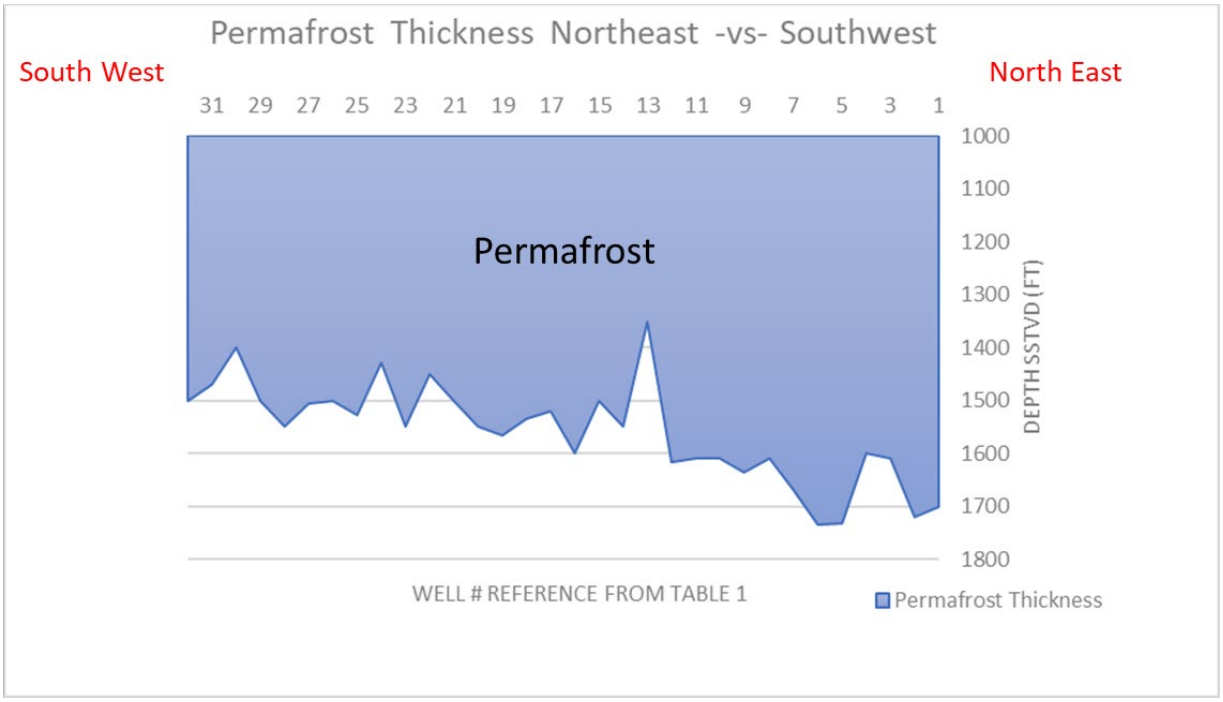

Figure 26. Permafrost depth taken from Table 5, shows a dip trend from the southwest to northeast cutting through the field represented by JJ-JJ'. This graph illustrates that the bottom of the permafrost may have talik formation across the field.

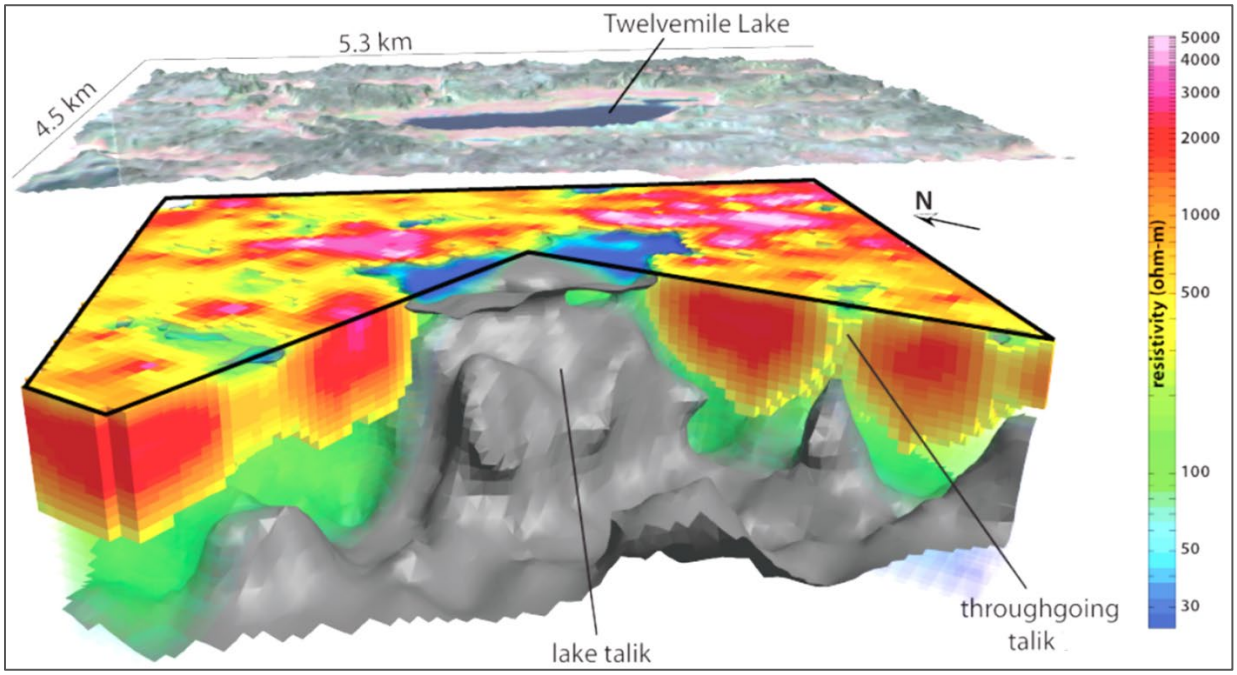

Figure 27. Three-dimensional model using resistivity near Twelvemile Lake, Alaska, illustrating how taliks form in the subsurface from water bodies (Abraham, 2011).

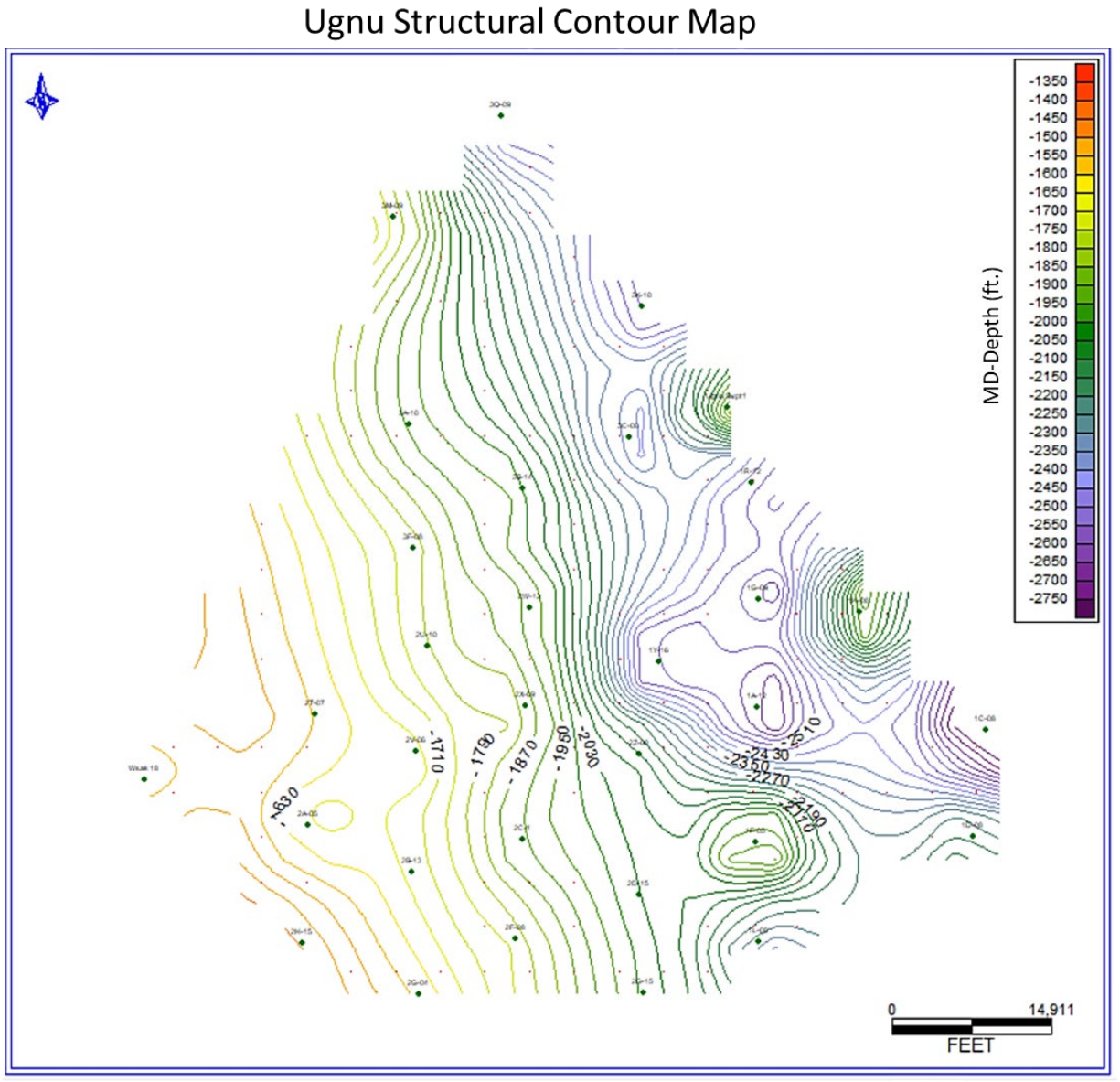

Figure 28. Structural contour map of the top of Ugnu sands that dip from the southwest to the northwest section of the map.

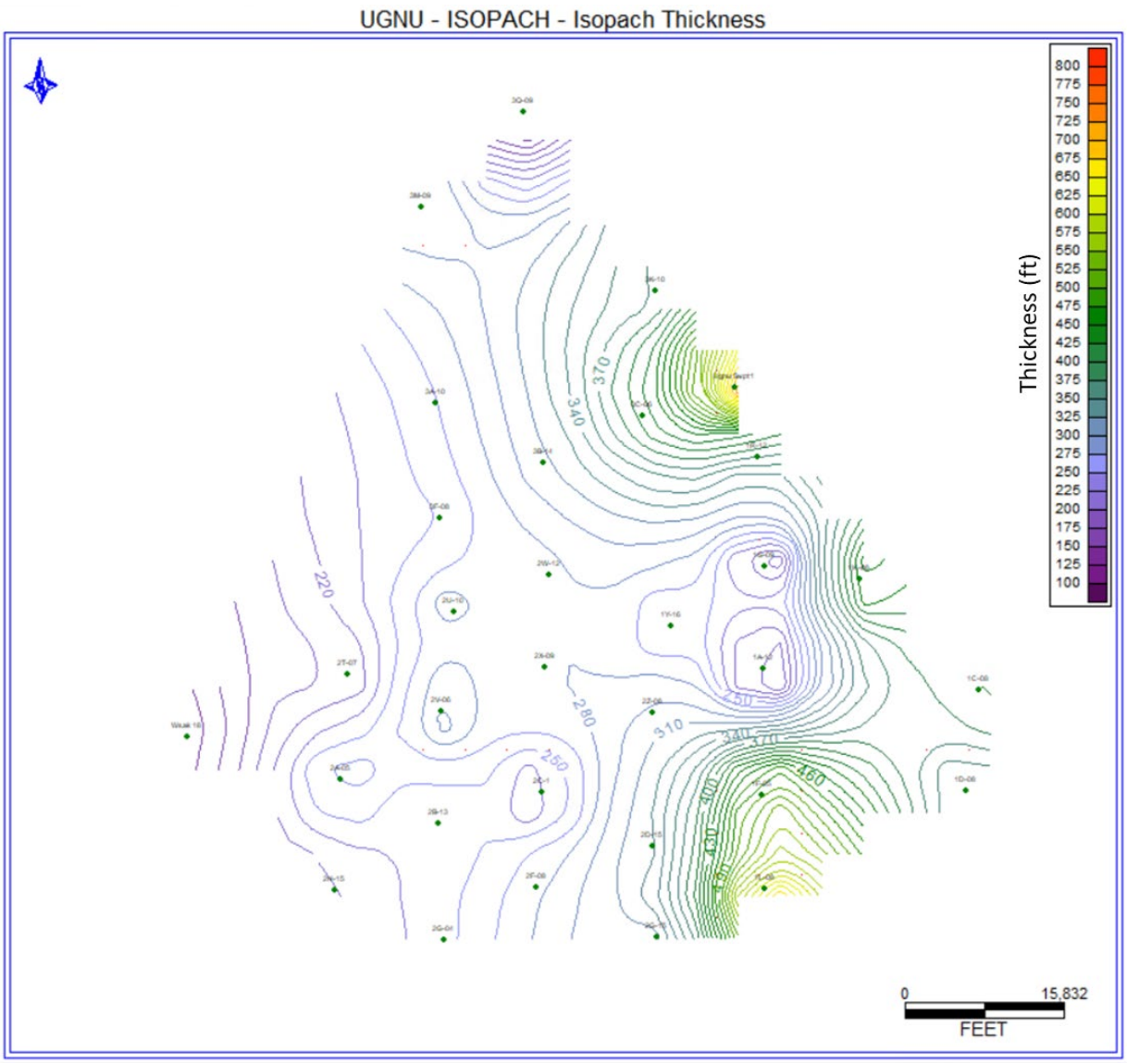

Figure 29. Isopach map of the Ugnu reservoir showing a thinning trend from the northeast to southwest section of the map.

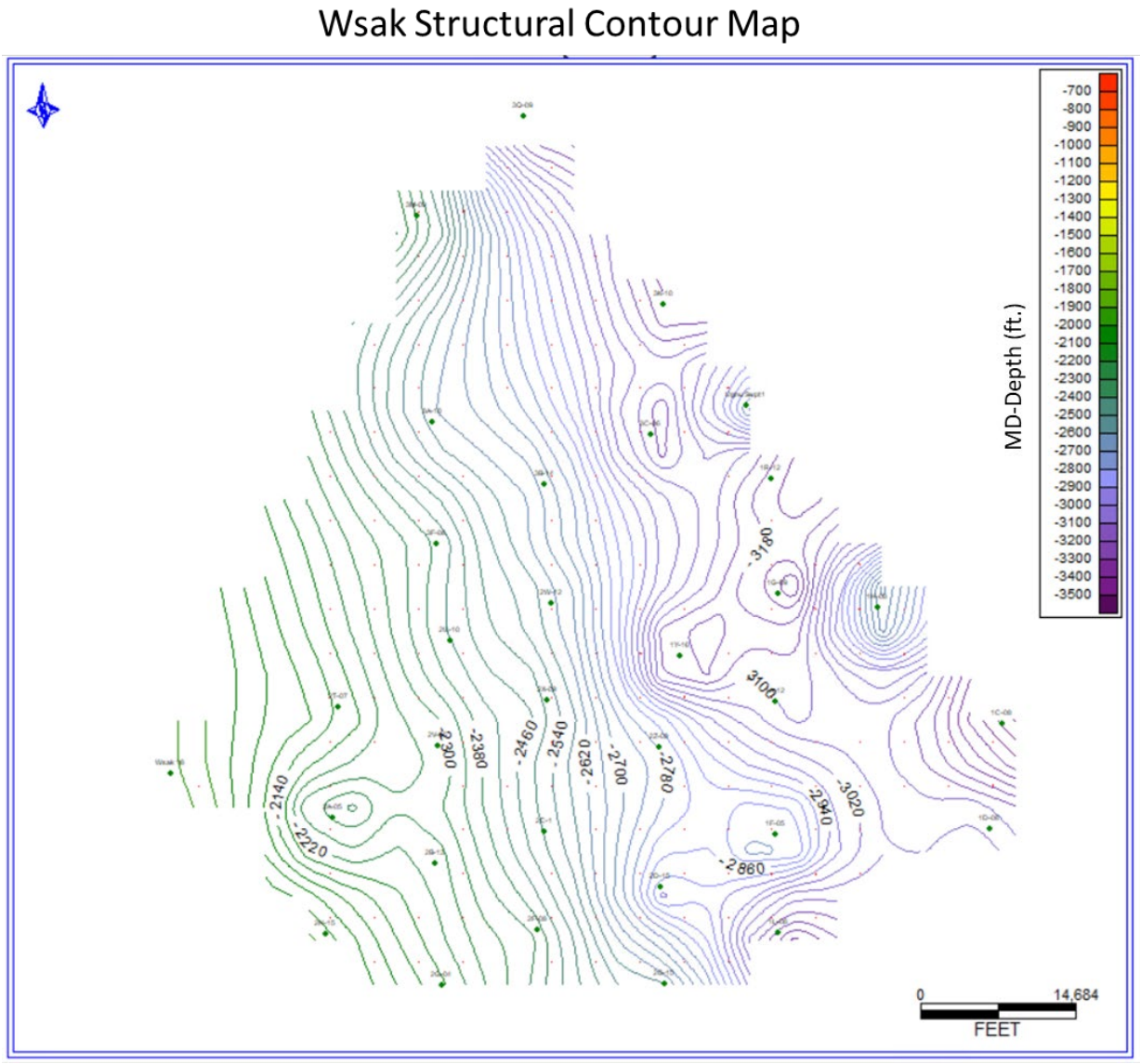

Figure 30. Structural contour map of the top of West Sak sands that dip from the southwest to the northeast section of the map.

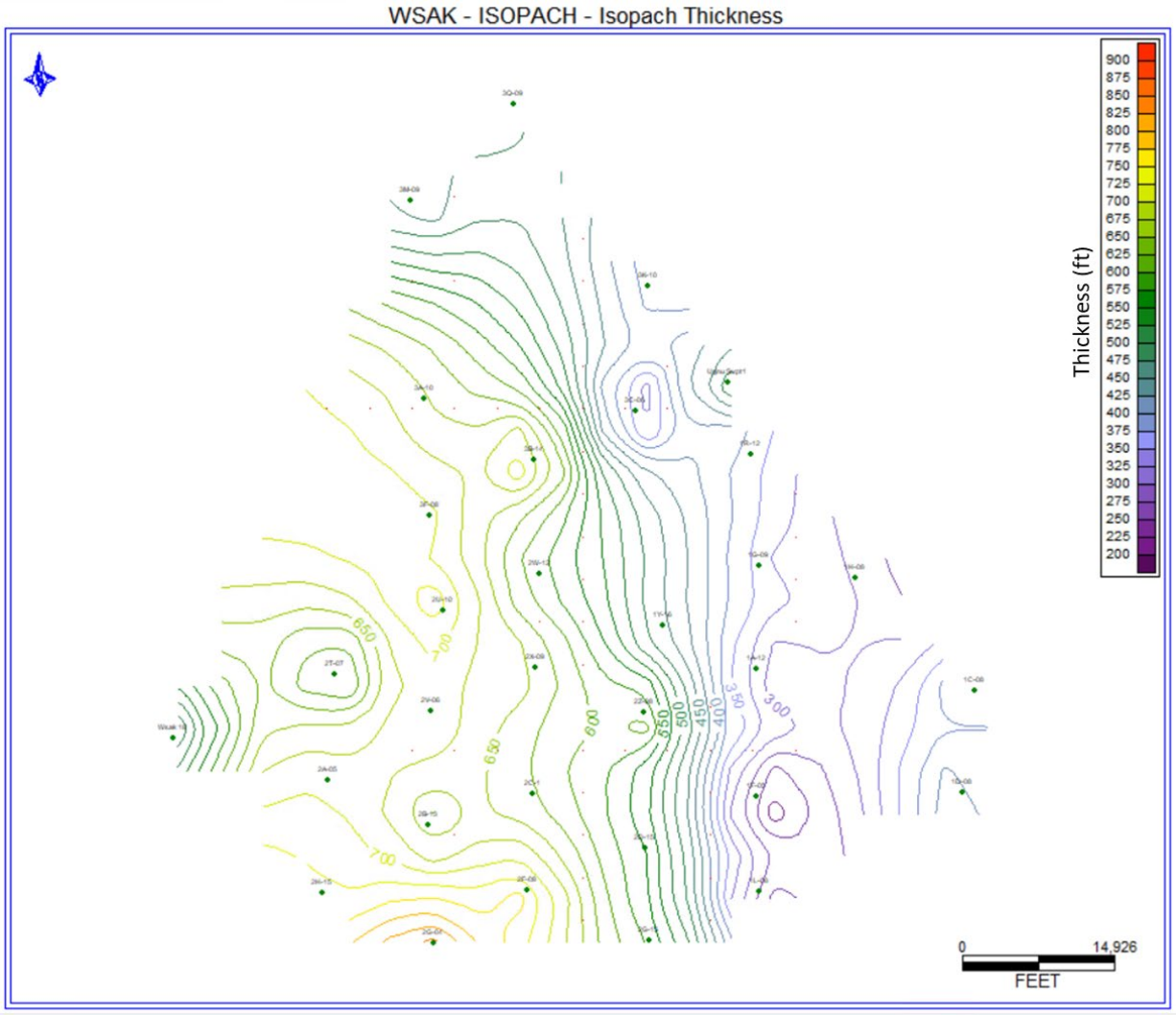

Figure 31. Isopach map of the West Sak sands showing a thinning trend from the northwest to southwest section of the map.

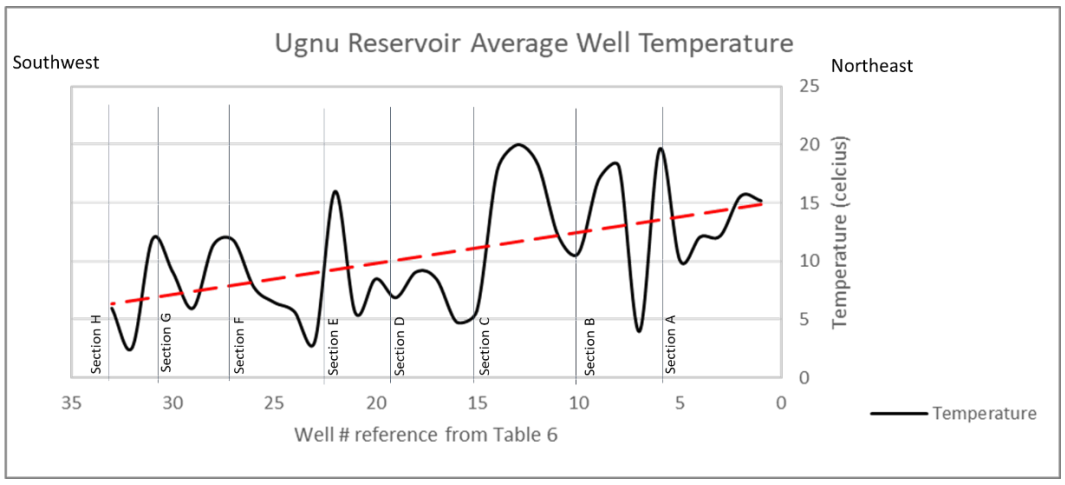

Figure 32. Temperature graphed from cross-section A-H representing the averages for the upper Ugnu reservoir. Shows a trend of warmer temperatures on the Northeastern section.

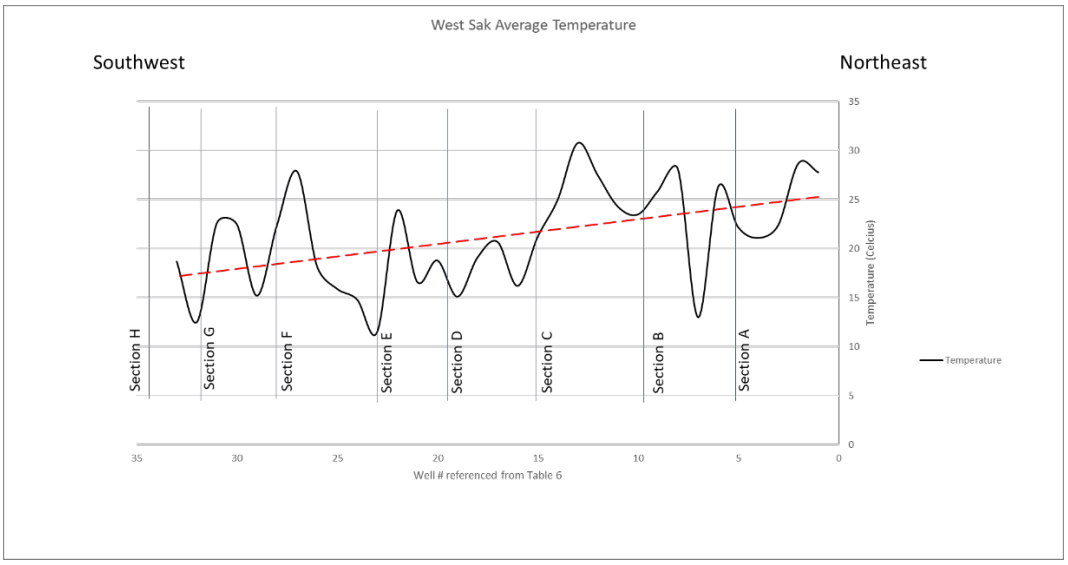

Figure 33. Temperature graphed from cross-section A-H representing the averages for the West Sak reservoir. Trend shows warmer reservoir on the northeastern section.

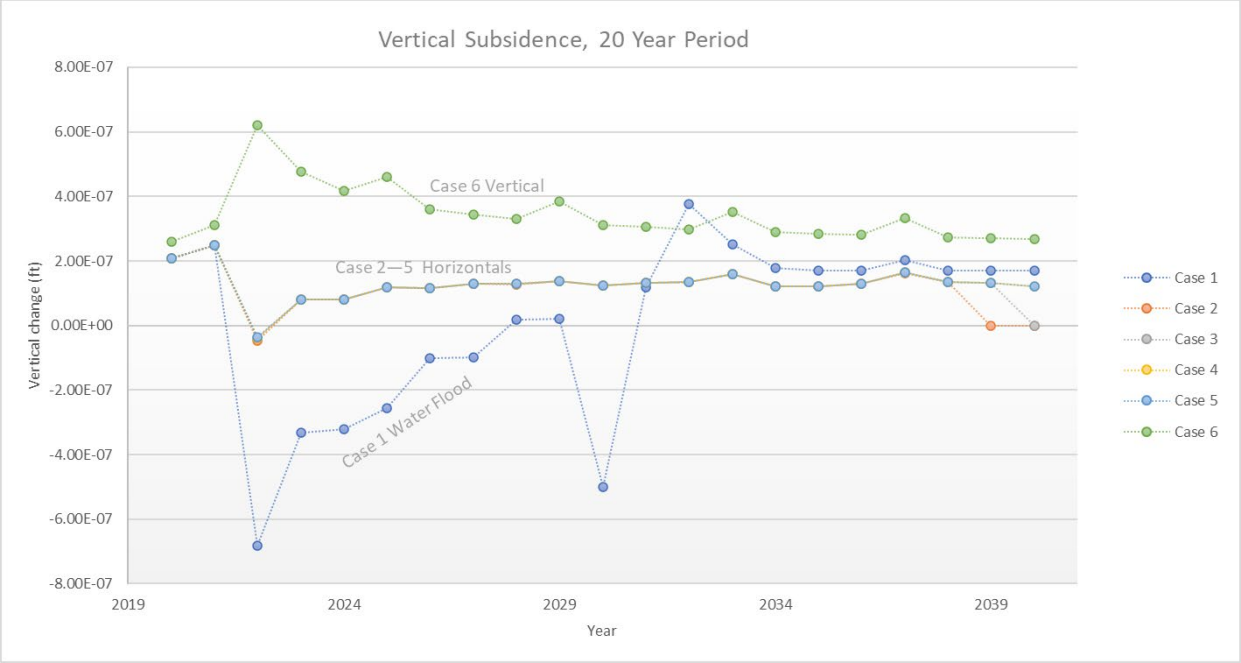

Figure 34. Case 1-6 total vertical subsidence Study area-1 West Sak reservoir, horizontal wells vs vertical wells using both waterflood and polymer flooding.

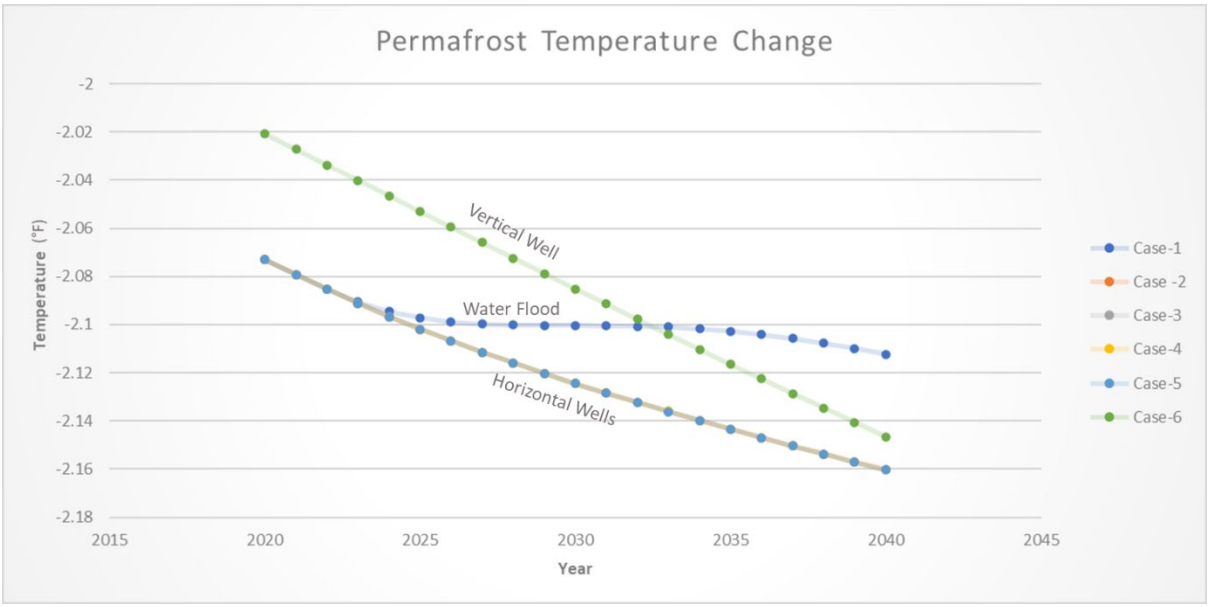

Figure 35. Case 1-6 Temperature profile Study area-1 West Sak reservoir.

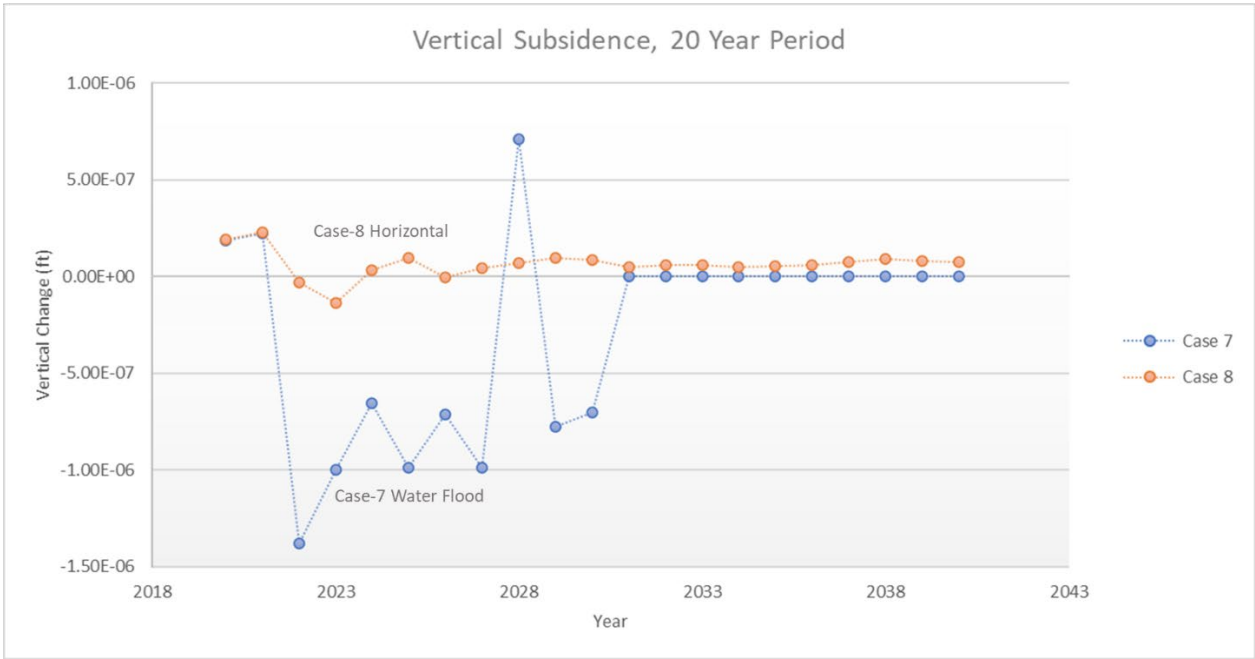

Figure 36. Case 7-8 total vertical subsidence Study area-1 Ugnu reservoir using polymer and waterflood methods.

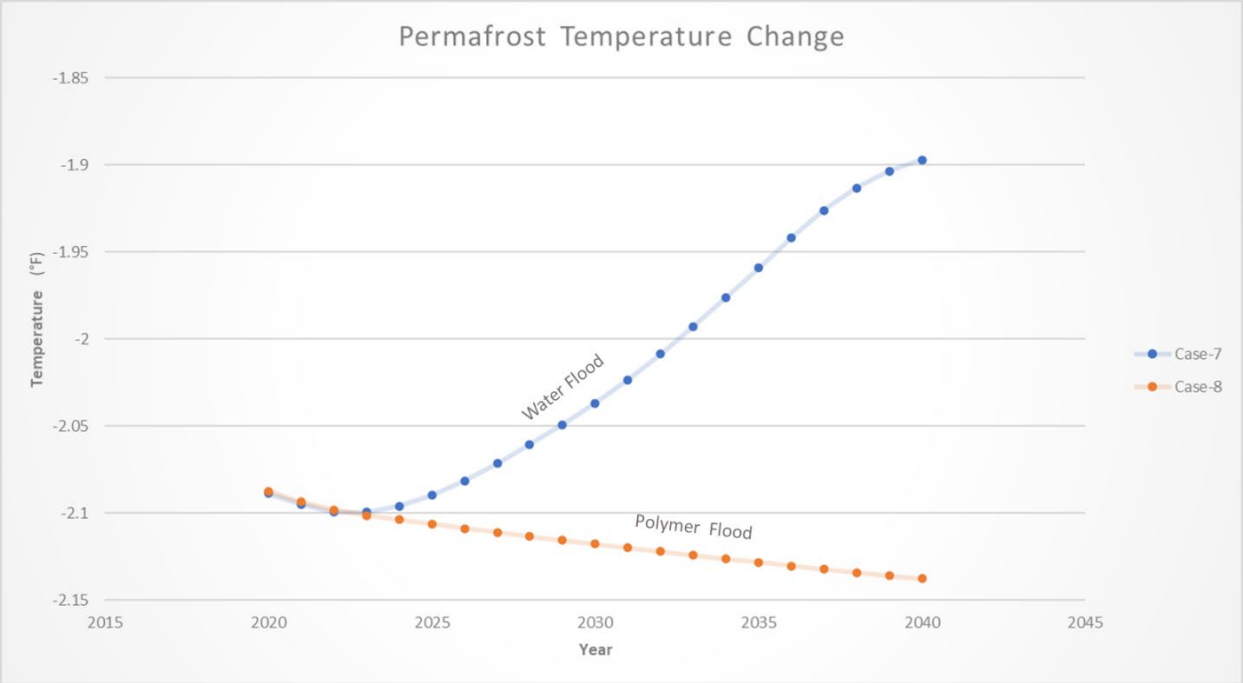

Figure 37. Case 7-8 temperature change Study area-1 Ugnu reservoir.

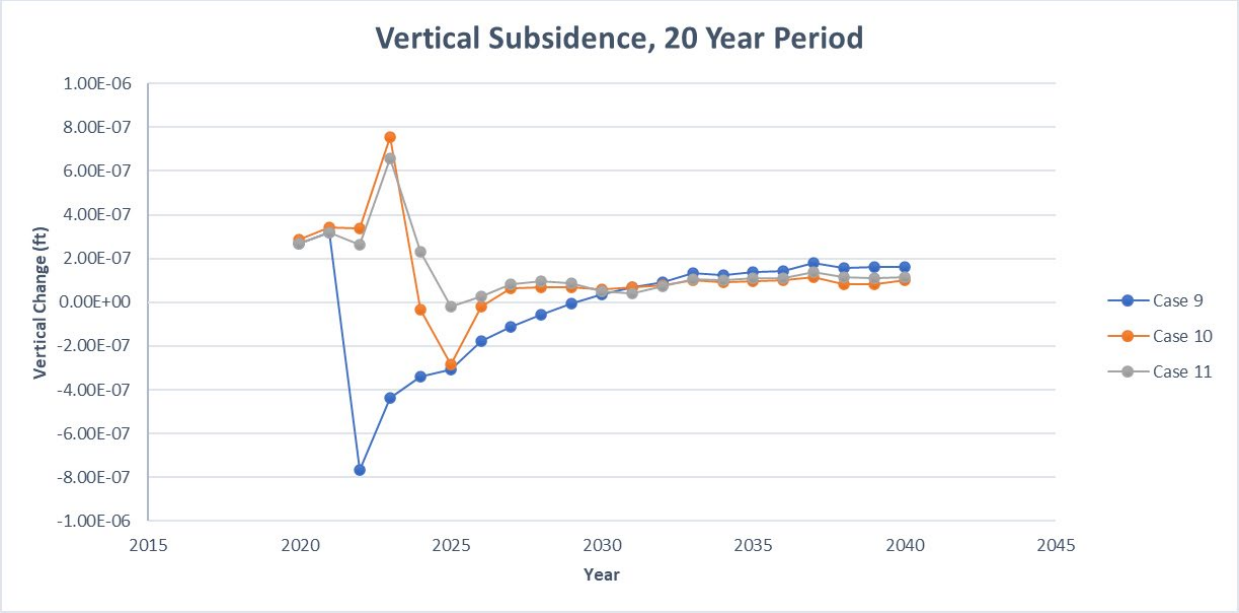

Figure 38. Case 9-11 total vertical subsidence Study area-1 West Sak reservoir using horizontals wells with waterflood and polymer injection.

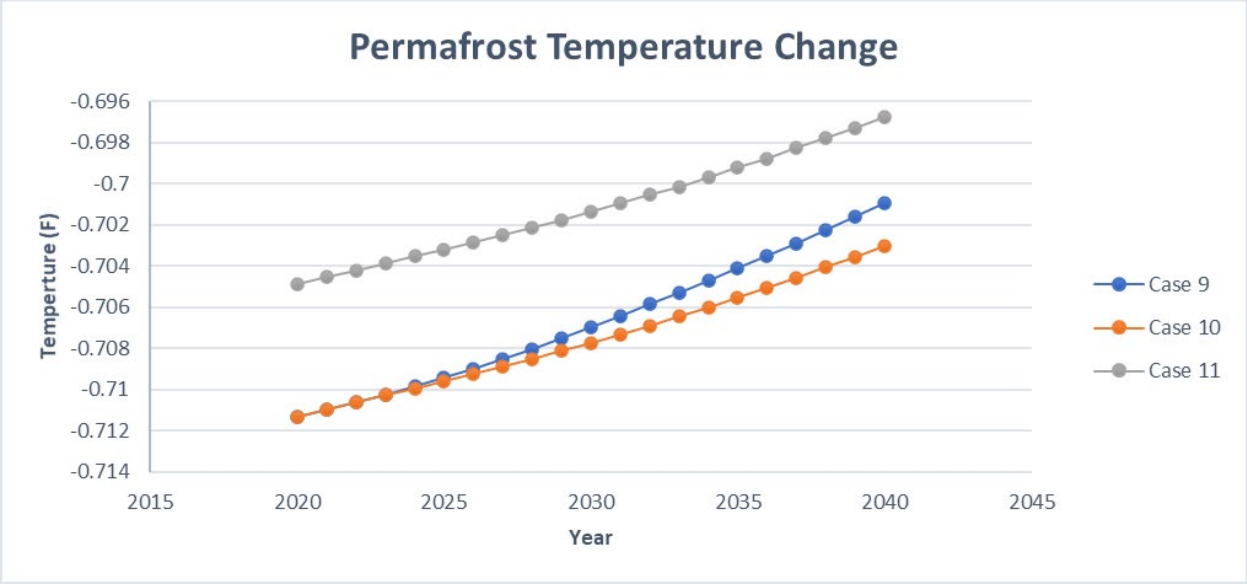

Figure 39. Case 9-11 total temperature change northeast West Sak.

TABLES

Table 1. Change in economically recoverable reserves (reserve growth) from discovery to December 31, 2007. Kuparuk River and Milne Point estimated ultimate recovery is considering advancement in technology and recovery of heavy oil from West Sak and Ugnu sands (Thompson, 2017).

Producing Field	Original Reserve Estimate (MMBO)	Estimated Ultimate Recovery (MMBO)	Difference (MMBO)	Percent Difference (%)
Prudhoe Bay	9590	14066	4476	46.7
Lisburne	400	244	-156	-39.0
Kuparuk River	600	3090	2490	415.0
Milne Point-Kuparuk	110	413	303	275.5
Endicott	375	599	224	59.7
Point Mcintyre	300	611	311	103.7
Northstar	210	210	0	0.0
Badami	120	60	-60	-50.0
Tarn	42	160	118	281.0
Alpine	430	564	134	31.2
TOTAL	**12177**	**20017**	**7840**	**64**

* MMBO - Million barrels of crude oil.

Table 2. Crude oil classification by the American Petroleum Institute Agency (API Manual, 1980).

Oil Class	°API
Light	°API $\geq$ 31.1
Medium	22.3 $\leq$ °API < 31.1
Heavy	10 $\leq$ °API < 22.3
Extra-Heavy	°API $\leq$ 10

Table 3. Static and Dynamic geomechanical properties from the Mallik and MT. Elbert deposits (Rutqvist et al., 2009).

Property	Hydrate Saturation	Static Properties	Dynamic Properties
Cohesion Cm (Mpa)	$S_h = 0$	0.5	5.0
	$S_h = 1$	2.0	20.0
Friction angle (°)	$S_h = 0$	30.0	30.0
	$S_h = 1$	30.0	30.0
Dilation angle (°)	$S_h = 0$	10.0	10.0
	$S_h = 1$	10.0	10.0
Youngs Modulus E (Gpa)	$S_h = 0$	0.5	5.0
	$S_h = 1$	1.8	18.0
Poisson's ratio v	$S_h = 0$	0.2	0.4
	$S_h = 1$	0.2	0.4

Table 4. Geomechanical properties from prior numerical simulation Wang et al (2019), modified from Rutqvist et al., 2009.

Layer (Top Down)	Subdivision/Rock Type	Geomechanical Property	Dynamic Value
1	Permafrost/silts/sand/clay	Young's Modulus E, Gpa	Yet to be calculated
		Poisson's ratio, v	0.3
2	Silty clay	Young's Modulus E, Gpa	1.7
		Poisson's ratio, v	0.28
3	Ugnu, Unconsolidated sands	Young's Modulus E, Gpa	5
		Poisson's ratio, v	0.4
		Friction Angle, degree	30
		Cohesion, Cm, Mpa	5
4	Silty clay	Young's Modulus E, Gpa	1.7
		Poisson's ratio, v	0.28
5	Wsak, Unconsolidated sands	Young's Modulus E, Gpa	5
		Poisson's ratio, v	0.4
		Friction Angle, degree	30
		Cohesion, Cm, Mpa	5
6	Silty clay	Young's Modulus E, Gpa	1.7
		Poisson's ratio, v	0.28

Table 5. Calculated reservoir properties from wireline logs (AOGCC, 2020).

Cross Section A	Ugnu				West Sak				Silt/Sand/Clay 1				Silt/Sand/Clay 2				Silt/Sand/Clay 3			
API No	Formation top (ft)	Net Thickness (ft)	K (Avg md)	Φ (Avg %)	SW (Avg %)	Formation top (ft)	Net Thickness (ft)	K (Avg md)	Φ (Avg %)	SW (Avg %)	K (Avg md)	Φ (Avg %)	SW (Avg %)	K (Avg md)	Φ (Avg %)	SW (Avg %)	K (Avg md)	Φ (Avg %)	SW (Avg %)
50029216740000	25.85	125	-	-	-	3290	480	-	-	-	-	-	-	-	-	-	-	-	-	-
50029216530000	2694	368	-	-	-	3339	360	-	-	-	-	-	-	-	-	-	-	-	-	-
50029209140000	2702	391	-	-	-	2799	499	-	-	-	-	-	-	-	-	-	-	-	-	-
50029213530000	2684	321	-	-	-	3359	348	-	-	-	-	-	-	-	-	-	-	-	-	-
50029207630000	2347	270	919.0	34.0	27.0	3219	321	918.0	33.0	38.0	410.0	33.0	34.0	513.0	32.0	24.0	145.0	25.0	28.0	
50029205850000	3000	400	839.0	32.0	23.0	3500	400	450.0	30.0	31.0	440.0	31.0	25.0	907.0	32.0	21.0	100.0	21.0	28.0	
Cross Section Avg			**879.0**	**33.0**	**25.0**			**684.0**	**31.5**	**34.5**	**425.0**	**32.0**	**29.5**	**710.0**	**32.0**	**22.5**	**122.5**	**23.0**	**28.0**	
Cross Section B	**Ugnu**				**West Sak**				**Silt/Sand/Clay 1**				**Silt/Sand/Clay 2**				**Silt/Sand/Clay 3**			
API No	Formation top (ft)	Net Thickness (ft)	K (Avg md)	Φ (Avg %)	SW (Avg %)	Formation top (ft)	Net Thickness (ft)	K (Avg md)	Φ (Avg %)	SW (Avg %)	K (Avg md)	Φ (Avg %)	SW (Avg %)	K (Avg md)	Φ (Avg %)	SW (Avg %)	K (Avg md)	Φ (Avg %)	SW (Avg %)	
50029217100000	1791	315	258.0	33.0	47.0	2357	428	378.0	33.0	41.0	300.0	36.0	66.0	556.0	34.0	35.0	1119.0	28.0	19.0	
50029210960000	2564	416	1700.0	36.0	24.0	3279	279	400.0	36.0	31.0	783.0	36.0	35.0	492.0	35.0	29.0	220.0	24.0	24.0	
50029210010000	2692	170	760.0	30.0	24.0	3675	549	450.0	27.0	36.0	870.0	35.0	26.0	600.0	30.0	27.0	300.0	25.0	25.0	
50029210660000	2237	332	837.0	32.0	27.0	3140	423	281.0	26.0	28.0	575	33	23	731	29	25	64	17	22	
Cross Section Avg			**871.8**	**32.8**	**30.5**			**376.5**	**29.0**	**32.8**	**632.0**	**34.5**	**37.5**	**593.3**	**32.0**	**29.0**	**425.8**	**23.5**	**22.5**	
Cross Section C	**Ugnu**				**West Sak**				**Silt/Sand/Clay 1**				**Silt/Sand/Clay 2**				**Silt/Sand/Clay 3**			
API No	Formation top (ft)	Net Thickness (ft)	K (Avg md)	Φ (Avg %)	SW (Avg %)	Formation top (ft)	Net Thickness (ft)	K (Avg md)	Φ (Avg %)	SW (Avg %)	K (Avg md)	Φ (Avg %)	SW (Avg %)	K (Avg md)	Φ (Avg %)	SW (Avg %)	K (Avg md)	Φ (Avg %)	SW (Avg %)	
50029214570000	1997	264	-	-	-	2682	652	-	-	-	-	-	-	-	-	-	-	-	-	
50029212870000	2036	308	-	-	-	2731	942	-	-	-	-	-	-	-	-	-	-	-	-	
50029209270000	2832	243	616.0	34.0	30.0	3626	439	300.0	27.0	29.0	375.0	33.0	30.0	216.0	28.0	31.0	251.0	26.0	22.0	
50029206880000	2860	140	775.0	33.0	26.0	3220	280	620.0	30.0	32.0	990.0	34.0	26.0	600.0	32.0	29.0	25.0	24.0	99.0	
50029204720000	2890	160	-	-	-	3456	84	-	-	-	-	-	-	-	-	-	-	-	-	
Cross Section Avg			**695.5**	**33.5**	**28.0**			**460.0**	**28.5**	**30.5**	**682.5**	**33.5**	**28.0**	**408.0**	**30.0**	**30.0**	**138.0**	**25.0**	**60.5**	
Cross Section D	**Ugnu**				**West Sak**				**Silt/Sand/Clay 1**				**Silt/Sand/Clay 2**				**Silt/Sand/Clay 3**			
API No	Formation top (ft)	Net Thickness (ft)	K (Avg md)	Φ (Avg %)	SW (Avg %)	Formation top (ft)	Net Thickness (ft)	K (Avg md)	Φ (Avg %)	SW (Avg %)	K (Avg md)	Φ (Avg %)	SW (Avg %)	K (Avg md)	Φ (Avg %)	SW (Avg %)	K (Avg md)	Φ (Avg %)	SW (Avg %)	
50029214640000	1884	248	400.0	36.0	28.0	2494	985	700.0	29.0	25.0	1100.0	40.0	35.0	393.0	32.0	30.0	420.0	20.0	18.0	
50029212400000	1965	272	-	-	-	2625	612	-	-	-	-	-	-	-	-	-	-	-	-	
50029208240000	2156	300	447.0	31.0	28.0	2835	623	445.0	31.0	32.0	-	-	-	356.0	33.0	29.0	128.0	26.0	32.0	
50029208070000	1872	461	650.0	34.0	31.0	2606	303	700.0	33.0	29.0	600.0	38.0	34.0	450.0	32.0	23.0	210.0	25.0	30.0	
Cross Section Avg			**499.0**	**33.7**	**29.0**			**615.0**	**31.0**	**28.7**	**850.0**	**39.0**	**34.5**	**399.7**	**32.3**	**27.3**	**252.7**	**23.7**	**26.7**	
Cross Section E	**Ugnu**				**West Sak**				**Silt/Sand/Clay 1**				**Silt/Sand/Clay 2**				**Silt/Sand/Clay 3**			
API No	Formation top (ft)	Net Thickness (ft)	K (Avg md)	Φ (Avg %)	SW (Avg %)	Formation top (ft)	Net Thickness (ft)	K (Avg md)	Φ (Avg %)	SW (Avg %)	K (Avg md)	Φ (Avg %)	SW (Avg %)	K (Avg md)	Φ (Avg %)	SW (Avg %)	K (Avg md)	Φ (Avg %)	SW (Avg %)	
50029213020000	1901	399	800.0	38.0	30.0	2535	443	800.0	33.0	23.0	750.0	40.0	34.0	405.0	32.0	27.0	900.0	30.0	21.0	
50029211860000	1882	280	-	-	-	2562	666	-	-	-	-	-	-	-	-	-	-	-	-	
50029211750000	2468	665	400.0	32.0	30.0	3379	251	150.0	26.0	38.0	800.0	35.0	28.0	107.0	23.0	36.0	390.0	25.0	23.0	
Cross Section Avg			**600.0**	**35.0**	**30.0**			**475.0**	**29.5**	**30.5**	**775.0**	**37.5**	**31.0**	**256.0**	**27.5**	**31.5**	**645.0**	**27.5**	**22.0**	
Cross Section F	**Ugnu**				**West Sak**				**Silt/Sand/Clay 1**				**Silt/Sand/Clay 2**				**Silt/Sand/Clay 3**			
API No	Formation top (ft)	Net Thickness (ft)	K (Avg md)	Φ (Avg %)	SW (Avg %)	Formation top (ft)	Net Thickness (ft)	K (Avg md)	Φ (Avg %)	SW (Avg %)	K (Avg md)	Φ (Avg %)	SW (Avg %)	K (Avg md)	Φ (Avg %)	SW (Avg %)	K (Avg md)	Φ (Avg %)	SW (Avg %)	
50103200690000	1701	203	-	-	-	2249	501	-	-	-	-	-	-	-	-	-	-	-	-	
50029210540000	1740	361	644.0	34.0	36.0	2365	702	670.0	31.0	27.0	600.0	37.0	38.0	390.0	29.0	34.0	-	-	-	
50029210620000	1986	176	683.0	37.0	31.0	2557	623	380.0	26.0	38.0	303.0	35.0	40.0	767.0	33.0	35.0	293.0	27.0	22.0	
50029211840000	2146	318	720.0	32.0	31.0	3067	552	163.0	24.0	21.0	800.0	37.0	36.0	300.0	27.0	34.0	400.0	19.0	24.0	
Cross Section Avg			**682.3**	**34.3**	**32.7**			**337.7**	**27.0**	**28.7**	**567.7**	**36.3**	**38.0**	**485.7**	**29.7**	**34.3**	**346.5**	**23.0**	**23.0**	
Cross Section G	**Ugnu**				**West Sak**				**Silt/Sand/Clay 1**				**Silt/Sand/Clay 2**				**Silt/Sand/Clay 3**			
API No	Formation top (ft)	Net Thickness (ft)	K (Avg md)	Φ (Avg %)	SW (Avg %)	Formation top (ft)	Net Thickness (ft)	K (Avg md)	Φ (Avg %)	SW (Avg %)	K (Avg md)	Φ (Avg %)	SW (Avg %)	K (Avg md)	Φ (Avg %)	SW (Avg %)	K (Avg md)	Φ (Avg %)	SW (Avg %)	
50103200190000	1748	145	-	-	-	2056	447	-	-	-	-	-	-	-	-	-	-	-	-	
50103200300000	2120	382	-	-	-	2713	694	-	-	-	-	-	-	-	-	-	-	-	-	
50029211380000	1805	202	-	-	-	3377	253	-	-	-	-	-	-	-	-	-	-	-	-	
50029210770000	1887	278	-	-	-	2467	954	-	-	-	-	-	-	-	-	-	-	-	-	
50029212060000	2113	302	575.0	35.0	30.0	2693	569	700.0	30.0	28.0	900.0	39.0	38.0	500.0	31.0	31.0	190.0	21.0	20.0	
Cross Section Avg			**575.0**	**35.0**	**30.0**			**700.0**	**30.0**	**28.0**	**900.0**	**39.0**	**38.0**	**500.0**	**31.0**	**31.0**	**190.0**	**21.0**	**20.0**	
Cross Section H	**Ugnu**				**West Sak**				**Silt/Sand/Clay 1**				**Silt/Sand/Clay 2**				**Silt/Sand/Clay 3**			
API No	Formation top (ft)	Net Thickness (ft)	K (Avg md)	Φ (Avg %)	SW (Avg %)	Formation top (ft)	Net Thickness (ft)	K (Avg md)	Φ (Avg %)	SW (Avg %)	K (Avg md)	Φ (Avg %)	SW (Avg %)	K (Avg md)	Φ (Avg %)	SW (Avg %)	K (Avg md)	Φ (Avg %)	SW (Avg %)	
50103200340000	1595	218	-	-	-	2125	725	-	-	-	-	-	-	-	-	-	-	-	-	
50029211670000	1738	245	-	-	-	2309	831	-	-	-	-	-	-	-	-	-	-	-	-	
Cross Section Avg			-	-	-			-	-	-	-	-	-	-	-	-	-	-	-	

Table 6. Numerical model properties.

Property	Units	Field Scale	Study-1	Study-2
Number of Blocks	I*J*K	300*300*7	150*100*7	150*150*7
Block Width (ft)	I	364.4	146.893	112.267
	J	380.9	80.594	134.41
	K	Variable	Variable	Variable
Ugnu Reservoir Temperature	° C	33	-6.11	7.2
Wsak Reservoir Temperature	° C	10.4	0	18
Oil Density	g/mol	398.12	398.12	398.12
Water Density	g/mol	18.02	18.02	18.02
Initial Reservoir Pressure	psi	1600	1600	1600
Number of Layers		7	7	7
Ugnu Reservoir Permeability	md	697	575-683	700-1700
Wsak Reservoir Permeability	md	539	337-700	400-549
Ugnu Reservoir Porosity		34	29-31	30-35
Wsak Reservoir Porosity		30	27-30	27-30
Ugnu Res Water Saturation		29	27-28	29-31
Wsak Res Water Saturation		31	27-29	29-32
Compressibility	psi	3.00E-05	3.00E-05	3.00E-05
Thermal Expansivity				
Water	° F	1.84E-04	1.84E-04	1.84E-04
Polymer	° F	1.84E-04	1.84E-04	1.84E-04
Oil	° F	4.87E-04	4.87E-04	4.87E-04

Table 7. Well geometry, includes well type, reservoir location, perforation distance, polymer concentration, elastic modulus.

Expermental Model	Well Type	Reservoir	Perforation Distance to Permafrost (ft)	Distance between Injectore & Producer	Polymer Concentration (ppm)	PV	Elastic Modulus (lb/ft^2)
Case 1	Horizontal Well	West Sak	900-1000	550	0	-	1.30E+05
Case 2	Horizontal Well	West Sak	900-1000	550	1000	0.948	1.30E+05
Case 3	Horizontal Well	West Sak	900-1000	550	1800	0.951	1.30E+05
Case 4	Horizontal Well	West Sak	900-1000	550	2000	0.957	1.30E+05
Case 5	Horizontal Well	West Sak	900-1000	550	2500	0.981	1.30E+05
Case 6	Vertical Well	West Sak	900-1000	584	1000	0.625	1.30E+05
Case 7	Horizontal Well	Ugnu	350-1000	550	0	-	1.30E+05
Case 8	Horizontal Well	Ugnu	350-1000	550	1000	0.758	1.30E+05
Case 9	Horizontal Well	Wsak north	1700	600	0	-	2.20E+05
Case 10	Horizontal Well	Wsak north	1700	600	1800	0.617	2.20E+05
Case 11	Horizontal Well	Wsak north	1700	600	2500	0.578	2.20E+05

Table 8. Wireline log and completion reports derived data showing reservoir tops and estimated depths to TVD of the permafrost zone, Ugnu and West Sak sands (AOGCC, 2020).

API No	Ugnu Sands		West Sak Sands		Permafrost
	Reservoir top (ft)	Net Thickness (ft)	Reservoir top (ft)	Net Thickness (ft)	Bottom (ft)
5002921674	2585	125	3290	480	1700
5002921653	2694	368	3339	360	1721
5002920914	2202	391	2799	499	1610
5002921353	2684	321	3359	348	1600
5002920763	2347	270	3219	321	1732
5002920585	3000	400	3500	400	1734
5002921710	1791	315	2357	428	1670
5002921096	2564	416	3279	279	1610
5002921001	2692	170	3075	549	1635
5002920266	2237	332	3140	423	1610
5002921457	1997	264	2682	652	1610
5002921287	2036	308	2731	942	1616
5002920927	2832	243	3626	439	1350
5002920688	2860	140	3220	280	1550
5002920472	2890	160	3456	84	1500
5002921464	1884	248	2494	985	1600
5002921240	1965	272	2625	612	1519
5002920924	2156	300	2835	623	1534
5002920807	1872	461	2606	303	1565
5002921302	1901	399	2535	443	1550
5002921186	1882	280	2562	665	1500
5002921175	2468	665	3379	251	1450
5010320069	1701	203	2249	501	1550
5002921054	1740	361	2365	702	1429
5002920962	1986	176	2557	623	1526
5002921184	2146	318	3067	552	1500
5010320019	1748	145	2056	447	1505
5010320030	2120	382	2713	694	1550
5002921138	1805	202	3377	253	1500
5002921077	1887	278	2467	954	1400
5002921206	2113	302	2693	569	1470
5010320034	1595	218	2125	725	1500
5002921167	1738	245	2309	831	1450

Table 9. Wellbore temperature calculation indicating an increase in temperature towards the northeast vs the southwest in both the Ugnu and West Sak reservoir (AOGCC, 2020).

API No	Cross Section	Ugnu Reservoir (ft) Avg (°C)	West Sak Reservoir (ft) Avg (°C)
5002921674	A	15.2	27.8
5002921653	A	15.6	28.7
5002920914	A	12.2	22.4
5002921353	A	12.1	21.1
5002920763	A	10.1	22.2
5002920585	A	19.6	26.3
Average		**14.1**	**24.8**
5002921710	B	4.0	13.0
5002921096	B	18.1	28.1
5002921001	B	17.0	25.9
5002920266	B	10.7	23.5
Average		**12.5**	**22.6**
5002921457	C	12.2	24.3
5002921287	C	18.3	27.5
5002920927	C	20.0	30.8
5002920688	C	17.8	25.0
5002920472	C	5.8	21.2
Average		**14.8**	**25.8**
5002921464	D	4.8	16.2
5002921240	D	8.5	20.7
5002920924	D	9.1	19.1
5002920807	D	6.9	15.1
Average		**7.3**	**17.8**
5002921302	E	8.5	18.8
5002921186	E	5.6	16.6
5002921175	E	16.0	23.9
Average		10.0	19.8
5010320069	F	3.1	11.5
5002921054	F	5.7	14.8
5002920962	F	6.5	15.9
5002921184	F	7.8	18.2
Average		**5.8**	**15.1**
5010320019	G	11.8	27.9
5010320030	G	11.4	22.4
5002921138	G	6.0	15.2
5002921077	G	9.1	22.5
5002921206	G	11.9	22.6
Average		**10.0**	**22.1**
5010320034	H	2.6	12.5
5002921167	H	6.0	18.7
Average		**4.3**	**15.6**

Table 10. Average permafrost temperatures calculated from average surface temperature with respect to wireline and completion depth reports. There was no difference across the field.

Surface - 500 (ft) Avg (°C)	500 - 1000 (ft) Avg (°C)	1000 - Permafrost Bottom (ft) Avg (°C)
-9.0	-6.0	-2.0

Table 11. Calculated variables used to build the mesh grids for the seven layers in the numerical field scale model.

Cross Section	Well	X	Y	Surface Top (ft)	K	Φ	Water Saturation	Temperature (°F)	Permafrost Thickness (ft)
E	184162	1658944.39	5970913.48	77	260.5	0.43	0.79	-2.3	1423
F	183083	1658655.65	5958522.40	67	225.0	0.44	0.66	-2.0	1459
F	183179	1648735.29	5966601.14	78	400.0	0.46	0.67	-1.7	1351
F	186108	1639361.85	5970118.16	41	260.5	0.43	0.79	-1.8	1509
G	184021	1658082.87	5949250.54	24	260.5	0.43	0.79	-1.9	1376
G	184104	1648459.82	5955469.78	84	260.5	0.43	0.79	-2.1	1416
G	181028	1623623.25	5963932.91	85	260.5	0.43	0.79	-1.9	1420
G	184067	1638757.61	5959819.54	94	260.5	0.43	0.79	-2.0	1456
H	184141	1649066.19	5944056.42	104	260.5	0.43	0.79	-2.1	1346
Cross Section	Well	X	Y	Silt 1	K	ϕ	Water Saturation	Temperature (°F)	Silt 1 Thickness (ft)
E	184162	1658944.39	5970913.48	1500	775.0	0.375	0.31	11.7	459
F	183083	1658655.65	5958522.40	1526	600.0	0.371	0.38	12.8	527
F	183179	1648735.29	5966601.14	1429	600.0	0.369	0.38	10.3	388
F	186108	1639361.85	5970118.16	1550	567.7	0.363	0.38	13.6	192
G	184021	1658082.87	5949250.54	1400	900.0	0.391	0.38	9.3	511
G	184104	1648459.82	5955469.78	1500	900.0	0.389	0.38	11.9	389
G	181028	1623623.25	5963932.91	1505	900.0	0.393	0.38	12.3	328
G	184067	1638757.61	5959819.54	1550	900.0	0.385	0.38	13.4	664
H	184141	1649066.19	5944056.42	1450	690.3	0.36	0.34	10.5	392
Cross Section	Well	X	Y	Ugnu top (ft)	K	ϕ	Water Saturation	Temperature (°F)	Ugnu Thickness
E	184162	1658944.39	5970913.48	1882	600.0	0.35	0.30	24.8	280
F	183083	1658655.65	5958522.40	1986	683.0	0.37	0.31	27.7	176
F	183179	1648735.29	5966601.14	1739	644.0	0.34	0.36	20.7	362
F	186108	1639361.85	5970118.16	1701	682.3	0.34	0.33	19.7	203
G	184021	1658082.87	5949250.54	1887	575.0	0.35	0.30	24.9	278
G	184104	1648459.82	5955469.78	1805	575.0	0.35	0.30	22.6	202
G	181028	1623623.25	5963932.91	1748	575.0	0.35	0.30	21.0	145
G	184067	1638757.61	5959819.54	2120	575.0	0.35	0.30	31.4	382
H	184141	1649066.19	5944056.42	1738	686.1	0.34	0.29	20.7	245
Cross Section	Well	X	Y	Silt 2	K	ϕ	Water Saturation	Temperature (°F)	Silt 2 Thick
E	184162	1658944.39	5970913.48	2162	256.0	0.28	0.32	32.6	400
F	183083	1658655.65	5958522.40	2162	390.0	0.29	0.34	32.6	394
F	183179	1648735.29	5966601.14	2101	390.0	0.29	0.34	30.9	263
F	186108	1639361.85	5970118.16	1904	485.7	0.30	0.34	25.4	345
G	184021	1658082.87	5949250.54	2165	500.0	0.31	0.31	32.7	302
G	184104	1648459.82	5955469.78	2007	500.0	0.31	0.31	28.3	343
G	181028	1623623.25	5963932.91	1893	500.0	0.31	0.31	25.1	163
G	184067	1638757.61	5959819.54	2502	500.0	0.31	0.31	42.2	211
H	184141	1649066.19	5944056.42	1983	478.9	0.31	0.29	27.6	326
Cross Section	Well	X	Y	Wsak Top	K	ϕ	Water Saturation	Temperature (°F)	Wsak Thick
E	184162	1658944.39	5970913.48	2562	475.0	0.30	0.31	43.8	665
F	183083	1658655.65	5958522.40	2556	180.0	0.26	0.38	43.7	624
F	183179	1648735.29	5966601.14	2364	670.0	0.31	0.27	38.3	703
F	186108	1639361.85	5970118.16	2249	337.7	0.27	0.29	35.1	501
G	184021	1658082.87	5949250.54	2467	700.0	0.31	0.28	41.2	954
G	184104	1648459.82	5955469.78	2350	700.0	0.30	0.28	37.9	620
G	181028	1623623.25	5963932.91	2056	700.0	0.30	0.28	29.6	447
G	184067	1638757.61	5959819.54	2713	700.0	0.30	0.28	48.1	694
H	184141	1649066.19	5944056.42	2309	521.2	0.30	0.31	36.7	831
Cross Section	Well	X	Y	Silt 3	K	ϕ	Water Saturation	Temperature (°F)	Silt 3 Thick
E	184162	1658944.39	5970913.48	3227	645.0	0.28	0.22	62.5	2134
F	183083	1658655.65	5958522.40	3180	346.5	0.23	0.23	61.2	2644
F	183179	1648735.29	5966601.14	3067	346.5	0.23	0.23	58.0	2715
F	186108	1639361.85	5970118.16	2750	346.5	0.23	0.23	49.1	3023
G	184021	1658082.87	5949250.54	3421	190.0	0.21	0.20	68.0	1651
G	184104	1648459.82	5955469.78	2970	190.0	0.22	0.20	55.3	2469
G	181028	1623623.25	5963932.91	2503	190.0	0.22	0.20	42.2	3517
G	184067	1638757.61	5959819.54	3407	190.0	0.21	0.20	67.6	1906
H	184141	1649066.19	5944056.42	3140	302.9	0.24	0.29	60.1	2807
Cross Section	Well	X	Y	Kuparuk	K	ϕ	Water Saturation	Temperature (°F)	Kup thick
E	184162	1658944.39	5970913.48	5361	475.0	0.30	0.31	122.4	696
F	183083	1658655.65	5958522.40	5824	180.0	0.26	0.38	135.4	221
F	183179	1648735.29	5966601.14	5782	670.0	0.31	0.27	134.2	267
F	186108	1639361.85	5970118.16	5773	337.7	0.27	0.29	134.0	986
G	184021	1658082.87	5949250.54	5072	700.0	0.31	0.28	114.3	1028
G	184104	1648459.82	5955469.78	5439	700.0	0.30	0.28	124.6	751
G	181028	1623623.25	5963932.91	6020	700.0	0.30	0.28	140.9	482
G	184067	1638757.61	5959819.54	5313	700.0	0.30	0.28	121.1	661
H	184141	1649066.19	5944056.42	5947	521.2	0.30	0.31	138.9	395

Table 12. Vertical subsidence and temperature results.

Expermental Model	Well Type	Polymer Concentration (ppm)	Vertical Subsidence (Gain/Loss, ft)	Permafrost Temperature (Increase/Decrease, °F)
Case 1	Horizontal	0	-8.52E-09	Decrease -2.50e-02
Case 2	Horizontal	1000	-1.15E-07	Decrease -4.85e-02
Case 3	Horizontal	1800	-1.22E-07	Decrease -4.85e-02
Case 4	Horizontal	2000	-1.28E-07	Decrease -4.86e-02
Case 5	Horizontal	2500	-1.29E-07	Decrease -4.86e-02
Case 6	Vertical	1000	-8.37E-08	Decrease -6.38e-02
Case 7	Horizontal	0	-4.77E-07	Increase 6.92e-02
Case 8	Horizontal	1000	-1.28E-07	Decrease -2.91e-02
Case 9	Horizontal	0	-2.78E-07	Increase 4.6e-03
Case 10	Horizontal	1800	-1.65E-07	Increase 3.8e-03
Case 11	Horizontal	2500	-1.20E-07	Increase 3.7e-03
Wang et al., 2019				
Case 1	Horizontal	1800	0.61	Increase 1.78
Case 2	Horizontal	2150	0.81	Increase 3.21
Case 3	Horizontal	2500	0.96	Increase 4.52
Case 4	Vertical	1800	1.47	Increase 1.75
Case 5	Vertical	2150	1.49	Increase 3.17
Case 6	Vertical	2500	1.50	Increase 4.47

Appendix A

Table A1. Logs-derived data for selected wells in the West Sak Sands (Panda et al., 1989).

Well Name	Interval* (ft)	Weighted Mean Effective Porosity (%)	Weighted Mean Water Saturation (%)	Net Pay Thickness (ft)	Net to Gross Ratio
West Sak No 1	3746-4044	34.6	32.5	116	0.39
West Sak No. 2	3304-3530	28.7	19.0	84	0.37
West Sak No 3	2628-2882	29.95	33.6	41	0.16
West Sak No. 5	3332-3428	26.8	18.0	12	0.13
West Sak No. 9	2678-2930	35.5	42.2	50	0.20
West Sak No 8-10	2695-3174	37.6	41.9	55	0.11
West Sak No. 11	2324-2694	28.6	44.3	27	0.07
West Sak No. 17	3516-3620	15.8	31.3	12	0.12
West Sak No. 18	2526-2720	36.3	38.3	13	0.07
East Ugnu No. 1	3386-3654	32.6	44.2	27	0.10
Kuparuk No 1G-7	3408-3638	24.8	34.6	64	0.28
Kuparuk No. 3B-14	2538-3025	38.3	41.0	136	0.28
Milne Pt No N-1B	3555-3806	24.2	24.1	56	0.22

* Represents interval that is potentially hydrocarbon bearing. Properties of individual West Sak sand members are listed in Tables 2-6.

Table 2A. Petrophysical properties of West Sak lower sands 1 (Panda et al., 1989)

Well Name	Interval (ft)	Net Pay (ft)	Average ϕ (%)	Average Sw (%)
West Sak No. 1	3860-3874	11	35.6	38.7
West Sak No. 2	3428-3434	5	28.3	16.5
West Sak No. 3	2753-2772	-	-	-
West Sak No. 5	No log data	available		
West Sak No. 9	2852-2860	6	33.5	40.5
West Sak No. 8-10	2934-2945	3	33.7	45.3
West Sak No. 11	2566-2575	-	23.9	59.3
West Sak No. 17	3714-3722	-	16.9	79.8
West Sak No. 18	2526-2536	4	36.4	35.4
East Ugnu No. 1	3511-3530	5	33.6	42.2
Kuparuk No. 1G-7	3533-3540	2	21.1	46.2
Kuparuk No. 3B-14	2698-2740	37	39.8	40.5
Milne Pt. No. N-1B	3677-3684	4	16.9	37.1

Appendix A, Continued

Table 3A. Petrophysical properties of West Sak upper Sands (Panda et al., 1989).

	SAND 1				SAND 2			
Well Name	Interval (ft)	Net Pay (ft)	Average ϕ (%)	Average Sw (%)	Interval (ft)	Net Pay (ft)	Average ϕ (%)	Average Sw (%)
West Sak No. 1	3746-3784	32	33.3	26.4	3810-3844	34	34.8	32.9
West Sak No. 2	3304-3334	30	29.2	9.1	3364-3404	37	29.2	13.8
West Sak No. 3	2628-2672	18	30.3	27.6	2706-2734	10	25.2	36.6
West Sak No. 5	3332-3374	10	27.0	18.1	3410-3428	1	24.5	17.5
West Sak No. 9	2678-2716	33	36.5	43.0	2770-2786	9	33.6	39.7
West Sak No. B-10	2695-2747	7	35.4	37.5	2804-2860	12	38.1	40.1
West Sak No. 11	2324-2364	17	27.7	43.5	2402-2432	9	30.7	45.2
West Sak No. 17	3516-3558	4	17.8	27.5	3597-3620	8	14.8	33.5
West Sak No. 18	No log data	available			No log data	available		
East Ugnu No. 1	3386-3424	8	34.0	42.5	3459-3490	14	31.6	45.5
Kuparuk No. 1G-7	3408-3455	23	28.1	36.6	3477-3512	27	21.9	30.7
Kuparuk No. 3B-14	2538-2559	21	40.0	37.1	2575-2613	36	39.1	42.8
Milne Pt. No. N-1B	3555-3570	10	21.3	32.1	3582-3617	20	32.8	19.0

Table 4A. Petrophysical properties of West Sak lower sands 2 (Panda et al., 1989).

Well Name	Interval (ft)	Net Pay (ft)	Average ϕ (%)	Average Sw (%)
West Sak No. 1	3930-3940	9	36.7	33.2
West Sak No. 2	3456-3460	4	31.8	18.4
West Sak No. 3	2796-2806	4	31.8	38.1
West Sak No. 5	No log data	available		
West Sak No. 9	2892-2904	1.5	35.4	47.9
West Sak No. B-10	3048-3076	20	37.9	41.2
West Sak No. 11	2630-2638	-	20.7	67.7
West Sak No. 17	3770-3790	-	16.9	79.8
West Sak No. 18	2612-2618	3	35.5	42.0
East Ugnu No. 1	3622-3654	2	31.6	47.7
Kuparuk No. 1G-7	3588-3605	5	26.8	38.3
Kuparuk No. 3B-14	2774-2807	29	39.8	42.7
Milne Pt. No. N-1B	3719-3750	12	17.2	26.1

Appendix A, Continued

Table 5A. Petrophysical properties of West Sak lower sands 3 (Panda et al., 1989).

Well Name	Interval (ft)	Net Pay (ft)	Average ϕ (%)	Average *Sw* (%)
West Sak No. 1	3972-3984	6	39.2	42.0
West Sak No. 2	3472-3476	4	28.9	20.3
West Sak No. 3	2815-2824	1	29.6	46.1
West Sak No. 5	No log data	available		
West Sak No. 9	2918-2930	0.5	31.3	44.8
West Sak No. B-10	3112-3132	11	37.7	45.8
West Sak No. 11	2688-2694	2	27.8	47.5
West Sak No. 17	3836-3844	-	18.3	79.8
West Sak No. 18	2692-2720	6	36.7	38.5
East Ugnu No. 1	-	-	-	-
Kuparuk No. 1G-7	3637-3658	8	24.6	35.6
Kuparuk No. 3B-14	2898-2907	2	26.6	49.8
Milne Pt. No. N-18	3786-3806	11	21.3	26.3

Table 6A. Petrophysical properties of West Sak lower sands 4 (Panda et al., 1989).

Well Name	Interal (ft)	Net Pay (ft)	Avg ϕ (%)	Avg SW (%)
Wsak no 1	4032-4044	4	27.6	45.8
Wsak no 2	3524-3530	4	29.8	14.5
Wsak no 3	2872-2882	8	31.3	41.3
Wsak no 5	-	-	-	-
Wsak no 9	-	-	-	-
Wsak no 8-10	3167-3174	4	45.2	43.8
Wsak no 11	2726-2730	-	18.9	67.3
Wsak no 17	3969-3974	-	13.4	91.3
Wsak no 18	-	-	-	-
East Ugnu no 1	-	-	-	-
Kuparuk 1G-7	-	-	-	-
Kuparuk 3B-14	2941-2969	6	26.8	42.8
Milne Pt no N-18	2888-3905		10.1	71

Appendix B

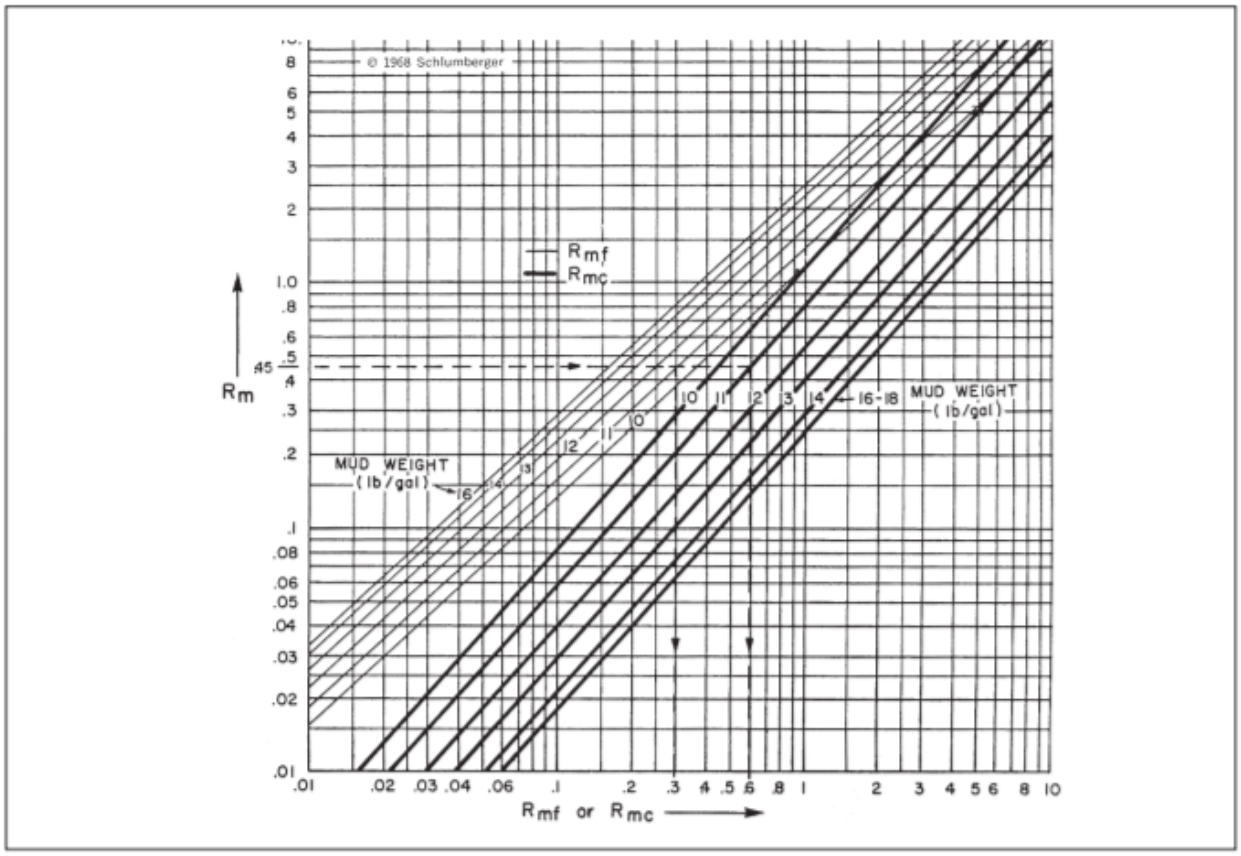

Figure 1B. Chart used to estimate Rmf from Rm located at the top of the wireline log header taken from schlumberger in (Hartmann et al., 1999).

Appendix B, Continued

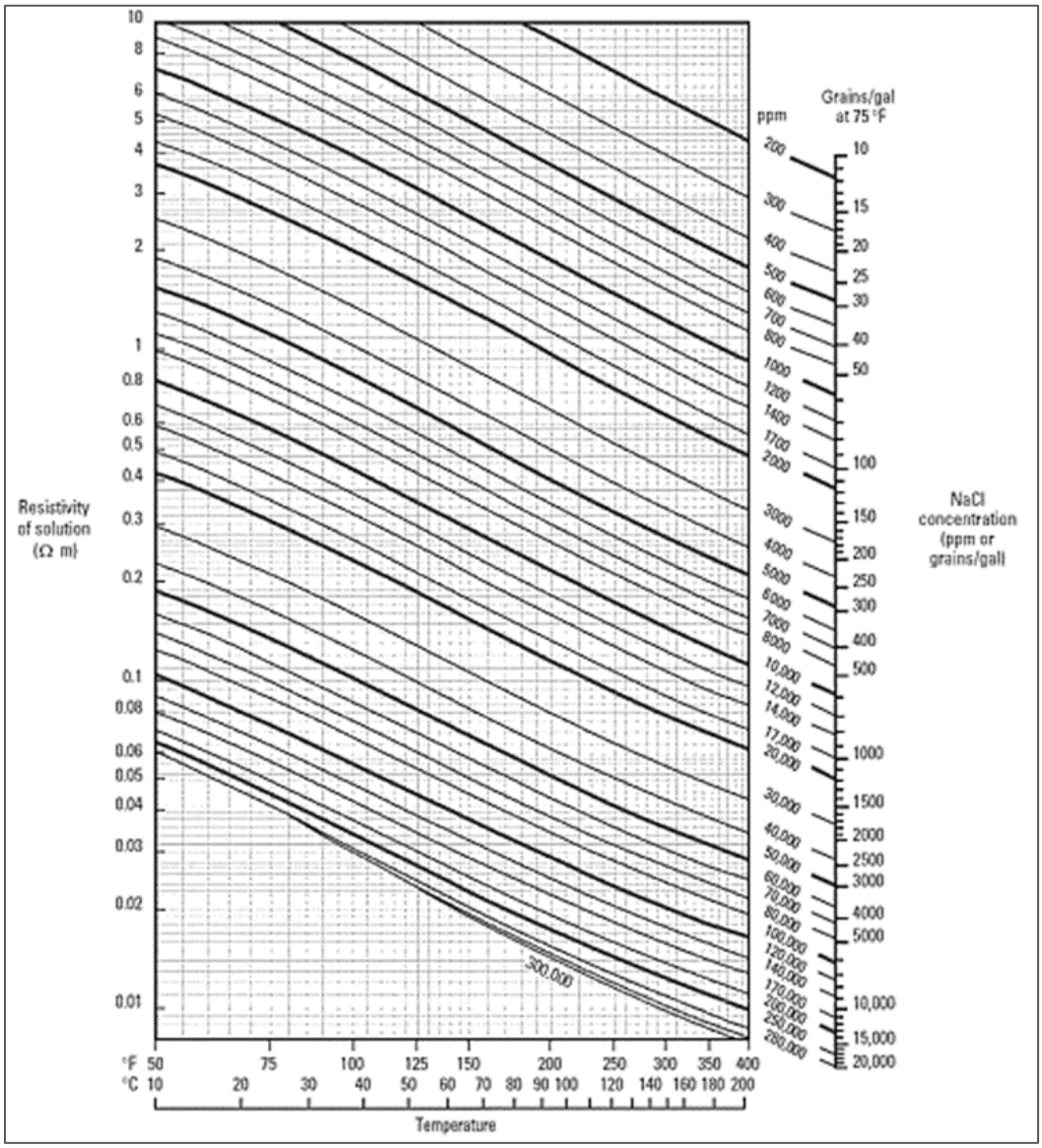

Figure 2B. Chart used to convert Rmf to reservoir temperature take from Schlumberger and modified by Hartmann et al (1999).

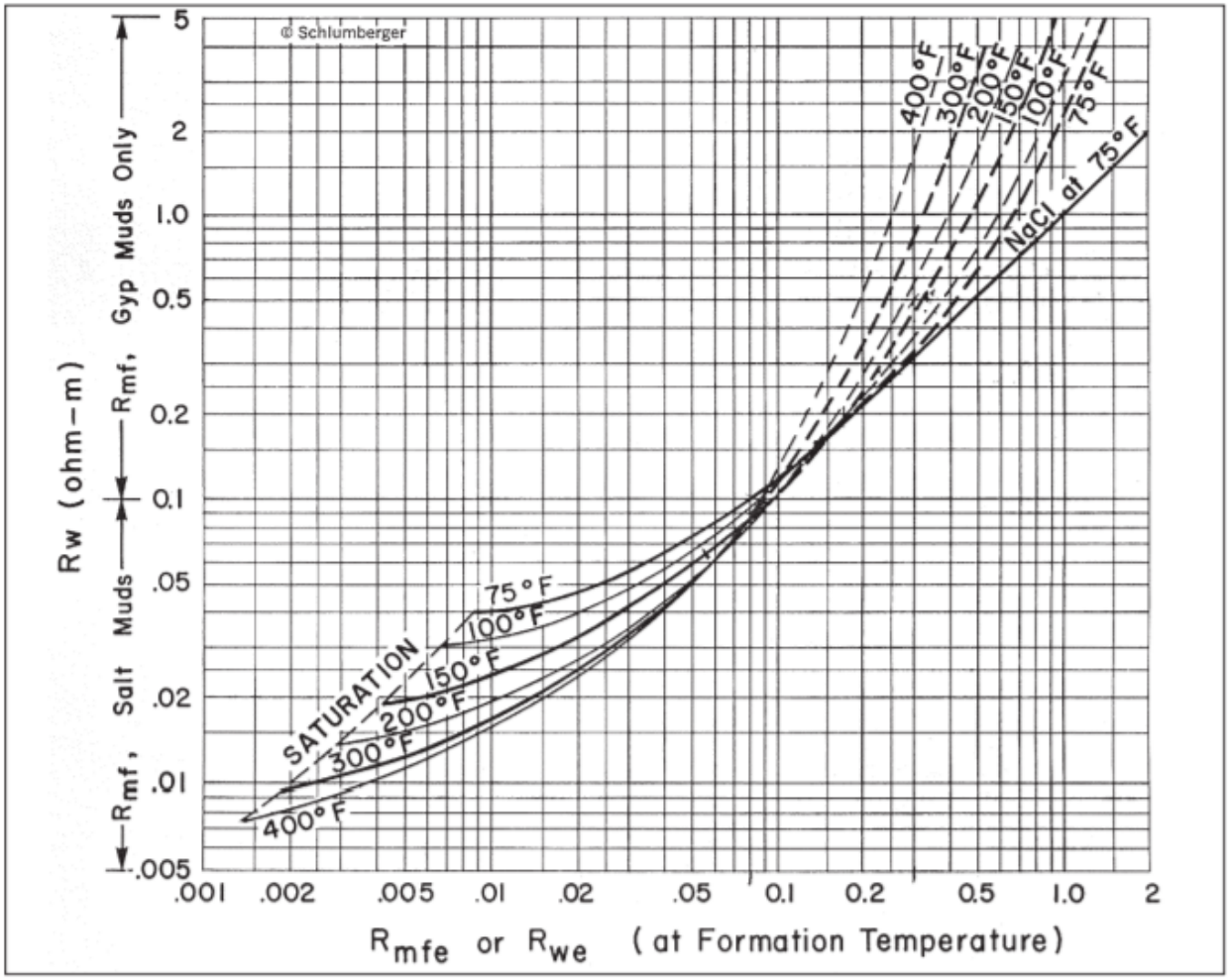

Figure 3B. Chart used to convert Rmf to Rmf_{eq} taken from Schlumberger and modified by Hartmann et al (1999).

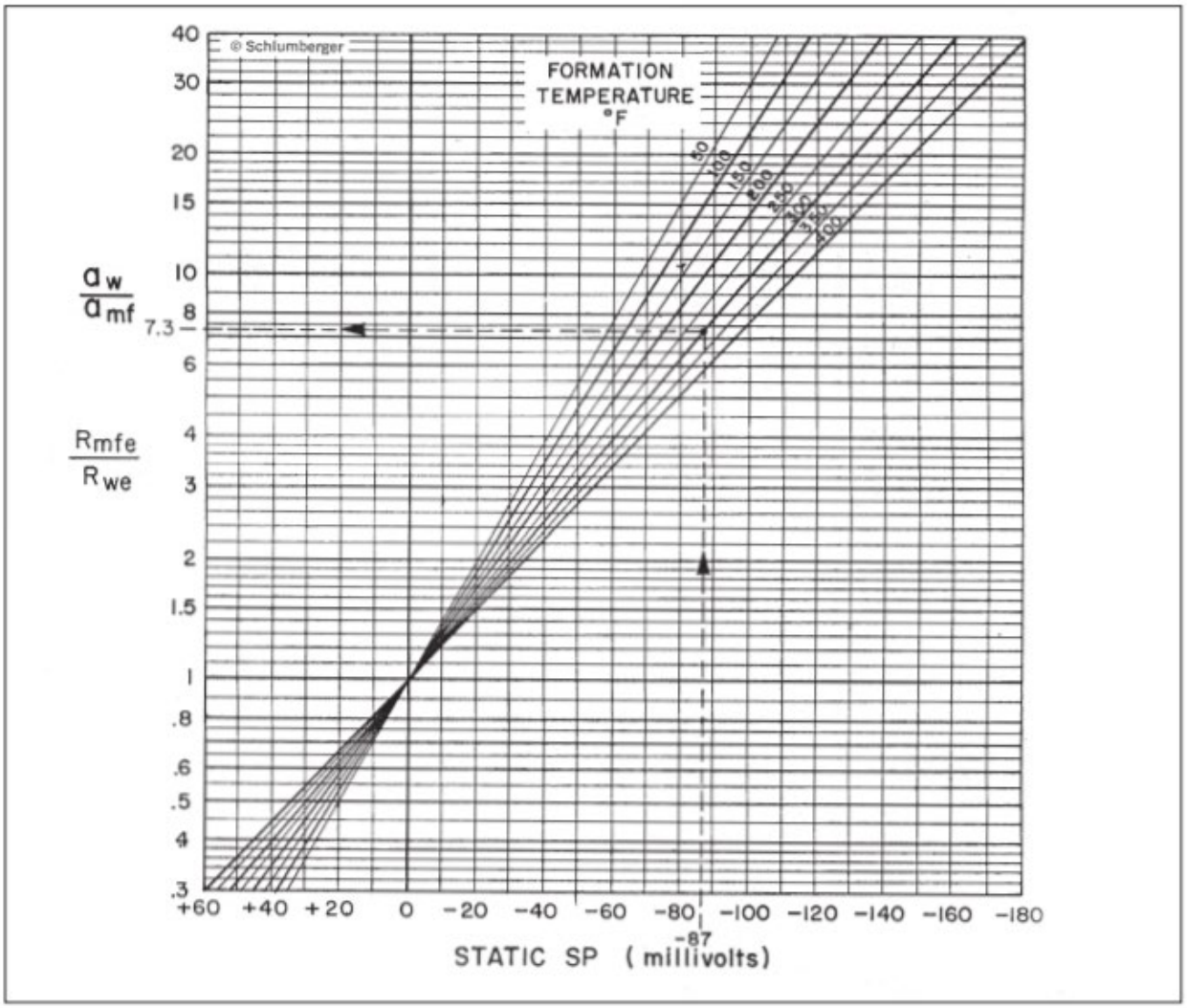

Figure 4B. Chart allows for converting SP from the zone of interest to equivalent formation water resistivity R_{we} taken from Schlumberger and modified by Hartmann et al (1999).

Appendix C

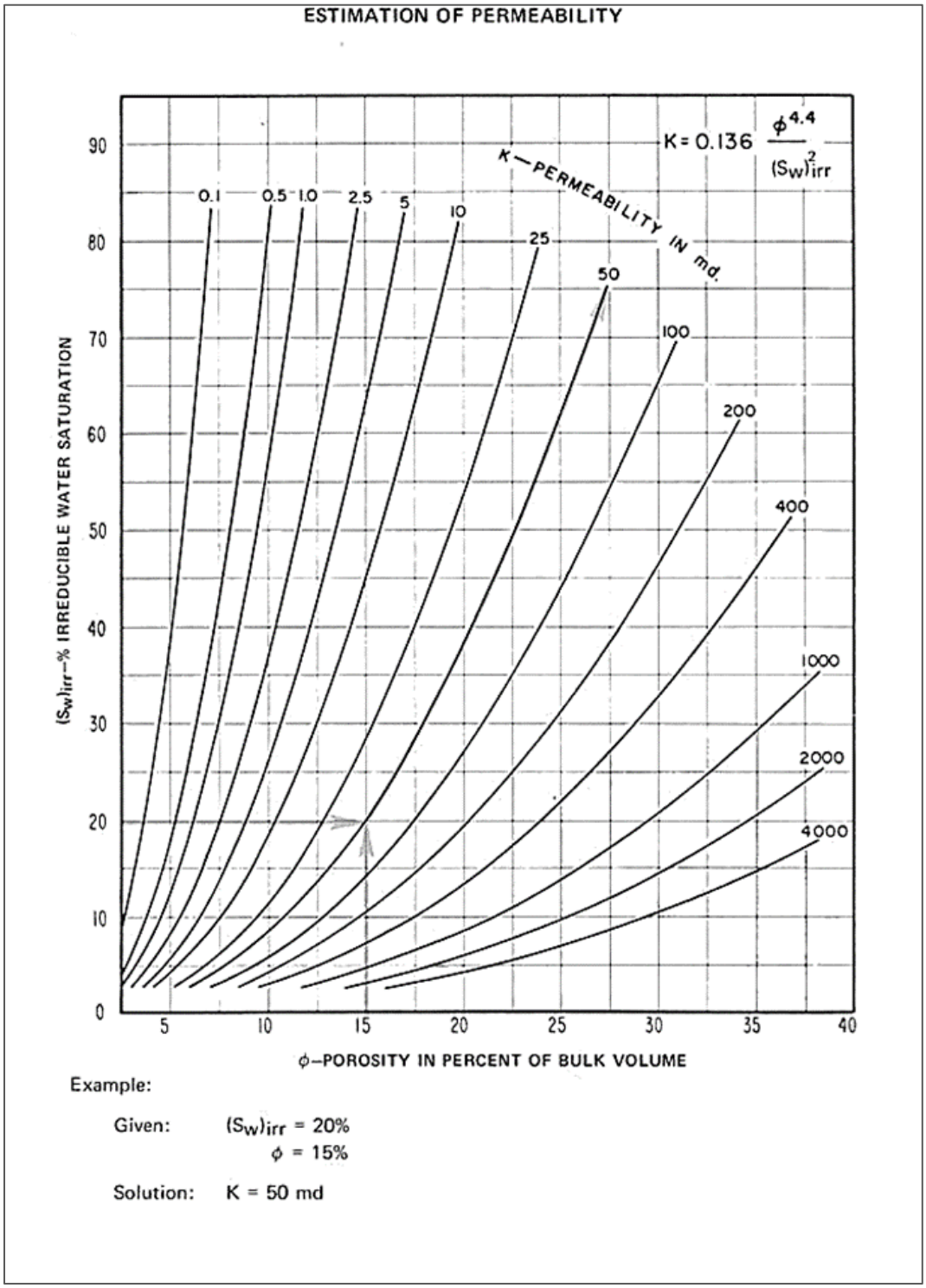

Figure 1C. Chart used to verify the math done in Petra that was used to estimate permeability from water saturation (sw) vs porosity (ϕ) (Timur, 1968).

Appendix D

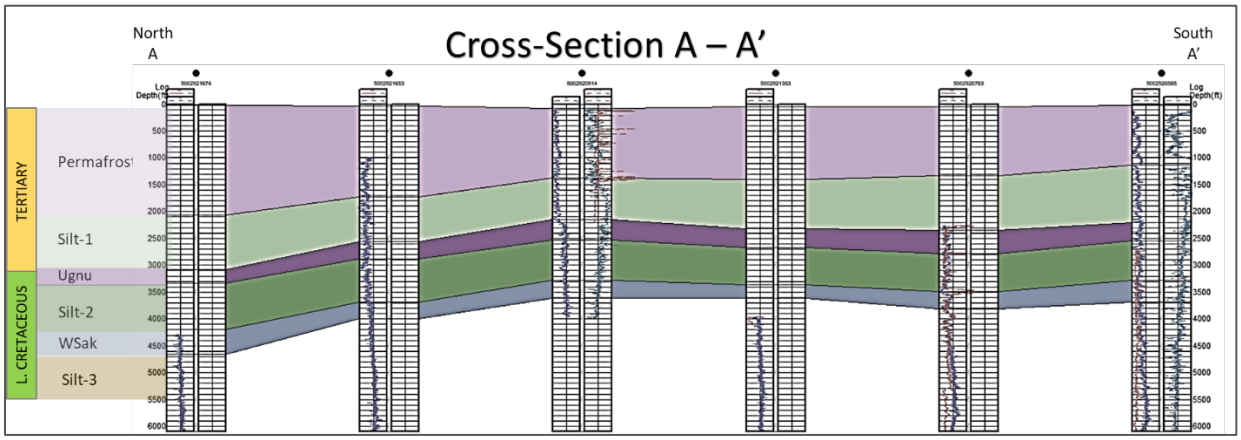

Figure 1D. Cross-section A-A’

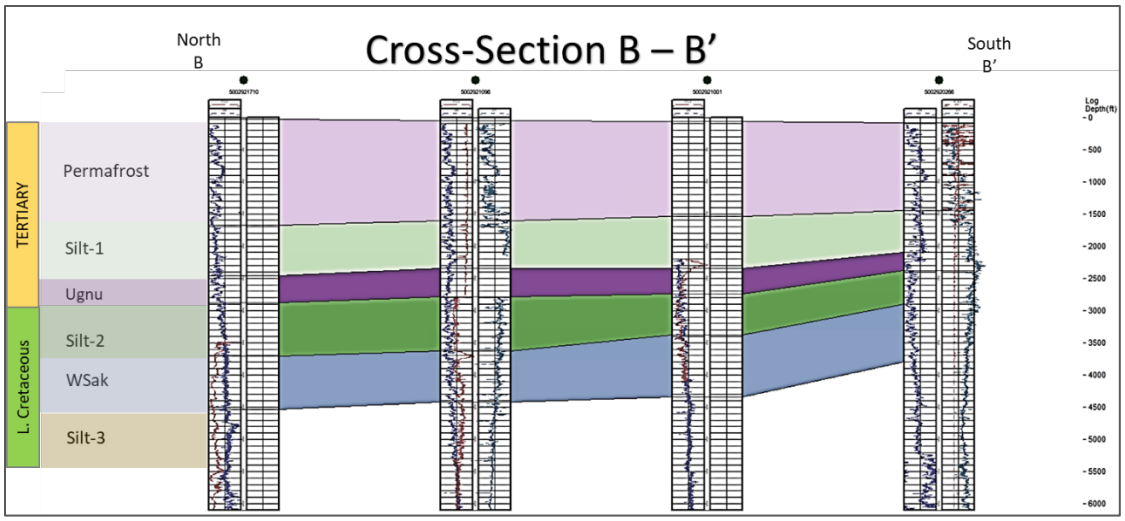

Figure 2D. Cross-section B-B’

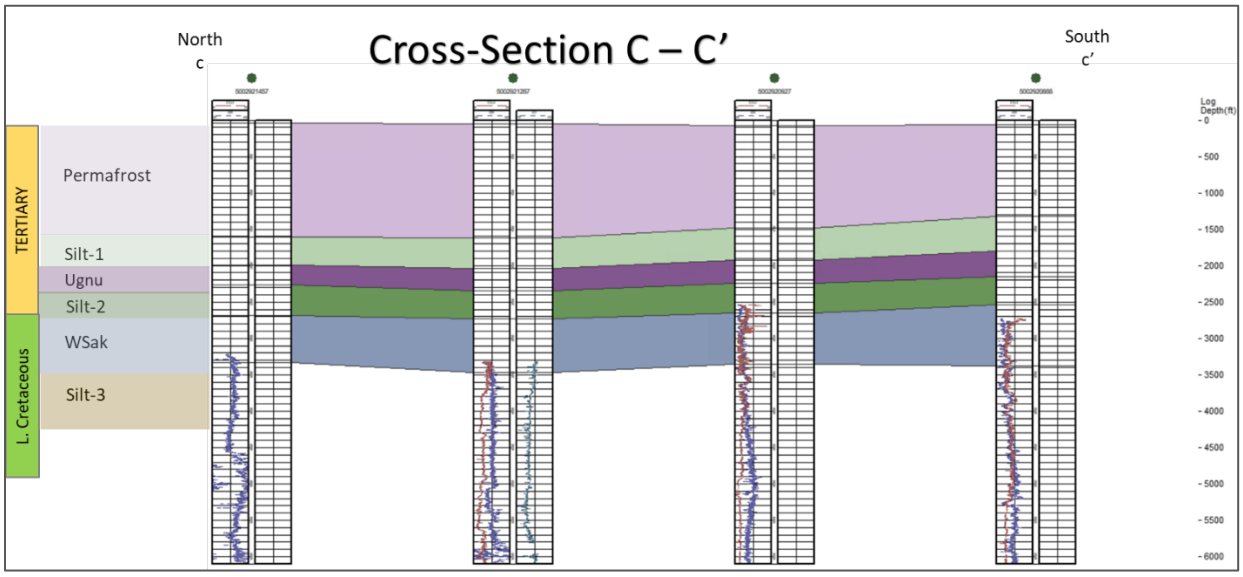

Figure 3D. Cross-section C-C’

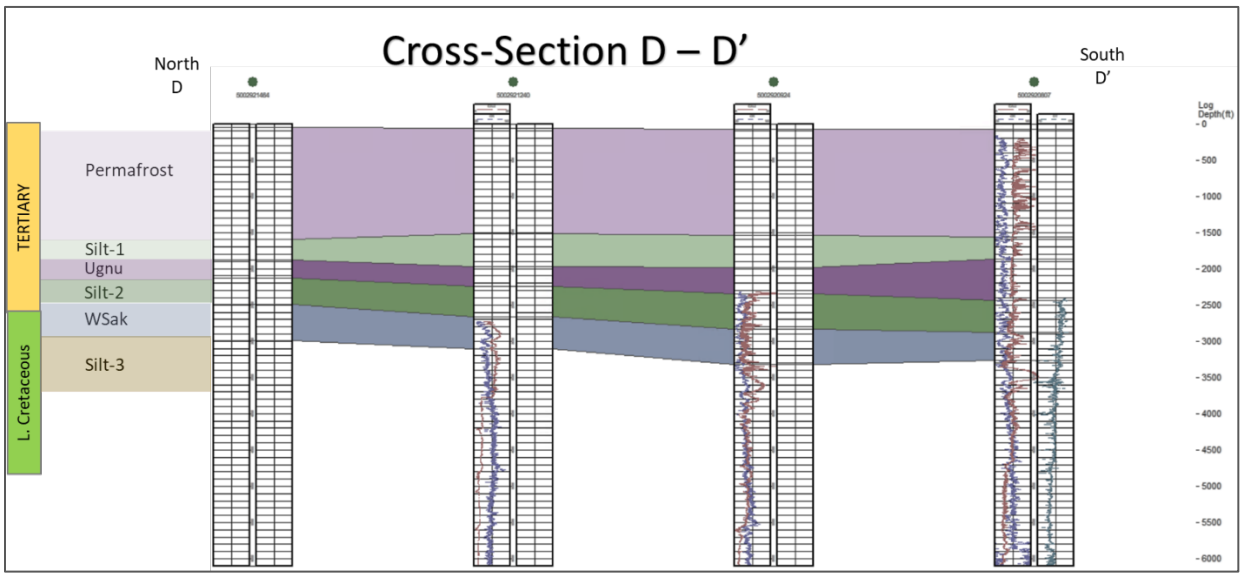

Figure 4D. Cross-section D-D’

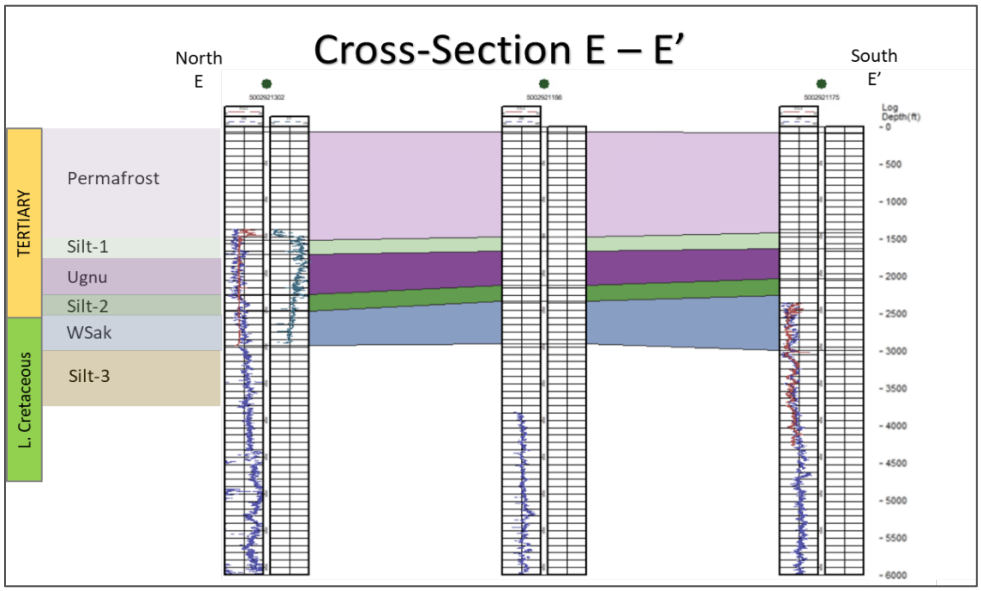

Figure 5D. Cross-section E-E’

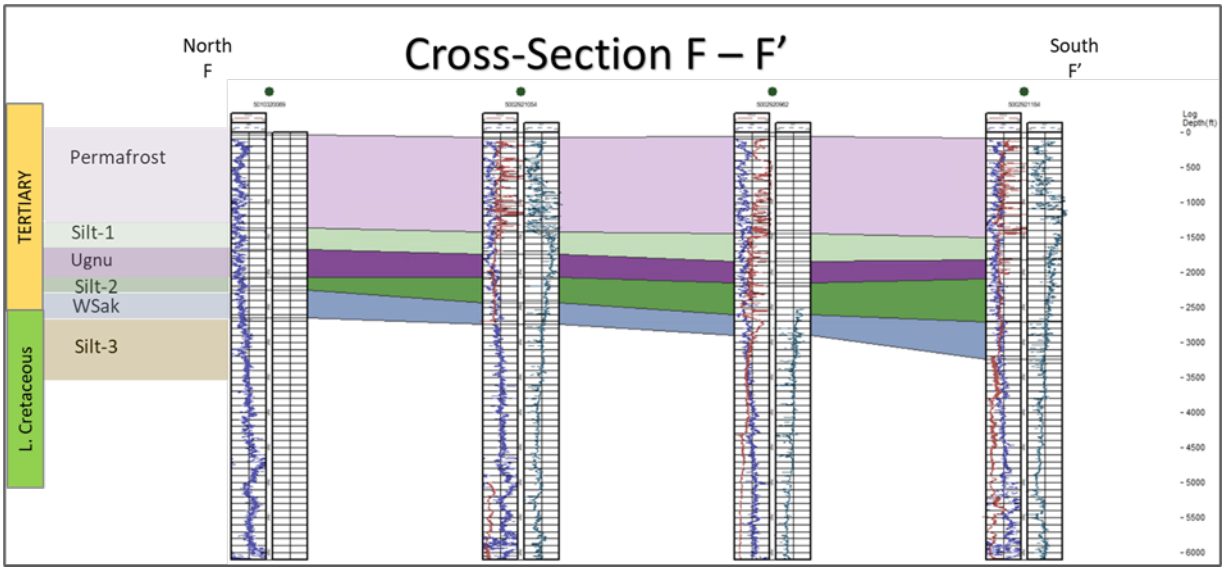

Figure 6D. Cross-section F-F’

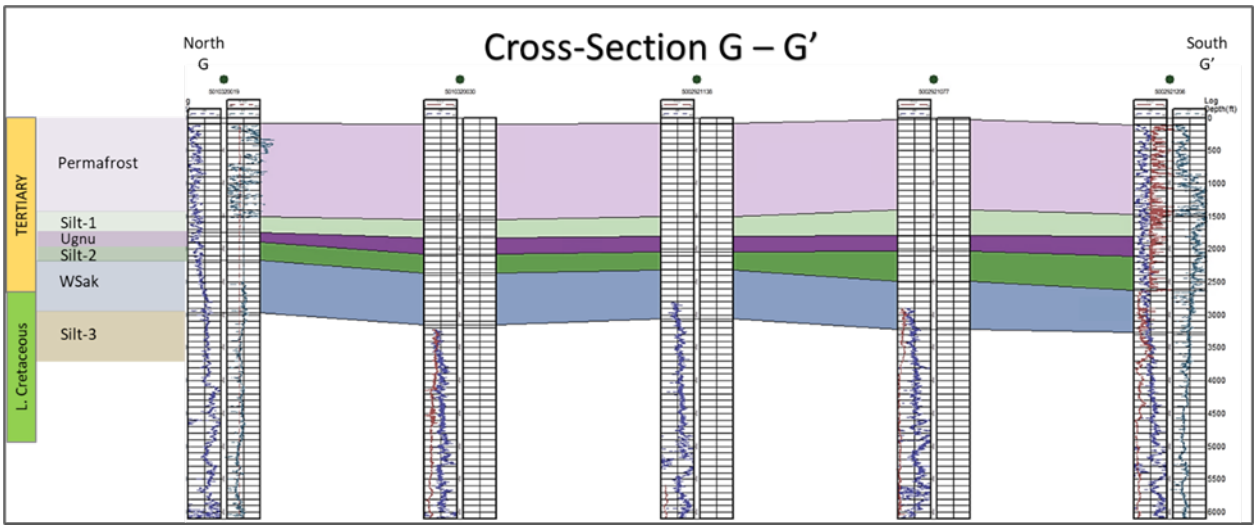

Figure 7D. Cross-section G-G'

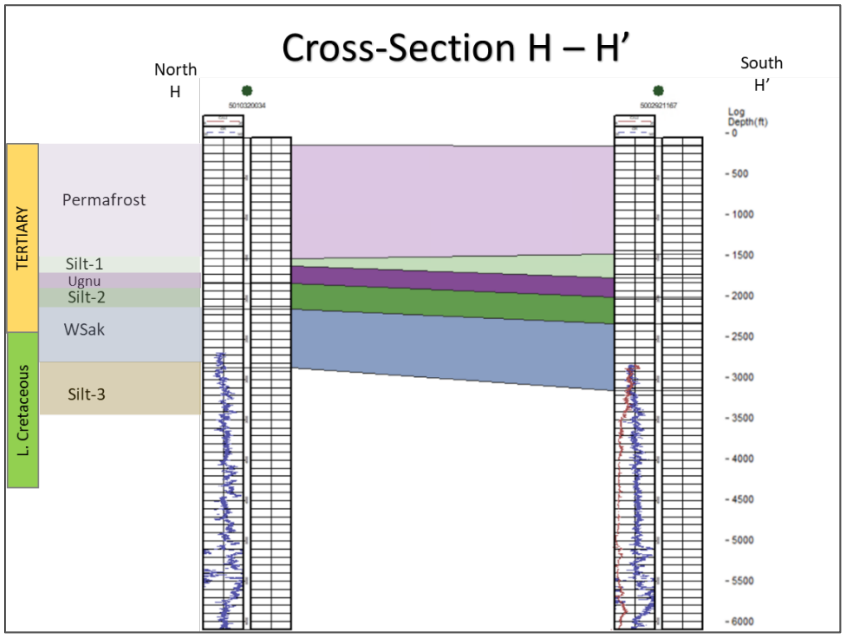

Figure 8D. Cross-section H-H'